2022

# DEVELOPING A LAGRANGIAN SEDIMENT TRANSPORT MODEL FOR NATURAL STREAMS

Saman Baharvand

# DEVELOPING A LAGRANGIAN SEDIMENT TRANSPORT MODEL FOR NATURAL STREAMS

By

Saman Baharvand

Dissertation

Submitted in partial fulfillment of the requirements

for the degree of Doctor of Philosophy at

The University of Texas at Arlington

August 2022

Arlington, Texas

Supervising Committee:

Dr. Habib Ahmari, Supervising Professor

Dr. Yu Zhang

Dr. Xinbao Yu

Dr. Ali Jon Khosronejad



# ABSTRACT

Sediment transport in natural streams is a complex process that can significantly affect the stream's water quality, ecosystem, and morphology. Suspended sediment concentrations can adversely affect the health of the ecosystem and aquatic species, and the deposited sediment particles can change the morphology and have irreparable environmental impacts. Several numerical models that can be used to manage and mitigate the adverse effects of sediment released into rivers by natural or anthropogenic activities have been developed to estimate the sediment and pollutant transport in waterbodies. However, the goal of the research for this thesis was to develop a Lagrangian stochastic sediment transport model, based on a particle tracking model (PTM), to simulate sediment transport in open channels. The sediment particle displacement was simulated using discretized advection and dispersion; the random walk approach was used to model the stochastic movement of the sediment particles. In advection, the displacement of the particle is based on its linearly interpolated velocity in the flow domain, derived from a 2D hydrodynamic model. In dispersion, using the random walk method, the stochastic movement of the particles is generated in a three-dimensional space. A conditional empirical equation was used to consider the effect of vertical dispersion in the top layers, near the water's surface. The PTM used the dimensionless mobility number that was developed based on the Shields diagram, to determine whether the particles remain suspended or are deposited onto the streambed. Using laboratory dataset, the ability of the PTM to calculate the sediment concentration of various classes of sediment (very fine, fine, and medium sand) was evaluated, and the results are presented with different dispersion coefficients. A comparison of the particle tracking model and the analytical solution of the advection-dispersion equation showed that the model was acceptably accurate. The

result of the sensitivity analysis and validation process showed that the model can be used to simulate sediment transport in open channel flows.

The sediment regime in natural streams can be altered by anthropogenic activities such as agriculture, logging, mining, urbanization, bridge and dam constructions, and hydrological alterations. This thesis examines the performance of the PTM at Wilson Creek in McKinney, Texas by utilizing empirical dispersion models that simulate the excess sediment load caused by bridge construction activities. The required hydrodynamic parameters including flow velocity, flow depth, and shear stress were obtained from the Hydrologic Engineering Center's River Analysis System (HEC-RAS 2 and were coupled with the PTM. A field monitoring program that included collecting suspended solids and surveying depositional areas in the creek, and observing the turbidity, bedload material, and substrate type was conducted during the bridge construction activities to evaluate the performance of the PTM. The PTM outputs included changes in the creek's sediment regime, suspended sediment concentration and depositional areas. A comparison of the field data and the PTM showed that the model accurately simulated the suspended sediment concentration distribution in the creek and the depositional areas correlated with the field investigations.

The use of machine learning-based dispersion models to improve the performance of the PTM was also investigated, and data obtained from previous studies was used to develop ensemble learning-based models to predict the longitudinal and transverse dispersion coefficients in natural streams. Several scenarios for developing prediction models were tested using the grid search cross-validation technique, and the model's optimal principal parameters (also known as hyperparameters) were presented, using different statistical measures. The dispersion models were coupled with the PTM to investigate the model's performance, using both empirical and learning-

based dispersion coefficients in natural streams. The field data collected at Wilson Creek was used to assess the performance of the model.

# ACKNOWLEDGEMENT

I am so grateful to my supervisor and chair of my committee Dr. Habib Ahmari for his always patience, feedback, and trust. Without his consistent inspiration, support, and guidance, this endeavor would not have been conceivable. I also want to acknowledge the rest of my dissertation committee: Dr. Yu Zhang, Dr. Xinbao Yu, and Dr. Ali Jon Khosronejad, for their insightful comments and for providing valuable knowledge throughout my Ph.D. program, which motivated me to widen my research from different perspectives. I would like to express my appreciation to Dr. Poorya Taghvaei for his continuous support throughout the second chapter of this work.

I am also grateful to former colleagues in the Civil Engineering Department at the University of Texas at Arlington, who helped me with research and coursework as well as with achieving a balance in my personal life: Ms. Roz Javadizadeh, Dr. Ali Jozaghi, Dr. Shah Md Imran Kabir, Md Arifur Rahman, Mr. Matthew Pebworth, Mr. Subhas Kandel, Mr. Mohammed Qays, Mr. Fahad Pervaiz, Mr. Mohammad Nabatian. A major part of the material presented in this dissertation is based upon work supported by the Texas Department of Transportation (Grant: 0-7023). This support is gratefully acknowledged.

I must express my gratitude to my wonderful parents, sister, and family members for their support and encouragement while studying a thousand miles from them. Words cannot express how grateful I am to my role models, my parents, for all of the sacrifices they have made on my behalf, and they have me to thank for all those grey hairs. Furthermore, thanks to all my friends, especially Dr. Alborz Fathinejad, Mr. Ruhi Nasiri, and Mr. Rumi, for making wonderful memories during the challenging stages of my life. Thanks to all of you.

# DEDICATION

*This work is dedicated to my parents and my sister, who have always loved me unconditionally and whose guidance taught me to work hard for the things I aspire to achieve.*

# CO-AUTHORSHIP

This thesis is part of the work conducted by the author to satisfy the requirements for a Ph.D. in civil engineering and includes developing numerical models, performing field studies, analyzing data, examining research results, and preparing the material for manuscripts. Dr. Habib Ahmari supported and supervised the research, which resulted in the following manuscripts, with co-authorship as stated below.

- Journal Papers

| Dissertation Chapter | Title | Authors | Status |
|---|---|---|---|
| 2 | Developing A Lagrangian Sediment Transport Model for Open Channel Flows | Baharvand, S., Ahmari, H., Taghvaei, P. | Submitted (under second review) |
| 3 | Modeling Non-cohesive Sediment Transport in Natural Stream Using a Lagrangian Approach - Case Study: Wilson Creek, McKinney, Texas, USA | Baharvand, S., Ahmari, H., Kandel, S., Goldsmith, A., Jaber, F., Yu, X., Randklev, C. | Not submitted |
| 4 | Application of Machine Learning Approaches in Particle Tracking Model to Estimate Sediment Transport in Natural Streams | Baharvand, S., Ahmari, H., | Not Submitted |

# TABLE OF CONTENTS

# LIST OF FIGURES

# LIST OF TABLES

# CHAPTER 1

# INTRODUCTION

## MOTIVATION

Water is one of our most important natural resources, yet anthropogenic activities are negatively impacting its quality. An accurate prediction of suspended sediment concentrations and sediment deposition rates is essential to assessing and predicting biological and biogeochemical regimes in streams, as well as the health of aquatic habitats and species. Several tools and methods have been developed to study sediment transport in natural streams, but most of the sediment transport models have been developed based on an Eulerian-Eulerian framework that solves sediment transport equations at a fixed point in space. Such models compute sediment transport rates over the modeling domain as a continuous phase, consider the statistical properties of the sediment cloud, and assess the morphological evolution of the stream bed. Eulerian modeling tools are vital components of engineers' analysis toolboxes, as the models require very little grid space to provide reasonable solutions in environments that experience a sudden change in their sediment regime, such as the accidental release of sediment plume from construction sites of stream-crossing structures. Lagrangian sediment transport models are also proven effective methods for tracking sediment particles in different environments, as they consider a number of moving mass particles, and different evolving scenarios can increase their similarity to the natural randomness properties of sediment transport.

Dispersion plays an important role in Lagrangian sediment transport models' simulation of sediment movement and the effect of turbulent flow on sediment properties. Several studies have used a particle tracking model (PTM) as a Lagrangian stochastic sediment transport model to

simulate the movement of sediment particles in open channels (Oh and Tsai 2018; Fan et al., 2016; Tsai et al., 2014). For example, a Lagrangian stochastic model was developed to predict 50 years of morphologic changes caused by the effects of climate change in the Mersey Estuary, U.K. (Lane and Prandle 2006); a particle-based sediment transport model was used to assess non-cohesive sediment transport in open channels (Taghvaei 2013); and a coastal risk management system was developed, using PTM, to determine the dispersion coefficient of toxic substances (i.e., dinoflagellate bloom) in Tampa Bay (Havens et al., 2010).

## BACKGROUND

Natural rivers have experienced an increase in pollution and contamination over the past few decades as a result of effluent discharge and anthropogenic activities. Rainfall, scouring, dam breaks, and landslides also generate a random quantity of sediment particles into waterbodies (streams, rivers, ponds, lakes, and estuaries) (Bennett et al., 2014), creating a need for a stochastic model that can consider the randomness of the sediment particles (Tsai et al., 2018).

Sediment particles are first eroded by wind and runoff and then transported in the water by suspended or bed loads and deposited in streams, lakes, and reservoirs (Malmon et al., 2003). Because their complex behavior makes it difficult to fully understand the mechanics of sediment transport (Tsai et al., 2018; Safari et al., 2016; Muste et al., 2009), various experimental and field investigations have been conducted, using empirical approaches (Lo´pez et al., 2014; Priya et al., 2016). The approaches used were drastically different from each other (Pinto et al., 2006), however, and the models were sensitive to small variations in sediment gradation and flow conditions, i.e., variability of flow depth, flow velocity, dispersion terms, etc. (Camenen and Larroudé 2003), making it impossible to select the most accurate empirical equation for a specific problem (Huntley and Bowen 1989).

Deterministic and stochastic approaches provide more reasonable results for sediment transport with less uncertainty and simplification assumptions (Hantush and Kalin 2004). However, numerical modeling of sediment transport has uncertainties that can be the result of dimensionality simplification for 1D, 2D, or 3D models or stream-specific coefficients such as Shields critical shear stress parameter (Beckers et al., 2018). Deterministic models use conservation of mass and momentum principles to model sediment transport and produce exact results for a particular set of inputs, but they usually require a longer simulation period than stochastic approaches. In contrast, stochastic approaches present data and predict outcomes that account for a certain level of unpredictability or randomness with a shorter simulation time. The first application of stochastic approaches for simulating bedload transport was proposed by Einstein in 1950; later, various studies showed the performance of Lagrangian stochastic approaches in modeling sediment transport (De Baas et al., 1986; Ley 1982; Ley and Thomson 1983).

Lagrangian stochastic sediment transport models consider a group of particles in the flow domain as mass transport elements to solve the advection-dispersion equation. Most of the stochastic models are Lagrangian models that simulate natural processes such as sediment entrainment or deposition (Oh 2011). Other studies have used particle tracking models (PTM) to simulate sediment and contaminant transport in rivers and estuaries. For instance, Lane and Prandle (2006) proposed a particle tracking model (PTM) to predict 50 years of morphologic changes caused by climate change in the Mersey Estuary, U.K.; Liu et al. (2007) studied the residence time in the Danshuei River estuarine system, Taiwan, using a 3D PTM coupled with a hydrodynamic model; Gong et al. (2008) developed a Lagrangian PTM to investigate the temporal evolution of flushing properties in the Xiaohai Lagoon; and Havens et al. (2010) presented a coastal risk management system using PTM with the dispersion coefficient of toxic substances in Tampa Bay and also

delineated the most probable areas affected by pollution, using probability functions. Oh (2011) proved the accuracy of a PTM in modeling sediment transport by using a stochastic diffusion particle tracking model (SD-PTM) and a stochastic jump-diffusion particle tracking model (SJD-PTM), and the results revealed the significant effect of dispersion in the stochastic sediment transport approach. Taghvaei (2013) showed the accuracy of the random walk method in a PTM when it is coupled with the 2D-CECAD hydrodynamic model to assess suspended sediment particles. The temporal changes in the suspended sediment concentration due to dredging at a port entrance showed an acceptable performance for the proposed model by Taghvaei (2013). Tsai et al. (2014) used various mathematical forms of particle tracking models to describe particle movements under different flow conditions. In their proposed particle tracking model, a random term primarily caused by fluid eddy motions was modeled as a Wiener process; in 2018, they introduced a probabilistic function to the model. Particle deposition and resuspension criteria were considered in the particle tracking system, and a discrete sediment transport was presented, based on the ensemble statistics of sediment concentrations and transport rates.

Dispersion plays an essential role in particle-based sediment transport models and is responsible for mixing the particles of open channels in longitudinal, transverse, and vertical directions. In rivers, the vertical mixing process usually occurs quickly at the contamination field near the pollutant discharge point. However, transverse and longitudinal mixing processes in streams take place in intermediate and distant fields, respectively, from the source of pollution (Najafzadeh et al., 2019). It is critical, therefore, to estimate the longitudinal and transverse dispersion coefficients in natural streams because these mechanisms are more important than vertical mixing in rivers (Rutherford, 1994).

In addition to the statistical and empirical-based estimations of dispersion coefficients of natural streams, various studies have discussed the efficacy of machine learning methods (also known as soft computing techniques or data-driven models). For instance, Etemad-Shahidi and Taghipour (2012) and Tu et al. (2015) developed an M5 model tree and genetic programming (GP) model, respectively, to estimate longitudinal dispersion, and both proved that ML-based methods more accurately estimate longitudinal dispersion than empirical approaches. Other studies have shown the superiority of soft computing techniques in estimating transverse dispersion in natural streams (Nezaratian et al., 2021; Azamathulla and Ahmad 2012). Due to the high performance of data-driven models, a machine learning approach can be used as an alternative method for estimating longitudinal and transverse dispersion in PTMs to enhance its applicability and compare it performance with the empirical-based dispersion equations.

## RESEARCH QUESTIONS AND OBJECTIVES

This research aims to develop a Lagrangian model based on a particle tracking model to simulate suspended sediment transport and sediment deposition in natural streams. Due to the broad scope of this topic, the research will address three specific research questions:

1. *Is the particle tracking model (PTM) able to simulate sediment transport in a straight prismatic channel using different empirical dispersion terms?*

The Lagrangian approach considers different equations and methods for modeling sediment transport. The performance of the PTMs in modeling sediment transport is acceptable; however, combining several methods to address the properties of sediment particles in waterbodies may change the model's performance. Advection, dispersion, the particles' settling velocity, and deposition and resuspension criteria are the most critical factors for modeling sediment transport

in PTMs. The first part of this study aims to investigate the performance of PTMs in prismatic straight open channels by utilizing different empirical dispersion terms, coupled with a stochastic approach, such as the random walk method, to increase the accuracy of the PTM in simulating sediment transport. The performance of the PTM will be evaluated using laboratory data and analytical solutions of the advection-dispersion model. Three widely used empirical equations form the basis of the longitudinal dispersion, which is the most important dispersion coefficient for solving the discretized transport relationship for each sediment particle. A variety of sediment gradations, from fine to coarse materials, will be used to evaluate the ability of the PTM to simulate the transport of sediment of different sizes, and the results will be compared to the laboratory dataset. Based on the results of this study, a PTM-based sediment transport model that utilizes empirical dispersion equations will be proposed for sediment transport modeling in straight prismatic channels.

2. *Can the particle tracking model accurately simulate sediment transport in natural streams? Is PTM able to predict the effects of sediment entrainment on the distribution of the sediment concentration?*

Field data is essential for developing an accurate PTM model for open channels in natural streams that, coupled with a 2D hydrodynamic model, will be able to simulate sediment transport. Wilson Creek in McKinney, Texas was studied to assess the performance of the PTM by comparing the results of the developed model with the field measurements, and several quantitative and qualitative assessments were made to evaluate the ability of the PTM to simulate the transport of suspended sediment and sediment deposition in natural streams.

3. *What is the advantage of the machine learning-based dispersion approach in the PTM model?*

Previous studies have not investigated the applicability of machine learning (ML) methods for estimating dispersion in natural streams; however, a few studies have shown the results of using specific ML methods to estimate the dispersion in different case studies. For instance, one of the widely used ML-based methods, ensemble models, has not been used to predict the transverse dispersion coefficient in natural streams. In the present study, a dataset of flow hydraulic parameters including flow depth, flow velocity, and shear velocity will be derived from several case studies and used to predict the longitudinal and transverse dispersion, using ensemble machine learning methods. Then, the ML-based dispersion models will be integrated into the PTM to model sediment transport in a natural stream, and the models' performance will be evaluated using the sediment concentration dataset obtained from field samples taken from a section of Wilson Creek.

**THESIS OVERVIEW**

This thesis is presented in manuscript form, with Chapters 2, 3, and 4 corresponding to a manuscript written by the author. Chapter 1 consists of the motivation of the study, a background of previous studies conducted to develop Lagrangian particle tracking models for solving discrete advection and dispersion displacement equations to model sediment transport in natural streams, a summary of machine learning approaches used to predict the dispersion coefficient in natural streams, and the objective of the research. Chapter 2 discusses the general structure of a Lagrangian particle tracking model that was developed based on empirical dispersion equations. It also discusses the sensitivity of the PTM for several widely used empirical longitudinal dispersion coefficients and the analytical solution of an advection-dispersion equation in a prismatic open

channel. Chapter 3 integrates an Eulerian flow domain with the PTM discussed in Chapter 2 and assesses the ability of the model to simulate sediment transport in natural streams. It also describes the field monitoring program that was conducted to evaluate the performance of the PTM while a bridge was being built over Wilson Creek. Chapter 4 presents the results of an effort to develop machine learning-based dispersion coefficients in natural streams. The ML-based dispersion models were coupled with the PTM to assess the performance of the PTM with empirical and ML-based dispersion models to simulate sediment transport in natural streams. The performance of the models were evaluated using the field data derived from Wilson Creek. Chapter 5 presents the conclusions of the thesis and provides suggestions and recommendations for future research.

The material in these chapters is supplemented by Appendix A, which presents the dispersion coefficient data that was used in the machine learning methods described in Chapter 4 to build the ML-based dispersion coefficient prediction approaches.

## REFERENCES


Azamathulla, H. M., and Ahmad, Z. (2012). "Gene-expression programming for transverse mixing coefficient." *Journal of Hydrology*, 434–435, 142–148.

Bennett, G., Molnar, P., McArdell, B., Burlando, P. (2014). "A probabilistic sediment cascade model of sediment transfer in the Illgraben." *Water Resour Res.*, 50(2):1225–1244

Camenen, B., and Larroudé, P. (2003). "Comparison of sediment transport formulae for the coastal environment." *Coastal Engineering*, 48(2), 111–132.

De Baas, A. F., Van Dop, H., and Nieuwstadt, F. T. M. (1986). "An application of the Langevin equation for inhomogeneous conditions to dispersion in a convective boundary layer." *Quarterly Journal of the Royal Meteorological Society*, 112(471), 165–180.

Einstein, H. A. (1950). "The bedload function for sediment transportation in open channel flows." vol 1026. United States Department of Agriculture, U.S. Government Printing Office, Washington, D.C.

Etemad-Shahidi, A., and Taghipour, M. (2012). "Predicting longitudinal dispersion coefficient in natural streams using M5 Model Tree." *Journal of Hydraulic Engineering*, 138(6), 542–554.

Fan, N., Singh, A., Guala, M., Foufoula-Georgiou, E., and Wu, B. (2016). "Exploring a semimechanistic episodic Langevin model for bed load transport: Emergence of normal and anomalous advection and diffusion regimes." *Water Resources Research*, 52(4), 2789–2801.

Gong, W., Shen, J., and Jia, J. (2008). "The impact of human activities on the flushing properties of a semi-enclosed lagoon: Xiaohai, Hainan, China." *Marine Environmental Research*, 65(1), 62–76.

Havens, H., Luther, M. E., Meyers, S. D., and Heil, C. A. (2010). "Lagrangian particle tracking of a toxic dinoflagellate bloom within the Tampa Bay estuary." *Marine Pollution Bulletin*, 60(12), 2233–2241.

Lane, A., and Prandle, D. (2006). "Random-walk particle modelling for estimating bathymetric evolution of an estuary." *Estuarine, Coastal and Shelf Science*, 68(1–2), 175–187.

Ley, A. J. (1982). "A random walk simulation of two-dimensional turbulent diffusion in the neutral surface layer." *Atmospheric Environment*, (1967), 16(12), 2799–2808.

Ley, A. J., and Thomson, D. J. (1983). "A random walk model of dispersion in the diabatic surface layer." *Quarterly Journal of the Royal Meteorological Society*, 109(462), 867–880.

Liu, W.-C., Chen, W. B., Cheng, R. T., Hsu, M. H., and Kuo, A. Y. (2007). "Modeling the influence of river discharge on salt intrusion and residual circulation in Danshuei River estuary, Taiwan." *Continental Shelf Research*, 27(7), 900–921.

Macdonald, N. J., Davies, M. H., Zundel, A. K., Howlett, J. D., Demirbilek, Z., Gailani, J. Z., Lackey, T. C., and Smith, J. (2006). "PTM : Particle Tracking Model." 168.

Malmon, D. V., Dunne, T., Reneau, S. L. (2003). "Stochastic theory of particle trajectories through alluvial valley floors." *Journal of Geology*, 111(5):525–542.

Muste, M., Yu, K., Fujita, I., Ettema, R. (2009). "Two-phase flow insights into open-channel flows with suspended particles of different densities." *Environ Fluid Mech*, 9(2):161–186.

Najafzadeh, M., Noori, R., Afroozi, D., Ghiasi, B., Hosseini-Moghari, S.-M., Mirchi, A., Torabi

Haghighi, A., and Kløve, B. (2021). “A comprehensive uncertainty analysis of model-estimated longitudinal and lateral dispersion coefficients in open channels.” *Journal of Hydrology*, 603, 126850.

Nezaratian, H., Zahiri, J., Peykani, M. F., Haghiabi, A., and Parsaie, A. (2021). “A genetic algorithm-based support vector machine to estimate the transverse mixing coefficient in streams.” *Water Quality Research Journal*, 56(3), 127–142.

Oh, J., and Tsai, C.W. (2018). “A stochastic multivariate framework for modeling movement of discrete sediment particles in open channel flows.” *Stochastic Environmental Research and Risk Assessment*, 32(2).

Oh, J. (2011). “Stochastic particle tracking modeling for sediment transport in open channel flows.” Ph.D. dissertation. State University of New York at Buffalo.

Ouillon, S. (2018). “Why and How Do We Study Sediment Transport? Focus on Coastal Zones and Ongoing Methods.” *Water*, 10(4), 390.

Priya KL, Jegathambal P, James EJ (2016). “Salinity and suspended sediment transport in a shallow estuary on the east coast of India.” *Reg Stud Mar Sci* 7:88–99.

Rutherford, J. C. (1994). “River mixing.” Wiley, Chichester, UK.

Safari M-J-S, Aksoy H, Mohammadi M (2016). “Artificial neural network and regression models for flow velocity at sediment incipient deposition.” *J. Hydrol.*, 541:1420–1429

Taghvaei, P. (2013). “Simulating Transport and Deposition of Non-Cohesive Sediments by Applying Particle Tracking Method.” MSc Thesis. University of Tehran.

Tsai, C. W., Hung, S. Y., and Oh, J. (2018). “A stochastic framework for modeling random-sized batch arrivals of sediment particles into open channel flows.” *Stochastic Environmental Research and Risk Assessment*, 32(7), 1939–1954.

Tsai, C. W., Man, C., and Oh, J. (2014). “Stochastic particle based models for suspended particle movement in surface flows.” *International Journal of Sediment Research*, 29(2), 195–207.

Tu, Q., Li, H., Wang, X., and Chen, C. (2015). “Ant colony optimization for the design of small-scale irrigation systems.” *Water Resources Management*, 29(7), 2323–2339.

# CHAPTER 2

# DEVELOPING A LAGRANGIAN SEDIMENT TRANSPORT MODEL FOR OPEN CHANNEL FLOWS


## ABSTRACT

A three-dimensional stochastic Lagrangian particle tracking sediment transport model was developed to solve the discrete advection-dispersion equation by using a combination of empirical dispersion equations. The performance of three widely-used longitudinal dispersion coefficient equations was examined for the purpose of selecting one as the primary dispersion equation in the model. A conditional empirical equation was used to consider the effect of vertical dispersion in the top layers of the water, near the surface. The ability of the PTM to calculate the sediment concentration was evaluated for various sediment classes (very fine sand, fine sand, and medium sand) using available laboratory dataset. Multiple statistical measures were calculated using the Taylor diagram for each dispersion equation. The results showed that the particle tracking model estimated the suspended sediment concentration in a rectangular open channel with a correlation coefficient (R) of 0.96, standard deviation (STD) of 0.262, and root mean square deviation (RMSD) of 0.06 for three different sediment classes, proving the acceptable accuracy of the model for different ranges of sediment gradations. The accuracy of the PTM was also compared to a recently developed particle tracking model and analytical solution of the advection-dispersion equation and showed that the model's prediction of the maximum concentration of suspended sediment in a straight channel was 6% lower than the analytical solution's for 30 seconds of simulation time and 9.4% lower for 50 seconds of simulation. However, there was a good agreement between the model's longitudinal and transverse sediment concentration distributions

and that of the analytical solution approach. The result of the sensitivity analysis and validation process showed that the model can be used to simulate sediment transport in open channels.

**Author Keywords:** Sediment transport, Lagrangian Particle Tracking, Stochastic approach, Advection-dispersion, Random walk.

## INTRODUCTION

Natural sedimentation processes such as bed resuspension and longshore transport, and anthropogenic activities such as dredging and piling construction can cause sediment particle movement in streams and estuaries that may lead to a series of sediment management issues (Black et al., 2007). These issues have the potential to negatively affect the environment, aquatic habitats, and economic aspects of society (Oh 2011). Eroded materials released from anthropogenic activities can alter sediment regimes and geomorphological conditions of receiving streams and may have short- and long-term impacts on aquatic habitats. A systematic understanding of the sediment transport process is essential to creating effective water resources and sediment management plans to control or mitigate these problems.

Previous studies have used numerical sediment transport models to assess sediment movement in various environments (Papanicolaou et al., 2004; Li and Duffy 2011; Meselhe et al., 2012), and during the past two decades, several deterministic sediment transport models have been developed that use conservation of mass and momentum principles. Deterministic models produce exact results for a set of inputs, but they require a longer simulation time than stochastic approaches and do not consider the randomness of the data. In contrast, stochastic approaches present data and predict outcomes that account for a certain level of unpredictability or randomness and can generate different outputs for a given set of input variables (Kalin and Hantush 2003). Deterministic approaches are usually used for short- (hours to days) to medium-term (days to months) sediment transport modeling (Amoudry and Souza 2011) and are used to model sediment transport in streams (Wu 2004; Fang and Rodi 2003) and coastal environments (Mengual et al., 2021; Warner et al., 2008; Damgaard et al., 2002). Several studies have shown the application of stochastic models for simulating sediment transport (Tsai et al., 2020; Park and Seo, 2018;

Macdonald et al., 2006; Niño and García, 1998), and the majority of them are Lagrangian models that simulate natural processes such as sediment entrainment or deposition (Oh 2011).

Lagrangian stochastic models are a proven method for accurately tracking sediment particles in turbulent flows (Ley 1982; Ley and Thomson 1983; MacDonald et al., 2006). They consider a group of particles as mass transport elements in the flow domain, and discrete advection and dispersion equations model the relationship between the flow characteristics and the movement of particles during the simulation period. Several studies have shown the applicability of stochastic methods for assessing the evolution of pollutant and sediment particles in open channels and estuaries. For instance, Lane and Prandle (2006) proposed a particle tracking model (PTM) based on the random walk approach to be coupled with the POLCOMS 3D hydrodynamic model to simulate the tidal dynamics of an estuary. Their model considered longitudinal and transverse advection in conjunction with the vertical dispersion derived from an approximation based on the bed friction coefficient and water depth, as proposed by Fischer et al. (1979). The model developed by Lane and Prandle (2006) considered simple criteria for sediment particle deposition, i.e., sediment particles would be deposited when the height of the particle above the bed, calculated in a discrete advective settlement step, was less than zero. They used the PTM to predict 50 years of morphologic changes due to the transport of fine sediment particles in the Mersey Estuary, U.K. caused by climate change. Havens et al. (2010) presented a coastal risk management system using PTM to simulate the transport of toxic blooms in Tampa Bay resulting from unarmored dinoflagellate *Karenia brevis* in 2005. They used a random walk stochastic approach with a fourth-order Runge-Kutta scheme to estimate the dispersion in a Lagrangian PTM in a flow domain simulated by the Princeton ocean model. The flow characteristics were linearly interpolated to the particle position at each computation time step, and they forced the salinity data, obtained from

the Environmental Protection Commission (EPC), to the flow domain discrete points to assess the bay's salinity transport. Probability functions were used to identify the areas most likely to be affected by pollution. Oh (2011) showed the accuracy of the PTM for modelling sediment transport using a stochastic jump-diffusion particle tracking model (SJD-PTM), which revealed the significant effect of dispersion in the stochastic sediment transport approach. Taghvaei (2013) showed the accuracy of the random walk in the Lagrangian PTM, coupled with the 2D-CECAD hydrodynamic model, in assessing suspended sediment particles. The temporal changes of suspended sediment concentration, due to dredging at a port entrance, showed the acceptability of their proposed model. Tsai et al. (2014) used various mathematical forms of particle tracking models to describe particle movements under different flow conditions. In their proposed particle tracking model, a random term primarily caused by fluid eddy motions was modeled as a Wiener process. Later, Tsai et al. (2018) introduced a probabilistic function to the PTM model. The applicability of the proposed sediment transport model was also discussed, using the available dataset. They considered the mixing process of sediment particles in the vertical direction in transport equations but failed to consider the longitudinal dispersion. Particle deposition and resuspension criteria were considered in the particle tracking system, and a discrete sediment transport, based on ensemble statistics of sediment concentrations and transport rates, was presented.

In addition to suspended sediment transport modeling using Lagrangian PTMs, some studies have focused on the applicability of PTMs to simulate bedload transport in waterbodies. For instance, Kidanemariam and Uhlmann (2014) used a direct numerical simulation (DNS) for incompressible fluid flow over a mobile bed with spherical shape particles. The bed particle movement in their study was modeled using Newton’s equation and was driven by hydrodynamic and gravity forces

acting on sediment particles. They modeled the particle-particle collision effect using a discrete element model and found that a particle-based bedload transport model can accurately estimate the bedload transport rate and predict the bedform patterns in laminar and turbulent flows. Barati et al. (2018) developed a three-dimensional Eulerian-Lagrangian model to investigate bedload transport by considering hydrodynamic forces and turbulent fluctuations and to define a particle-based saltation transport model. They evaluated the performance of the Lagrangian modeling for a wide range of sediment gradations and investigated how the absence of different hydrodynamic forces on the model affected it. Zhao et al. (2020) developed a Eulerian hydrodynamic model, based on the large eddy simulation (LES) method and coupled with a Lagrangian PTM, to simulate a wall-shear turbulent flow over a sediment bed and calculate the forces acting on saltating particles. Their study discussed the particle shape factor in the Lagrangian saltation transport model, which led to proposing a new bedload transport formula that considered the shape factor of particles.

There is a lack of information on comprehensively assessing the impacts of different empirical dispersion coefficients on sediment transport by using Lagrangian PTMs. Some of the Lagrangian PTM studies consider longitudinal and transverse dispersion coefficients (Tsai et al., 2018), but some neglect the effect of dispersion and assume that particle transport is due to the advection coefficients (Park et al., 2018). The present study aims to fill the literature void and develop a novel particle tracking model, using a random walk stochastic approach to model sediment transport in open channels and coupling it with a two-dimensional Eulerian flow domain using different empirical dispersion equations. Instead of using the traditional parabolic vertical dispersion formula, known as the Rouse model, a few studies have used alternative theoretical approaches to define the vertical dispersion coefficient (Park et al., 2020; Tsai et al., 2020;

McDonald 2006; Oh 2011). Because the Rouse model cannot consider the dispersion coefficient in areas close to the water's surface, however, a conditional vertical dispersion equation was used in the present study to model the particle movement more accurately by considering the vertical diffusivity effects on particles for the entire water depth. The effect of some commonly used longitudinal dispersion coefficients was also assessed to model sediment transport in the open channels using laboratory datasets, and the performance of the PTM was compared to previously developed PTMs that model dispersion for various sediment gradations. After a sensitivity analysis of various empirical dispersion coefficient equations was conducted, the accuracy of the PTM with ideal dispersion coefficient equations was verified, using an analytical solution of the 2D advection-dispersion equation. Lastly, the limitations of the proposed model and recommendations for future research are provided. The methodology and validation processes of the PTM are discussed in the following sections.

## METHODOLOGY

A Lagrangian particle tracking model (PTM), the architecture of which is illustrated in Figure 2.1, was developed to simulate sediment transport in open channels. As shown, the flow parameters, location of the sediment source, and the number of particles injected at the sediment source are first introduced to the PTM. Streamwise and transverse flow velocities ($V_x$, $V_y$), shear stress ($\tau$), and flow depth ($H$) are the required spatial hydrodynamic parameters and may be produced by any 2D hydrodynamic model, such as the HEC-RAS 2D, CCHE2D, that is capable of generating spatial geodata for natural streams. Each of the spatial flow parameters is discretized to a fixed Eulerian mesh domain that is used to solve Lagrangian particle transport equations, using a stochastic approach. Once the flow domain has been generated, using the appropriate 2D hydrodynamic model, the preprocessed flow data and sediment properties are introduced to the

PTM, and it will track each particle in streamwise, transverse, and vertical directions. Advection and dispersion motion are updated for each computational time step after checking the deposition/resuspension criteria. The possibility of deposition/resuspension of particles is determined using a conditional mobility factor that measures the ratio of the applied shear stress parameter from the hydrodynamic model to the critical shear stress of particles at the particle's location. The model's architecture depicted in Figure 2.1 was programmed in Python 3.9.0, an interpreted high-level, general-purpose programming language (Rossum 1995). Several Python-based packages such as "NumPy", "SciPy", "Pandas", "Matplotlib", and "statistics" can be used to build the general structure of the model.

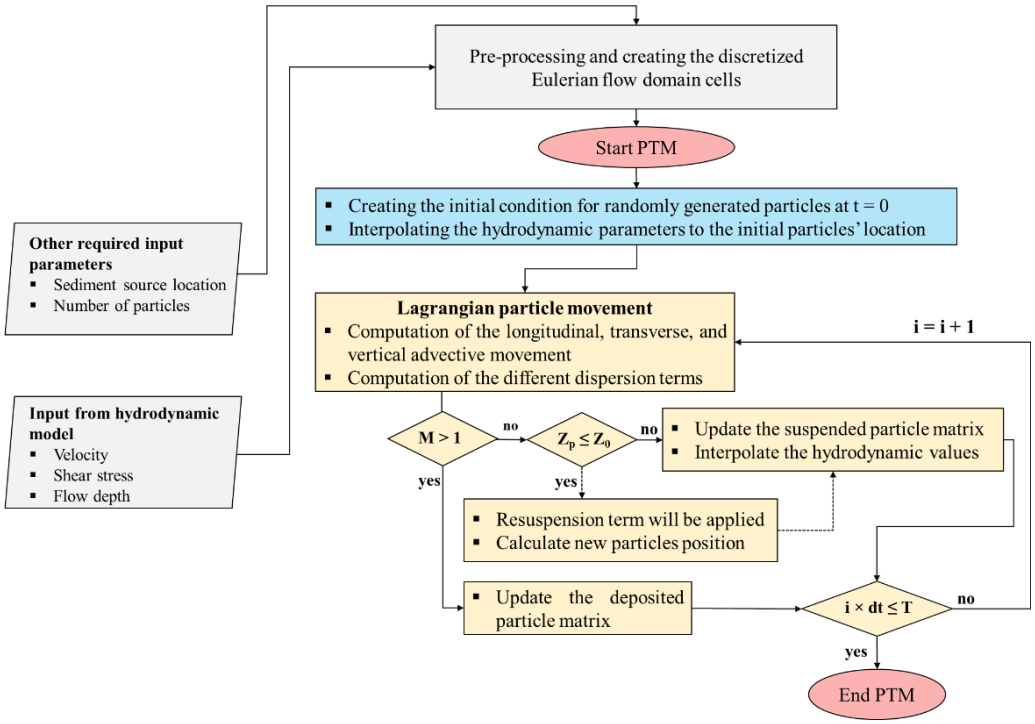


**Figure 2.1** Structure and input parameters of particle tracking sediment transport model

The performance of the particle tracking-based sediment transport model was investigated using available laboratory data and analytical solution of the advection-dispersion equation. The governing equations, interpolation techniques, and flow discretization process are discussed in the following section.

### 2.1.1 Particle Tracking Model

The Lagrangian approach considers the mass transport of particles in open channels, based on their specific physical features; therefore, there is no need for a direct solution of the advection-dispersion equation to track sediment movement in the flow domain. Each sediment particle can move in three directions simultaneously, and the movement of each is computed at each computational time step. Therefore, three separate mass transport equations considering the longitudinal, transverse, and vertical movement address the particles' potential movement path for each computational time step; however, the particles' transport equations neglect the vertical advection term. Figure 2.2 shows the forces acting on a suspended sediment particle, i.e., drag force ($F_D$), gravity force ($F_G$), and lift force ($F_L$), and the directions that a single particle can move in the discretized flow domain. As can be seen, the displacement caused by advection and dispersion in x, y, and z directions is shown with $\Delta x_t$, $\Delta y_t$, and $\Delta z_t$ vectors, respectively, in which subscript $t$ represents the computational time step. Advection and dispersion, as the fundamental basis of particle transport in each direction, are discussed in the following.

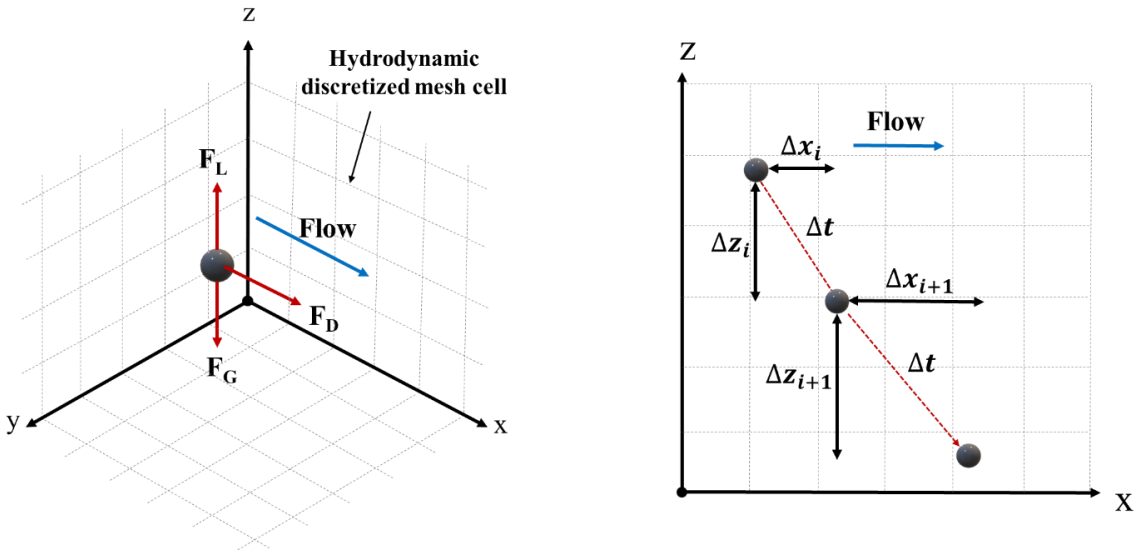


(a) (b)

**Figure 2.2** Schematic view of a) forces acting on a suspended sediment particle, and b) a hypothetical single sediment particle pathway in the flow column in x-z direction

*2.1.1.1 Advection-Dispersion Equation*

The advection-dispersion equation describes the transfer of a physical quantity through advection and dispersion motion. Equation 2.1 shows the advection-dispersion equation in a three-dimensional space (Van Rijn, 1993).

$$\frac{\partial c}{\partial t} + \frac{\partial (uc)}{\partial x} + \frac{\partial (vc)}{\partial y} + \frac{\partial (wc)}{\partial y} - \frac{\partial (w_s c)}{\partial z} - \frac{\partial}{\partial x}\left(D_x \frac{\partial c}{\partial x}\right) - \frac{\partial}{\partial y}\left(D_y \frac{\partial c}{\partial y}\right) - \frac{\partial}{\partial z}\left(D_z \frac{\partial c}{\partial z}\right) = 0 \qquad (2.1)$$

where $c$ is sediment concentration; $u$, $v$, $w$ are flow velocity in $x$, $y$, and $z$ directions; $D_x$, $D_y$, and $D_z$ are dispersion coefficients in the longitudinal, transverse, and vertical directions, respectively; $w_s$ is particle settling velocity; and $t$ is simulation time. The sediment dispersion reflects the amount of particle motion caused by turbulence and particle-particle interactions. Analytical, semi-analytical, and numerical methods are used to solve the advection-dispersion equation by considering initial and boundary conditions; however, the analytical solution of such an equation is very complicated. Therefore, numerical models are used to solve the advection-dispersion equation. In the present study, the two-dimensional flow domain was coupled with the Lagrangian PTM, and the vertical velocity component was neglected in the computation ($w = 0$).

In the Lagrangian particle tracking model, instead of solving Equation 2.1 directly, the displacement of sediment particles is modeled using discrete advection and dispersion to calculate the particles' location for the next computational time step. Equation 2.2 shows the sediment particle Lagrangian transport equation in the streamwise direction.

$$X_{t+1} = X_t + \Delta X_a + \Delta X_d \quad (2.2)$$

where $X_{t+1}$ refers to the location of a particle in a streamwise direction after one computational time step ($t$+1), $X_t$ is the current location of the particle, $\Delta X_a$ is the streamwise displacement of the particle due to advection term, and $\Delta X_d$ refers to the streamwise displacement of the particle caused by the dispersion term. It should be noted that similar transport equations are used to model particle movements in transverse and vertical directions.

According to Equation 2.2, the total displacement of a single particle depends on a linear combination of movement caused by advection and dispersion for a specific period. A random seed generator is used to produce spatially random particles at the sediment source for instantaneous and continuous sediment source conditions, and transport equations are applied to each cell of the discretized flow domain. Discretization of the flow domain depends on the spatial resolution of the data imported from the hydrodynamic model. After the flow domain discretization, the particle's new location is calculated using Equation 2.2. Therefore, the hydrodynamic parameters should be interpolated at the particle's location for the simulation time.

Velocity, shear stress, and flow depth are the main hydrodynamic characteristics that should be interpolated to where the particles end up for each computational time step. Pollock (1998), Goode (1990), Schafer-Perini and Wilson (1991), and Lane and Prandle (2006) used a simplified approach to show the accuracy of linear interpolation in sediment transport modeling. In the present study, hydrodynamic parameters are interpolated using the linear approach proposed by LaBolle and Fogg (1996).

*2.1.1.2 Advection Displacement*

The advection displacement of sediment particles depends on the average interpolated velocity in the longitudinal and transverse directions, fall velocity of particles, simulation time, and the distribution of the logarithmic velocity in the vertical direction. Table 2.1 shows the equations that were used to calculate the advection displacement of particles in the PTM. The average displacement caused by the advection term was computed using Equation 2.3, which expresses the mean drift motion and addresses the movement of a single particle in the streamwise direction ($x$-direction). Equation 2.4 by Van Rijn (1993) was used to estimate the logarithmic velocity distribution in the vertical direction; the zero-velocity level ($z_0$) was computed using the conditional approach indicated in Equation 2.5 (Van Rijn, 1993). Similarly, the transverse advection displacement was estimated using the dominant transverse velocity component on the particle's location. As mentioned, the PTM uses 2D flow velocity components as the advection velocity in longitudinal and transverse directions, and the vertical displacement of the particle is due to the gravitational forces acting on the sediment particles. Therefore, the vertical advection velocity of the particles was computed using the settling velocity ($w_s$) proposed by Van Rijn (1993) (Equation 2.6).

**Table 2.1** Advection Displacement Equations Used in the PTM

| Description | Equation | Equation No. |
|---|---|---|
| Longitudinal advection displacement | $\Delta L_{a-x} = u(t, x_t) \times \Delta t$ | (2.3) |
| Depth-averaged velocity logarithmic distribution | $u(z) = \left[\frac{\bar{u}}{\frac{z_0}{h} + ln\left(\frac{h}{z_0}\right) - 1}\right] ln\left(\frac{z}{z_0}\right)$ | 2.4) |
| Zero-velocity level | $z_0 = \begin{cases} 0.11\frac{\nu}{u_*} & \beta \leq 5 \\ 0.033\, k_s & \beta \geq 70 \\ 0.11\frac{\nu}{u_*} + 0.033\, k_s & 5 < \beta < 70 \end{cases}$ | 2.5) |
| Sediment particles settling velocity | $w_s = \begin{cases} \frac{(S-1)gd^2}{18\nu} & 1 < d \leq 100\ \mu m \\ \frac{10\nu}{d}\left[\left(1 + \frac{(S-1)gd^3}{100\nu^2}\right)^{\frac{1}{2}} - 1\right] & 100 < d \leq 1000\ \mu m \\ 1.1[(S-1)gd]^{\frac{1}{2}} & d \geq 100\ \mu m \end{cases}$ | 2.6) |

In the equations listed in Table 2.1, $u(t, x_t)$ is the average interpolated velocity of the particle in the streamwise direction at time *t*, $\Delta L_{a-x}$ is the particle movement distance due to the advection term, $\Delta t$ is the computational time step, *Z* is the vertical position of the particle in the water column, *h* is the average flow depth, $\bar{u}$ represents the mean streamwise velocity, $\nu$ is the kinematic viscosity of water, $k_s$ is bed roughness height, $u*$ is shear velocity, $\beta$ is boundary Reynolds number ($= \frac{u_* k_s}{\nu}$), $w_s$ is particle fall velocity, *S* is ratio of particle density to fluid density, and *d* is the particle diameter.

In addition to the advection and settling displacement effect on the particle movement, the dispersion coefficient significantly affects the accuracy of the PTM. There are several empirical equations that can be used for estimating the dispersion term, but not the advection. Widely used dispersion coefficient equations are discussed in the following section.

*2.1.1.3 Dispersion Displacement*

Various experimental and field studies have reported different values for three-dimensional dispersion coefficients ($D_x$, $D_y$, $D_z$). Table 2.2 shows the dispersion coefficient equations used to generate turbulent fluctuation effects on sediment transport. In the present study, the performance of three widely used longitudinal dispersion equations was investigated (Equations 2.7 to 2.9), and the PTM used empirical equations proposed by Gualtieri and Mucherino (2008) to estimate the transverse dispersion coefficient (Equations 2.10).

Tsai et al. (2020) used a theoretical approach developed by Absi et al. (2011) to estimate the vertical dispersion in their PTM. They showed less accuracy of the Rouse model, i.e., $D_z = \kappa u_* z\left(1 - \frac{z}{H}\right)$, in estimating the vertical dispersion coefficient because this model does not accurately consider the vertical dispersion coefficient values in layers close to the water surface. In the present study, a conditional vertical dispersion coefficient equation proposed by Van Rijn (1987) was used to compute the vertical dispersion coefficient, even in the top layers adjacent to the water surface (Equations 2.11).

**Table 2.2** Empirical Dispersion Equations Used in the Development of PTM

| Dispersion term | Equation | Reference | Equation No. |
|---|---|---|---|
| Longitudinal | $D_x = 5.93\, Hu_*$ | Elder (1959) | 2.7) |
| Longitudinal | $D_x = 10.612\, Hu\left(\frac{u}{u_*}\right)$ | Kashefipour and Falconer (2002) | 2.8) |
| Longitudinal | $D_x = 2\,(Hu_*)\left(\frac{u}{u_*}\right)^{1.25}\left(\frac{B}{H}\right)^{0.96}$ | Sahay and Dutta (2009) | 2.9) |
| Transverse | $D_y = 0.166\, Hu_*$ | Gualtieri and Mucherino (2008) | 2.10) |
| Vertical | $D_z = \begin{cases} D_{zm} - D_{zm}\left(1 - \frac{2z}{H}\right)^2 & \frac{z}{H} < 0.5 \\ D_{zm} & \frac{z}{H} \geq 0.5 \end{cases}$ | Van Rijn (1987) | 2.11) |

In the equations listed in Table 2.2, water depth ($H$), depth-average velocity ($u$), shear velocity ($u_*$), and stream width ($B$) are the effective parameters in dispersion. Equation 2.11 uses the maximum vertical dispersion coefficient ($D_{zm} = \frac{\kappa u_* H}{4}$, $\kappa$ refers to the von Kármán constant $\kappa$ = 0.4) and relative particle depth in the water column ($z/H$) to calculate the vertical dispersion coefficient. Several methods consider the stochastic motion of particles resulting from dispersion; the random walk method is used in this study.

*2.1.1.4 Random Walk Method*

Radom walk, a stochastic or random process, generates random steps in computational space. The method has been employed in several studies for computing the random motion of sediment particles in turbulent flows (Lane and Prandle 2006; Salamon et al., 2006; Taghvayi 2013; Shi and Yu 2015). Equation 2.12 represents the movement distance associated with the stochastic displacement parameter ($\sigma$).

$$\Delta L_d = N(0,1) \times \sigma \tag{2.12}$$

where $N(0,1)$ is a random number with normal distribution, a mean of 0, and a standard deviation of 1. $\sigma$ refers to the stochastic displacement computed from Equation 2.13.

$$\sigma = \sqrt{2D\Delta t} \tag{2.13}$$

where $D$ represents the general sediment dispersion coefficient, which is calculated in $x$, $y$, and $z$ directions based on the empirical dispersion equations mentioned in Table 2.2.

*2.1.1.5 Particle Deposition Process*

According to the Shields diagram, if the critical shear stress ($\tau_{cr}$) of a particle is greater than the applied shear stress ($\tau_{app}$), the particle deposits; otherwise, it stays in suspension. Macdonald et al. (2006) used the Shields diagram to determine the initiation of motion of bed material in a

stochastic sediment transport model. Equation 2.14 describes the dimensionless mobility number (*M*), indicating the deposition or resuspension of sediment particles.

$$M = \frac{\tau_{cr}}{\tau_{app}} \tag{2.14}$$

*M* >1 indicates that the particle will deposit on the streambed. If M < 1, a vertical resuspension movement using pure dispersion will be applied to the particles' centroid elevation to keep them in suspension mode. In the present model, the mobility number of each particle was calculated once the particle reached the zero velocity level. Figure 2.3 depicts the schematics of the potential movement path of a single particle from the suspension mode towards either the deposition or resuspension mode.

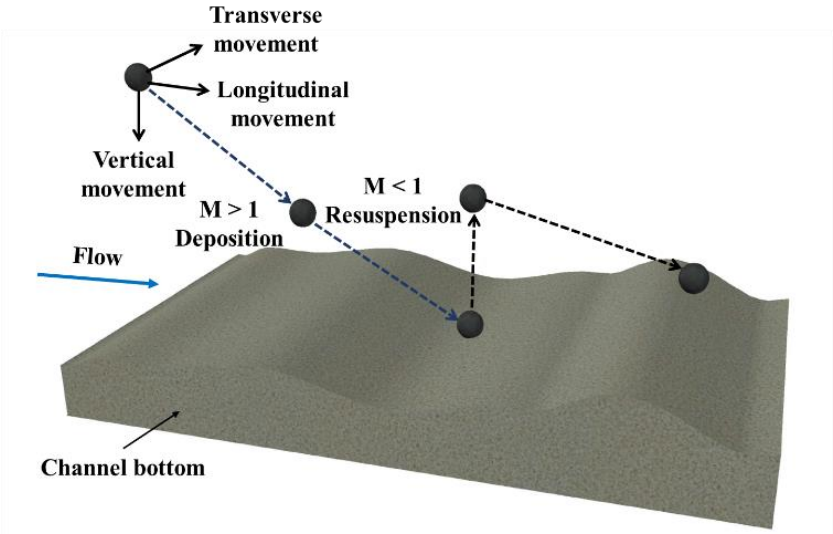


**Figure 2.3** Illustration of sediment deposition and resuspension processes in the water column

The model was designed for a specified range of sediment particle sizes; the sediment gradation and corresponding critical shear stress that were incorporated were obtained from a study by Berenbrock and Tranmer (2008). The critical shear stress of the desired sediment gradation was interpolated based on the third-degree polynomial interpolation approach known as the cubic interpolation technique.

### 2.1.2 Calculation of Sediment Concentration

Suspended sediment concentration was used to validate the model in the present study. To generate the suspended sediment concentration distribution, the nearest mesh grid was selected for each individual sediment particle in the flow domain, then the accumulated sediment particles on each grid generated the sediment concentration values. Figure 2.4 illustrates the preprocess of generating the suspended sediment concentration distribution in the flow domain by the PTM.

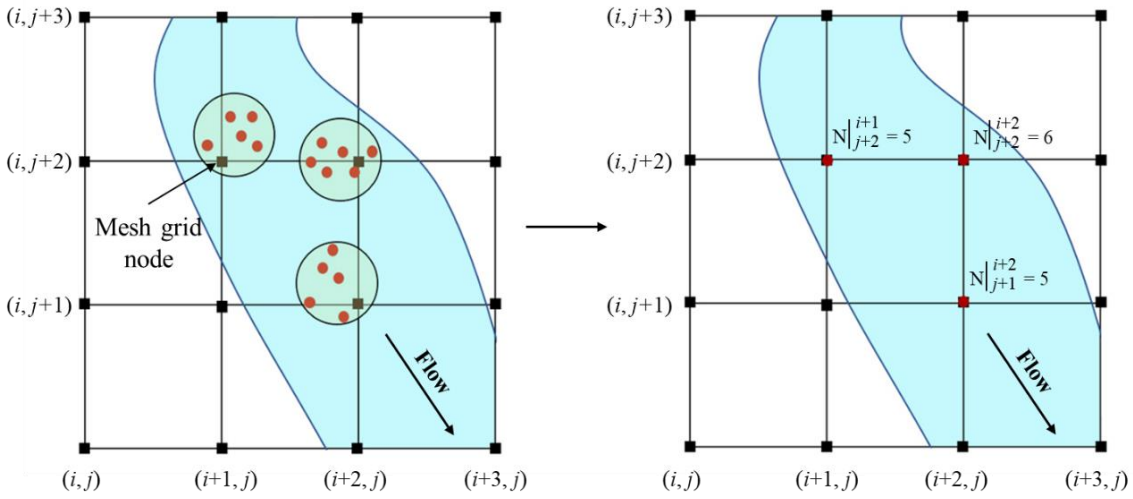


(a) (b)

**Figure 2.4** A schematic plan view of: a) mesh domain, suspended particles, and particle group closest to each node, and b) value of accumulated sediment particles generated at each node by the PTM

Equation 2.15 was used to calculate suspended sediment concentration (SSC) at each grid.

$$C = \frac{V_p \, \rho_s N_p(x,y,t)}{\Delta x \ \Delta y \ \Delta z} \tag{2.15}$$

where $C$ is the sediment concentration at each cubic mesh cell ($kg/m^3$), $V_p$ is the total sediment particle volume within the corresponding mesh cell ($m^3$), and $\rho_s$ is sediment density ($kg/m^3$). $\Delta x, \Delta y,$ and $\Delta z$ are the dimensions of the mesh cell in horizontal, transverse, and vertical directions,

respectively. $N_p(x, y, t)$ represents the number of particles assigned to the mesh grid node with coordination of (x, y) at time *t*.

## MODEL VALIDATION

The performance of the Lagrangian stochastic sediment transport model was assessed using both experimental data and analytical solutions of the advection-dispersion equation.

### 2.1.3 Validation of PTM Using Laboratory Data

Coleman (1986) investigated the effect of variations in the suspended sediment concentration on the characteristics of the velocity profile. Three sediment classes with diameters of 0.105 mm, 0.21 mm, and 0.42 mm were used in the experiments to explore a wide range of particles, from very fine sand to medium sand. The properties of each sediment class are shown in Table 2.3. The experiments were conducted in a 0.356 m wide and 15 m long rectangular flume. The discharge was fixed at 0.064 $m^3/s$, the average velocity was 1.04 m/s, the shear velocity was 0.041 m/s, the shear stress was 1.68 $N/m^2$, and the average water depth was 0.169 m. The flume and hydraulic conditions in the Coleman's 1986 experiments were simulated. Three sediment classes, each with a total mass of 0.91 kg, were introduced at the water's surface, upstream of the flume, at the source of the sediment (Table 2.3).

**Table 2.3** Properties of Sediment Classes Used for Model Validation

| Class no. | Sediment type | Diameter (mm) | Total mass (kg) |
|---|---|---|---|
| 1 | Very fine sand | 0.105 | 0.91 |
| 2 | Fine sand | 0.21 | 0.91 |
| 3 | Medium sand | 0.42 | 0.91 |

Each sediment class was applied to the sediment source located upstream of the flume. The sediment concentrations derived from the PTM 12 m downstream of the channel entrance were compared with Coleman's 1986 laboratory data to assess the accuracy of each dispersion model in generating concentration values.

*2.1.3.1 Sediments' Particle Relaxation Time*

The particle's relaxation time indicates the lag time for a particle to respond to changes in flow velocity, especially in extreme events. The inertia effect is the main factor in estimating the relaxation time for different sizes of sediment. Generally, if the size of a sediment particle is greater than that of the fluid particles, a lag in time should be considered in the sediment transport modeling. For high relaxation time (especially for large particles), particles follow the streamlines with a velocity lag. Some studies propose using theoretical and experimental analysis to calculate the velocity lag caused by inertia forces (Shamskhany et al., 2021; Cheng 2004); however, in most sediment transport models, the sediment particle velocity is assumed to be the same as the flow velocity (Oh, 2011).

In the present study, the Stokes number (*Stk*), a measure of the particle's inertia, was used to investigate the behavior of the suspended particles in the flow domain and evaluate the response time of the particles that could generate a lag between the flow velocity and the particle velocity. The Stokes number is the ratio of characteristic relaxation time ($t_p$) of the particle to the characteristic flow time ($t_f$). The relaxation time was estimated for all the sediment classes listed in Table 2.3 using Equation 2.16.

$$t_p = \frac{\rho_p {d_p}^2}{18\mu} \tag{2.16}$$

where $\rho_p$ is particle's density ($kg/m^3$), $d_p$ refers to the particle diameter (m), and $\mu$ is the dynamic viscosity of water (kg/s.m). Equation 2.17 was used to calculate the Stokes number for sediment classes from 1 to 3 (Table 2.3).

$$Stk = t_p/t_f \tag{2.17}$$

In this equation $t_f = H/U$, where $U$ is the average velocity in the flume (m/s), and $H$ refers to the characteristic length of the flow (m).

Generally, a Stokes number less than one ($Stk$ <1) implies that a particle adopts the fluid velocity immediately. If the Stokes number is less than 0.1 ($Stk$ < 0.1), the particle follows the flow velocity with an average error of less than 1% (Teropea et al., 2007). The variations in the relaxation time and Stokes numbers with particle diameters are shown in Figure 2.5. The values of these parameters for different sediment classes in the present study are also indicated in the figure.

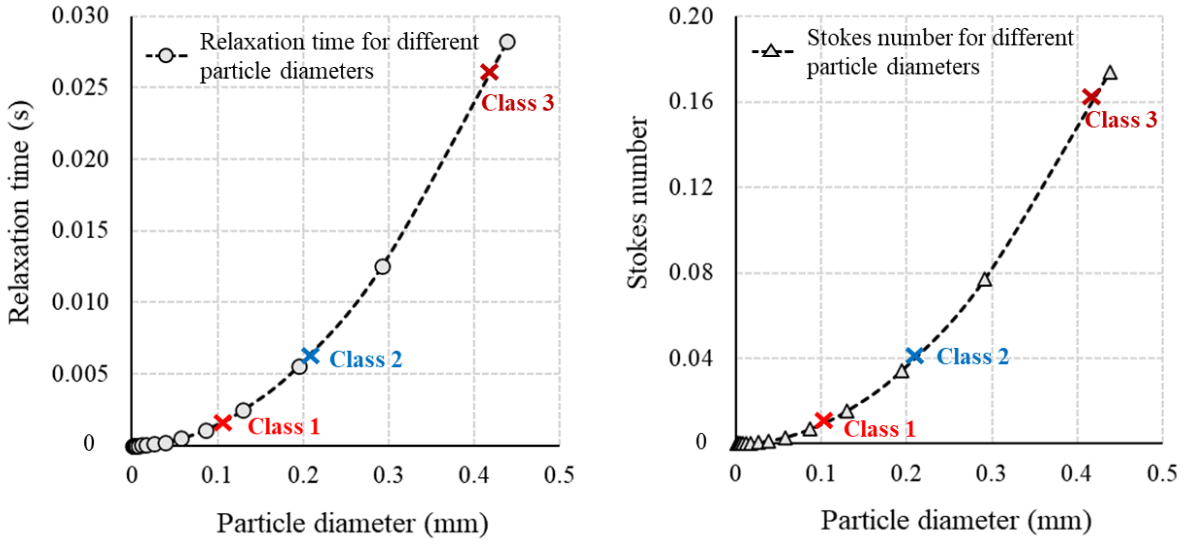


**Figure 2.5** a) Relaxation time, and b) Stokes number variations for particle's diameter in the range of 0 to 0.43 mm

As shown in Figure 2.5a, the relaxation time for Class 3 sediment with a diameter of 0.42 mm is about $t_p$ = 0.26 s, and for Classes 1 and 2, the relaxation times are less than 0.01 s. The small relaxation times for all three sediment classes demonstrate the negligible effects of particle size and density on the particles' response time. A Stokes number of less than one ($Stk$ < 1) for all sediment classes confirms the insignificant effect of inertia on the particles' movement (Figure 2.5b). Therefore, it can be assumed that the sediments of all three classes followed the flow velocity with acceptable accuracy. The linearly interpolated velocity components were used as the dominant advection velocity component for each sediment particle.

*2.1.3.2 Evaluation of Longitudinal Dispersion Equations*

A dimensionless concentration ratio ($C/C_{max}$) was used to compare the distribution of the SSC through the water column, using the relative depth ($z/H$) at the measuring station ($x$ = 12 m). Equations 2.7 to 2.9 were used to calculate the longitudinal dispersion of each sediment class listed in Table 2.3.

In the present study, the Taylor diagram (Taylor, 2001) was used to investigate the performance of the PTM, using the longitudinal dispersion models listed in Table 2.2 that summarize multiple aspects of the prediction model performance. Equations 2.18 to 2.20 indicate the statistical measures, including correlation coefficient (R), standard deviation (STD), and root mean square deviation (RMSD), that were used to generate the Taylor diagram. In addition to the Taylor diagram, the percentage errors (PE) between the observed and estimated concentration ratios for different sediment classes were calculated using Equation 2.21.

$$R = \frac{Cov(\hat{x}_i, x_i)}{STD_{\hat{x}_i} STD_{x_i}} \tag{2.18}$$

$$STD = \sqrt{\frac{\sum(x_i - \bar{x})}{N}} \tag{2.19}$$

$$RMSD = \sqrt{\sum_{i=1}^{N} \frac{(\hat{x}_i - x_i)^2}{N}} \tag{2.20}$$

$$PE = \left( \frac{|\hat{x}_i - x_i|}{x_i} \right) \times 100 \tag{2.21}$$

In the above equations, $\hat{x}_i$ is the predicted value, $x_i$ represents the observed value, $N$ is the total number of variables, and $\bar{x}$ is the average value of the entire dataset.

Figure 2.6 illustrates the distribution of the observed and estimated concentration ratios for Class 1 sediment. As can be seen, the estimated $C/C_{max}$ distribution follows an increasing trend from the water surface to the bottom of the water column for all three dispersion models. The concentration ratios calculated based on Equations 2.7 and 2.8 underestimated $C/C_{max}$ from $z/H$ = 0.65 to $z/H$ = 0.12; however, the results based on Equation 2.8 showed more deviation from the observed $C/C_{max}$ distribution. The concentration ratio from Equation 2.9 shows an overestimation in the mid-depth zone ($z/H$ = 0.60 – 0.47) near the channel bed ($z/H$ = 0.16 – 0.05).

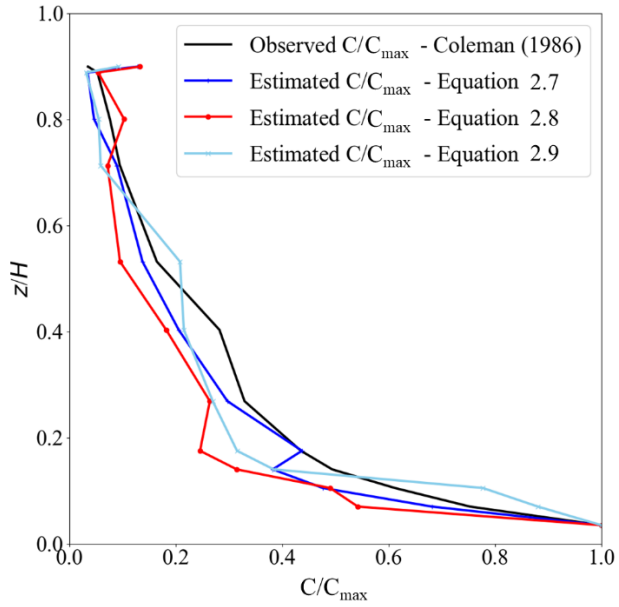


**Figure 2.6** Observed vs. estimated concentration ratios ($C/C_{max}$) for Class 1 sediment in PTMs

Figure 2.7 shows the Taylor diagram of the PTM results for Class 1 sediment and illustrates that the correlation coefficients of the three models were between contours 0.95 and 0.99, indicating high performance of all three dispersion equations in estimating the distribution of sediment concentration. Equation 2.8 shows the lowest performance, with a correlation coefficient of R = 0.95; estimations based on Equation 2.7 have the highest accuracy (R = 0.98). The maximum deviation of the estimated $C/C_{max}$ from the observed values occurred at $z/H$ = 0.165 for Equations 2.8 and 2.9, with PE = 39% and 25%, respectively.

The root mean square deviation (RMSD) contours in Figure 2.7 demonstrate the superiority of the PTM, based on Equation 2.7, in estimating $C/C_{max}$ with RMSD = 0.06. Furthermore, the standard deviation (STD) of the PTM, using Equation 2.9, shows that this model is less reliable than the results from Equations 2.7 and 2.8. The STDs for the results of these equations are located between contours 0.2 and 0.4.

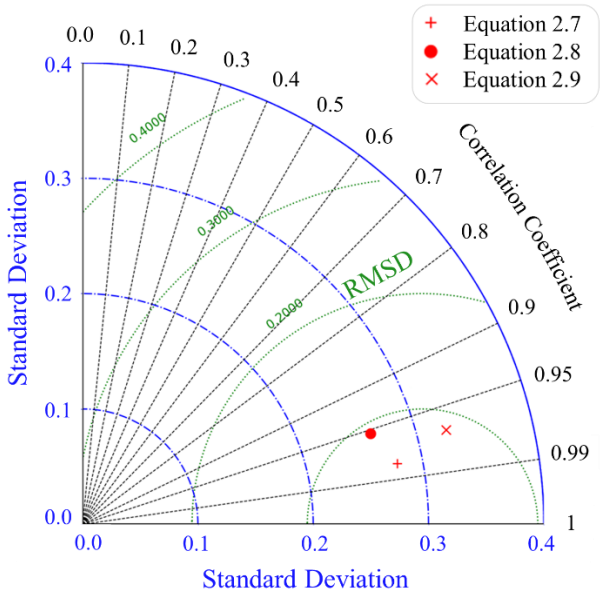


**Figure 2.7** Taylor diagram of the estimated concentration ratios for Class 1 sediment

Figure 2.8 demonstrates the distribution of observed and estimated concentration ratios for Class 2 sediment. The maximum deviation of the estimated $C/C_{max}$ from the observed values occurred at

$z/H$ = 0.168, with PE = 38% for all three PTM models. Equation 2.7 overestimates $C/C_{max}$ for $z/H$ > 0.42 and shows less deviation from the observed values than the other two models.

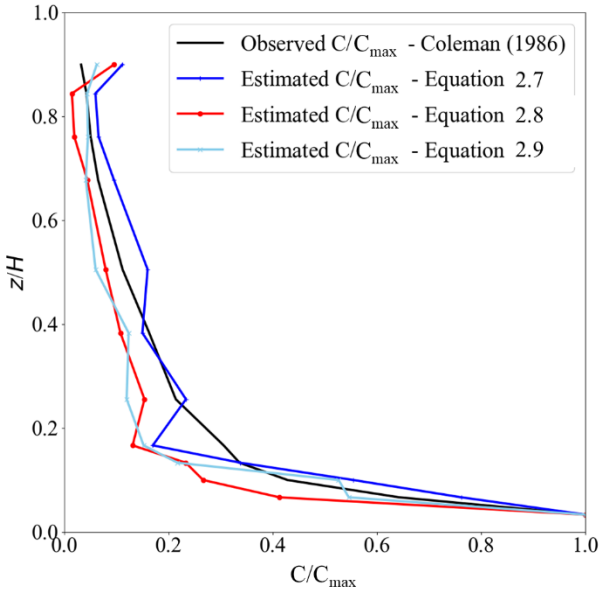


**Figure 2.8** Observed vs. estimated concentration ratios ($C/C_{max}$) for Class 2 sediment in PTMs

The Taylor diagram of the PTM models for Class 2 sediment shown in Figure 2.9 depicts a better performance of Equation 2.7 in estimating $C/C_{max}$ than Equations 2.8 and 2.9. The performance measures of Equation 2.7 are R = 0.97, RMSD = 0.07 and STD = 0.289.

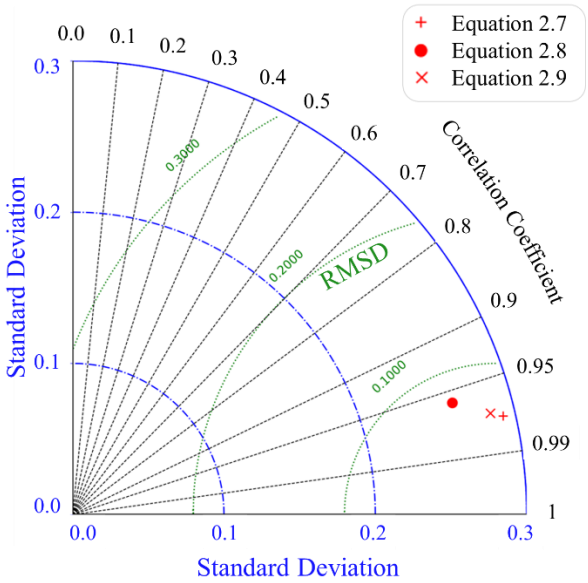


**Figure 2.9** Taylor diagram of estimated concentration ratios for Class 2 sediment

Figure 2.10 shows the distribution of the observed and estimated concentration ratios for Class 3 sediment. A comparison of Figure 2.10 with Figures 2.8 and 2.6 indicates that the PTM can estimate the concentration of coarser sand materials with a lower deviation from the laboratory values than finer sand. According to the Taylor diagram for Class 3 sediment shown in Figure 2.11, the correlation coefficient of the PTM, using Equation 2.7, is 0.96. The performance of Equations 2.8 and 2.9 are similar, with a correlation coefficient of 0.96 and 0.95, respectively. The results from Equation 2.9 are more widely spread around the mean of the concentration ratios, representing a higher standard deviation (0.29) than those generated by Equations 2.7 (0.26) and 2.8 (0.27). The maximum deviation of the estimated $C/C_{max}$ from the observed values occurred at $z/H$ = 0.136, with PE = 17% for all three PTM models.

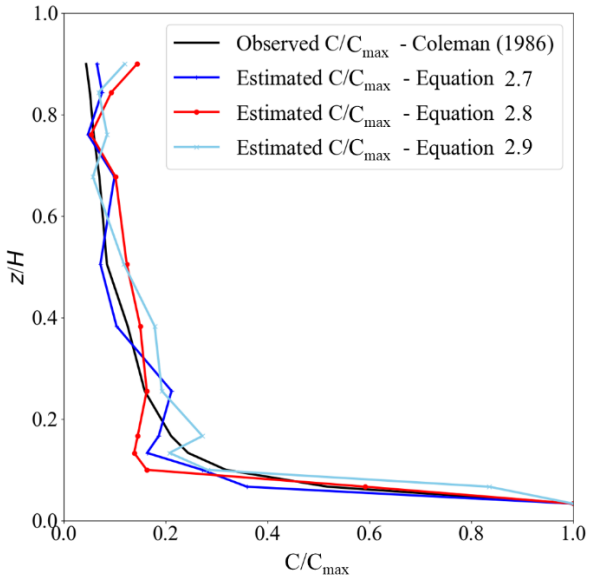


**Figure 2.10** Observed vs. estimated concentration ratios ($C/C_{max}$) for Class 3 sediment in PTMs

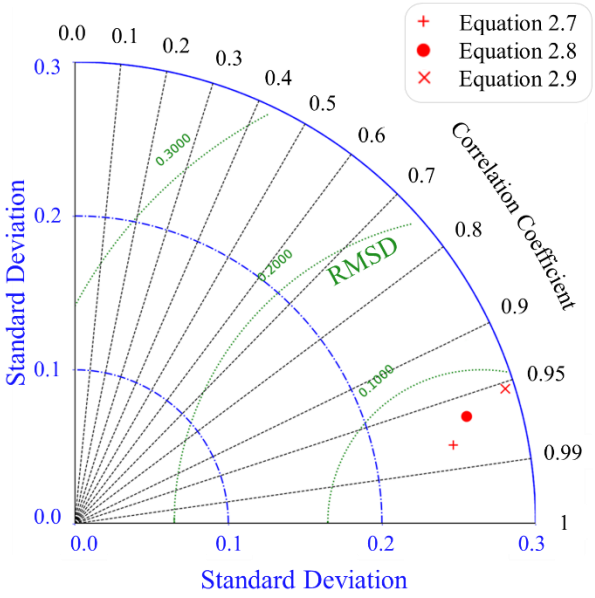


**Figure 2.11** Taylor diagram of the estimated concentration ratios for Class 3 sediment

A comparison between the PTM results with different dispersion approaches shows that the stochastic sediment transport model produced a more reliable sediment concentration, using Elder's (1959) dispersion equation (Equation 2.7). This equation was, therefore, selected as the longitudinal dispersion equation for the model.

### 2.1.4 Validation of PTM Using Analytical Solution

The advection-diffusion relationship (Equation 2.1) may be solved using analytical solutions with some assumptions. The instantaneous pollutant concentration in a straight rectangular channel with a uniform flow condition can be calculated using Equation 2.22 (Park et al., 2020; Park and Seo 2018).

$$C(x,y,t) = \frac{M_t/h}{4\pi t\sqrt{D_x D_y}}\left[\exp\left\{-\frac{(x-x_0-\bar{u}t)^2}{4D_x t} - \frac{(y-y_0)^2}{4D_y t}\right\}\right] \quad (2.22)$$

where $M_t$ is the total mass of pollutant (kg), ($x_0$, $y_0$) is the coordinate of the sediment point source in a 2D system, and $\bar{u}$ is the depth-averaged velocity (m/s). Equations 2.7 and 2.10 are used to estimate $D_x$ and $D_y$, respectively.

A 4 m-wide, 100 m-long straight rectangular channel was used to assess the PTM's performance, using the analytical solution (Figure 2.12). The depth-averaged velocity was assumed 1 m/s and the water depth = 0.3 m. A total of 1500 particles were injected instantaneously into the flow at the sediment source ($x_0$ = 0 m, $y_0$ = 2 m). The concentration of the suspended sediments was calculated by counting the number of particles on each computational node, using Equation 2.15 with $\Delta z = H(x, y, t)$, in which $H$ represents the water depth.

Figure 2.12a shows the temporal 3D visualization of solute mixing at $t$ = 10, 30, 50, and 80 seconds from the time that the sediment was injected.

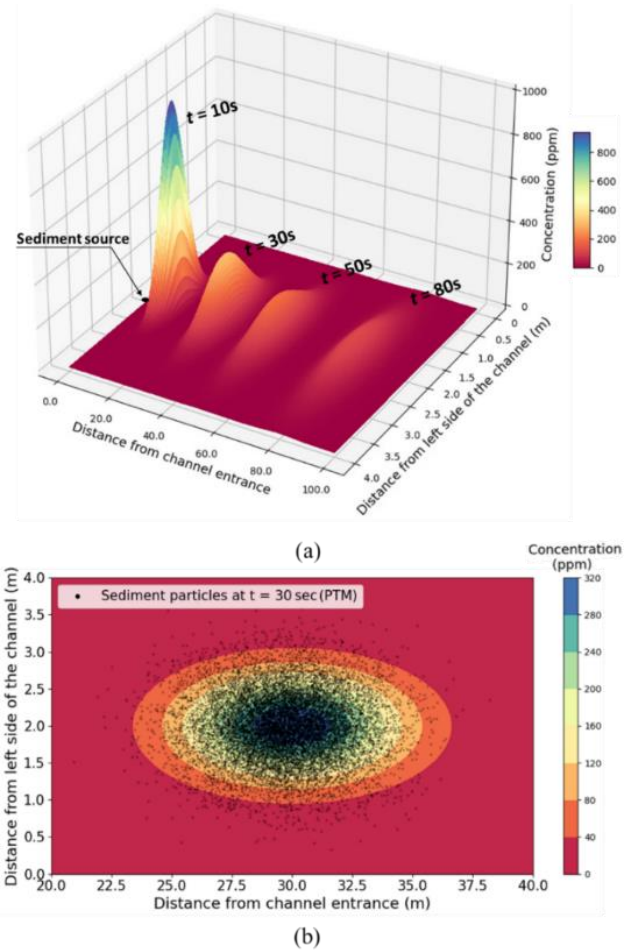


**Figure 2.12** Comparison between the analytical solution and the PTM results: a) Distribution of sediment concentration using the analytical solution at different simulation times (3D view), b) Concentration distribution contours using analytical solution (background color map contours), and distribution of sediment particles from PTM (black dots) at $t$ = 30 seconds (plan view)

Figure 2.12 shows that the maximum concentration at the centroid of the sediment plumes spread in the longitudinal and transverse directions due to the dispersion effect. Computational time steps of 30 and 50 seconds were selected to compare sediment concentrations from the solute mixing model and the PTM in the longitudinal and transverse directions. Figure 2.12b shows the particle distribution resulting from the PTM with the corresponding analytical concentration contours at $t$ = 30 seconds. Both models showed a high density of sediment particles at the centroid of the plume.

The longitudinal and transverse concentration distributions from both methods at $t$ = 30 and 50 seconds were used to assess the accuracy of the PTM in estimating sediment concentration in a straight channel. As presented in Figure 2.13a, there was an acceptable agreement between the PTM results and the analytical solution in estimating longitudinal concentration at both time steps; however, a small shift was detectable in the PTM results at $t$ = 30 seconds. At $t$ = 50 seconds, the PTM result showed a larger shift of the maximum concentration than at $t$ = 30 seconds.

The concentration distribution in the transverse direction is shown in Figure 2.13b. Unlike the longitudinal concentration distribution, no shift in the maximum concentration was observed in the transverse direction. The PTM results at $t$ = 50 seconds showed more deviation from the analytical solution in the areas outside the central part of the channel ($x$ < 1 m and $x$ > 3 m) than the results at $t$ = 30 seconds.

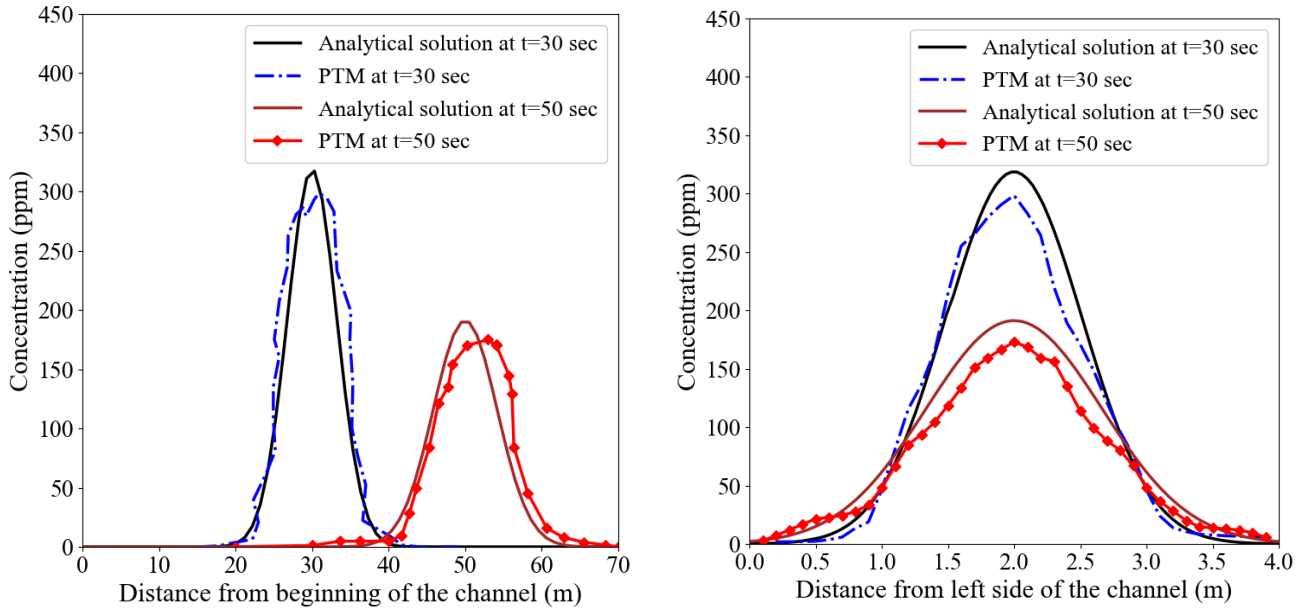


(a) (b)

**Figure 2.13** Comparison between concentration distributions estimated using the analytical solution and the PTM: (a) Longitudinal concentration, and (b) Transverse concentration

The maximum concentrations for the two time steps are summarized in Table 2.4. The PTM underestimated the maximum concentration with an error of 6.3% and 9.4% at $t$ = 30 and $t$ = 50 seconds, respectively.

**Table 2.4** Maximum Concentration (in ppm) Estimated by the PTM and Analytical Solution at Different Simulation Times

| **Model** | **t = 30 s** | **t = 50 s** |
|---|---|---|
| PTM | 298 | 173 |
| Analytical Solution | 318 | 191 |
| Error (%) | 6.3 | 9.4 |

### 2.1.5 Comparison of PTM with Previous Models

#### *2.1.5.1 Two-particle Stochastic Diffusion PTM by Tsai et al. (2020)*

Tsai et al. (2020) developed a two-particle stochastic diffusion particle tracking model (SD-PTM) that uses the distance between particles to address the interparticle correlation in a two-dimensional

flow domain and utilized the Class 1 sediment data from Coleman's 1986 experiments to evaluate its performance. A comparison of the results of their model and the one developed in this study, using Elder's 1959 dispersion equation, is depicted in Figure 2.14 for Class 1 sediment.

According to Figure 2.14a, the two-particle SD-PTM showed less deviation from the observed concentration values for Class 1 sediment than the PTM model, especially for depth ratios less than 0.2. Also, the coefficient of determination of the Tsai et al. (2020) model is $R^2$ = 0.99, which is slightly higher than the coefficient of determination of the PTM model ($R^2$ = 0.97).

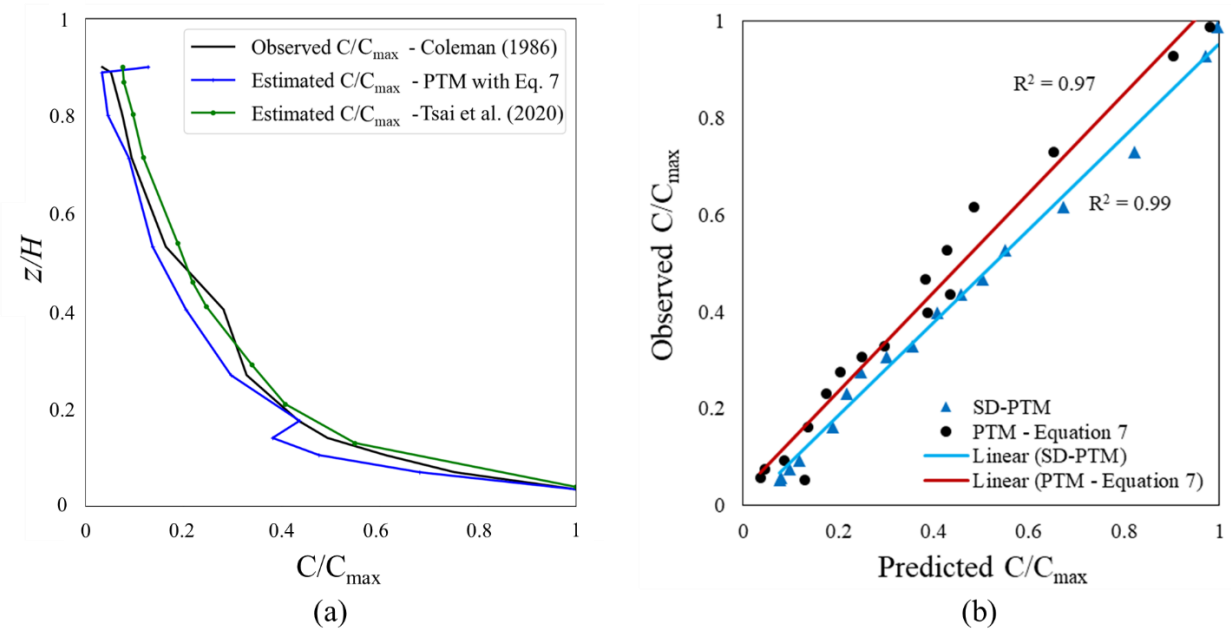


**Figure 2.14** a) Estimated sediment concentration ratios ($C/C_{max}$) at different depth ratios ($z/H$), and b) observed and predicted sediment concentrations using the PTM with Elder (1959) dispersion equation (Equation 2.7) vs. SD-PTM (Tsai et al., 2020) for Class 1 sediment

The two-particle SD-PTM overestimated the concentration ratios for $z/H < 0.44$ with a maximum percentage error of 12% at $z/H$ = 0.13. The PTM developed in this study underestimated the concentration ratios with a maximum percentage ratio of 21% at $z/H$ = 0.17 for the same range of depth ratios (i.e., $z/H < 0.44$). It should be noted that the PTM underestimated the concentrations for most depth ratios higher than 0.44 except for those in the top layers that could be affected by the sediment entrainment at the sediment source. The model developed by Tsai et al.

underestimated the concentration for $0.44 < z/H < 0.7$ and overestimated the concentration for $z/H > 0.7$; however, both models predicted the concentration ratios at different depths with an acceptable percentage of error.

*2.1.5.2 Stochastic Jump Diffusion PTM by Oh (2011)*

Oh (2011) developed a stochastic diffusion PTM (SJD-PTM) by adding a stochastic jump to the particles' transport equation and evaluated its performance using Class 2 sediment of the Coleman experiments conducted in 1986. Figure 2.15a shows the variations in the concentration at different depth ratios for Oh's PTM and the one developed for this study, using dispersion Equation 2.7 for the Class 2 sediment. The observed and predicted concentrations for both models illustrated in Figure 2.15b show a slight difference in predicting the sediment concentration values of Class 2 sediment: the coefficient of determination $R^2$ for Oh's PTM is 0.96 and for the PTM in this study is 0.95.

The PTM with dispersion (Equation 2.7) overestimated the concentration in most of the depth ratios except at $z/H = 0.17$; the SJD-PTM overestimated the concentrations in lower depth ratios from the bottom of the channel to $z/H = 0.28$ and underestimated the sediment concentrations for depth ratios larger than 0.38. Both models showed the highest accuracy for depth ratios between 0.3 to 0.36 with a PE of less than 5%.

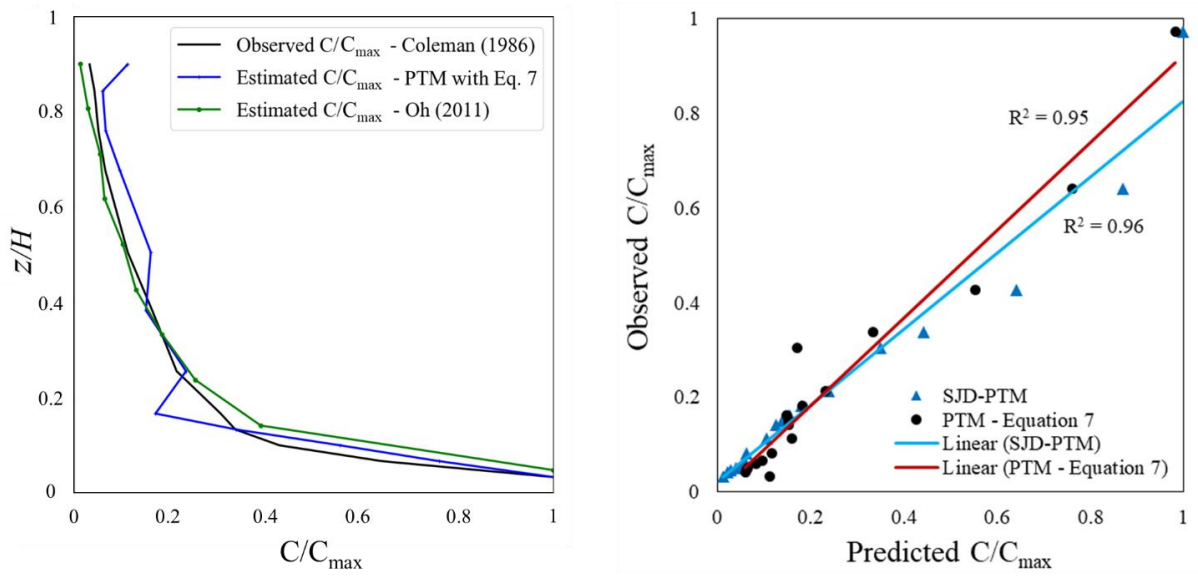


**Figure 2.15** a) Estimated concentration ratios ($C/C_{max}$) for different depth ratios ($z/H$), and b) observed and predicted sediment concentrations, using PTM with Elder (1959) dispersion equation (Equation 2.7) and SJD-PTM (Oh 2011) for Class 2 sediment

## CONCLUSION

A three-dimensional Lagrangian stochastic particle tracking model was developed to simulate sediment transport in open channels when coupled with any 2D hydrodynamic model able to generate the geospatial flow parameters of depth, velocity, and shear stress. The model simulates the movement of sediment particles in suspension, deposition, and resuspension. The performances of three longitudinal dispersion equations (Elder (1959), Kashefipour and Falconer (2002), and Sahay and Dutta (2009)) were examined with the aim of selecting one to be employed in the PTM. Unlike the majority of Lagrangian PTMs (McDonald 2006; Oh 2011), a conditional vertical dispersion coefficient equation was used as an alternative approach for defining the vertical dispersion coefficient. In previous studies, the Rouse model, a parabolic vertical dispersion formula, was used to address the dispersion effect on particles in the top layers of the water column, close to the surface of the water. The Rouse model estimates the dispersion coefficient as

approximately zero ($D_z \approx 0$) in the top layers, which might affect the suspended sediment concentration calculated by the PTM.

The dimensionless sediment concentration data ($C/C_{max}$) from Coleman's 1986 laboratory experiments were used to assess the performance of each equation in predicting the suspended sediment concentration for a variety of sediment gradations. In most of the Lagrangian PTMs (e.g., Lane and Prandle 2006; Tsai et al., 2020), fine particles are used to evaluate the performance of the models in simulating sediment transport; only a few studies use coarse particles to evaluate the PTMs (e.g., Shi et al. 2015). Therefore, the ability of the PTM to simulate sediment transport of different sizes (very fine sand, fine sand, medium sand) was considered in the present study. The Pearson correlation coefficient, standard deviation, and root mean square deviation parameters were plotted using the Taylor diagram for each dispersion equation to identify the best dispersion model to be utilized in the developed PTM. According to the result of the Taylor diagram and concentration distribution trends, Elder's equation distributed the suspended sediment concentration more accurately with a mean statistical value of R = 0.96, STD = 0.262, and RMSD = 0.06 for the three different sediment classes. Therefore, this equation was selected as the longitudinal dispersion coefficient for the PTM developed in this study. A comparison of the PTM-estimated $C/C_{max}$ with the Coleman's (1986) laboratory data showed less deviation from the observed values for coarser materials (medium sand) than for finer sediment.

In addition to the validation with laboratory data, the PTM results were compared to the analytical solution of the advection-dispersion model for a straight rectangular channel with an instantaneous sediment source. The longitudinal and transverse sediment concentrations from the analytical solution and the PTM showed an acceptable level of agreement, which confirms the ability of the PTM to predict the SSC variation in a straight rectangular channel. A comparison of the SSC from

the PTM and the analytical solution showed that the PTM estimated the maximum sediment concentration with 6.3% error and the analytical solution estimated the maximum sediment with 9.4% error for time steps of $t$ = 30 s and 50 seconds, respectively.

The ability of the PTM developed with Elder's (1959) longitudinal dispersion coefficient to predict suspended sediment concentrations in open channels was compared to the stochastic jump-diffusion PTM developed by Oh in 2011 and the two-particle stochastic diffusion PTM developed by Tsai et al., in 2020. Despite the fact that the model developed for this study is slightly less accurate than the other two PTMs with more complex displacement computations, its simplicity makes it an acceptable alternative PTM for modeling sediment transport in open channels.

Although the PTM showed an acceptable level of accuracy, some of the assumptions made in developing the model may limit its use in different environments. These limitations are described in the following, and recommendations are made for future research.

- The sediment particles were assumed to be spherical, and the interactions of the were not considered in the particle transport calculations.
- The lag velocity of the particle sizes used for modeling was negligible; however, the effect of inertia on the velocity of sediment particles for larger sediment sizes should be investigated to determine the appropriate criteria for addressing it.
- The proposed model fails to consider bedload transport and the geomorphologic evolution of the channel bed; therefore, it is suggested that a bedload transport model be coupled with the PTM developed for this study to provide a full range of sediment transport in open channels, including suspended and bedload transport.

This study showed that the PTM can accurately simulate sediment transport in open channels and can be used by hydro-environmental agencies and researchers to estimate changes in SSC, identify potential depositional areas, and provide best management practices to control and mitigate the possible impacts on water quality. Future research is needed to evaluate the performance of the model in simulating sediment transport in natural streams. Lastly, with recent developments in artificial intelligence approaches, the dispersion term in each flow direction could be modeled using soft computing techniques instead of the empirical equations used in the present study.

**Acknowledgment**

This research was made possible through funding from the Texas Department of Transportation (TxDOT) awarded to the co-author Habib Ahmari: Project Number 0-7023. The authors acknowledge the valuable comments offered by the editor and two anonymous reviewers in improving the technical contents of this paper.

## List of symbols

| Symbol | Description | Symbol | Description |
|---|---|---|---|
| $u$, $v$, $w$ | Flow velocity in $x$, $y$, $z$ directions | $z$ | Vertical elevation of the particle in the water column |
| H | Flow depth | $v_x$ | Interpolated velocity of the particle in the streamwise direction |
| $k_s$ | Bed roughness height | M | Mobility coefficient |
| $u_*$ | Shear velocity | $D_x$ | Longitudinal dispersion coefficient |
| $\beta$ | Boundary Reynolds number ($=\frac{u_* k_s}{\nu}$) | $D_y$ | Transverse dispersion coefficient |
| $z_0$ | Zero-velocity level | $D_z$ | Vertical dispersion coefficient |
| $\rho_s$ | Sediment density (kg/m$^3$) | C | Sediment concentration |
| $\nu$ | Kinematic viscosity of water | $\Delta L_t$ | Total displacement of a particle in each time step in PTM |
| $\bar{u}$ | Depth-averaged velocity | $\Delta L_a$ | Total displacement caused by the advection term |
| $B$ | Stream width | $\Delta L_d$ | Total displacement caused by the dispersion term |
| $\tau_{app}$ | Applied shear stress | $\Delta L_f$ | Particle's vertical movement |
| $t$ | Total simulation time | $\sigma$ | Stochastic displacement = $\sqrt{2Ddt}$ |
| $\Delta t$ | Computational time step | S | Ratio of particle density |
| $w_s$ | Sediment particle settling velocity | $V_{x_p}$ | Streamwise interpolated velocity component of particle |
| $x_0$, $y_0$ | Coordinates of the sediment source | $V_{y_p}$ | Transverse interpolated velocity component of particle |
| $x_p^t$, $y_p^t$, $z_p^t$ | Particle's 3D location at time t | $V_p$ | Total sediment particle volume in 3D mesh cell |
| $\tau_{cr}$ | Critical shear stress of particle | $\Delta x, \Delta y, \Delta z$ | Dimensions of the mesh cell |
| $Stk$ | Stokes number | $t_p$ | Relaxation time |

## REFERENCES


Absi, R., Marchandon, S., and Lavarde, M. (2011). "Turbulent diffusion of suspended particles: Analysis of the turbulent Schmidt number." *Defect and Diffusion Forum*, 312–315, 794–799.

Amoudry, L. O., and Souza, A. J. (2011). "Deterministic coastal morphological and sediment transport modeling: A review and discussion." *Reviews of Geophysics*, 49(2), RG2002.

Berenbrock, C., and Tranmer, A.W., (2008). "Simulation of flow, sediment transport, and sediment mobility of the lower Coeur d'Alene River, Idaho." U.S. Geological Survey Scientific Investigations Report 2008–5093, 164 p.

Black, K. S., Athey, S., Wilson, P., and Evans, D. (2007). "The use of particle tracking in sediment transport studies: A review." *Geological Society, London, Special Publications*, 274(1), 73–91.

Cheng, N.-S. (2004). "Analysis of velocity lag in sediment-laden open channel flows." *Journal of Hydraulic Engineering*, 130(7), 657–666.

Coleman, N. L. (1986). "Effects of suspended sediment on the open-channel velocity distribution." *Water Resources Research*, 22(10), 1377–1384.

Damgaard, J., Dodd, N., Hall, L., and Chesher, T. (2002). "Morphodynamic modeling of rip channel growth." *Coastal Engineering*, 45(3–4), 199–221.

De Baas, A. F., Van Dop, H., and Nieuwstadt, F. T. M. (1986). "An application of the Langevin equation for inhomogeneous conditions to dispersion in a convective boundary layer." *Quarterly Journal of the Royal Meteorological Society*, 112(471), 165–180.

Elder, J. W. (1959). "The dispersion of marked fluid in turbulent shear flow." *Journal of Fluid Mechanics*, 5(4), 544–560.

Fang, H.W., and Rodi, W. (2003). "Three-dimensional calculations of flow and suspended sediment transport in the neighborhood of the dam for the Three Gorges Project (TGP) reservoir in the Yangtze River." *Journal of Hydraulic Research*, 41(4), 379–394.

Fischer, H.B., List, E.J., Koh, R. C. Y., Imberger, J., and Brooks, N.H. (1979). "Mixing in Inland and Coastal Waters." Academic Press, New York, 483 pp.

Goode, D.J. (1990). "Particle velocity interpolation in block-centered finite difference groundwater flow models." *Water Resources Research*, 26, 925–940.

Gualtieri, C., and Mucherino, C. (2008). "Comments on 'Development of an empirical equation for the transverse dispersion coefficient in natural streams' by Tae Myoung Jeon, Kyong Oh Baek and Il Won Seo." *Environmental Fluid Mechanics*, 8(1), 97–100.

Havens, H., Luther, M. E., Meyers, S. D., and Heil, C. A. (2010). "Lagrangian particle tracking of a toxic dinoflagellate bloom within the Tampa Bay estuary." *Marine Pollution Bulletin*, 60(12), 2233–2241.

Kalin, L., and Hantush, M. M. (2003). "Evaluation of sediment transport models and comparative application of two watershed models." US Environmental Protection Agency, Office of Research and Development, National Risk Management Research Laboratory.

Kashefipour, S. M., and Falconer, R. A. (2002). "Longitudinal dispersion coefficients in natural channels." *Water Research*, 36(6), 1596–1608.

LaBolle, E.M., Fogg, G.E. (2001). “Role of molecular diffusion in contaminant migration and recovery in an alluvial aquifer system.” *Transport in Porous Media*, 42, 155–179.

Lane, A., and Prandle, D. (2006). “Random-walk particle modelling for estimating bathymetric evolution of an estuary.” *Estuarine, Coastal and Shelf Science*, 68(1–2), 175–187.

Ley, A. J. (1982). “A random walk simulation of two-dimensional turbulent diffusion in the neutral surface layer.” *Atmospheric Environment (1967)*, 16(12), 2799–2808.

Ley, A. J., and Thomson, D. J. (1983). “A random walk model of dispersion in the diabatic surface layer.” *Quarterly Journal of the Royal Meteorological Society*, 109(462), 867–880.

Li, S., and Duffy, C. J. (2011). “Fully coupled approach to modeling shallow water flow, sediment transport, and bed evolution in rivers.” *Water Resources Research*, 47(3).

Macdonald, N. J., Davies, M. H., Zundel, A. K., Howlett, J. D., Demirbilek, Z., Gailani, J. Z., Lackey, T. C., and Smith, J. (2006). “PTM : Particle Tracking Model.” 168.

Meselhe, E. A., Georgiou, I., Allison, M. A., and McCorquodale, J. A. (2012). “Numerical modeling of hydrodynamics and sediment transport in lower Mississippi at a proposed delta building diversion.” *Journal of Hydrology*, 472–473, 340–354.

Mengual, B., Le Hir, P., Rivier, A., Caillaud, M., and Grasso, F. (2021). “Numerical modeling of bedload and suspended load contributions to morphological evolution of the Seine Estuary (France).” *International Journal of Sediment Research*, 36(6), 723–735.

Niño, Y., and García, M. (1998). “Using Lagrangian particle saltation observations for bedload sediment transport modelling.” *Hydrological Processes*, 12(8), 1197–1218.

Oh, J. (2011). “Stochastic particle tracking modeling for sediment transport in open channel flows.” *Ph.D. dissertation.* State University of New York at Buffalo.

Park, I., and Seo, I. W. (2018). “Modeling non-Fickian pollutant mixing in open channel flows using two-dimensional particle dispersion model.” *Advances in Water Resources*, Elsevier, 111(August 2016), 105–120.

Park, I., Shin, J., Seong, H., and Rhee, D. S. (2020). “Comparisons of two types of particle tracking models including the effects of vertical velocity shear.” *Water (Switzerland)*, 12(12), 1–18.

Papanicolaou, A. N., Bdour, A., and Wicklein, E. (2004). “One-dimensional hydrodynamic/sediment transport model applicable to steep mountain streams.” *Journal of Hydraulic Research*, 42(4), 357–375.

Pollock, D.W., (1988). “Semianalytical computation of path lines for finite-difference models.” *Ground Water*, 26, 743–750.

Rossum, G. van. (1995). “Python tutorial.” Technical Report CS-R9526, Centrum voor Wiskunde en Informatica (CWI), Amsterdam.

Sahay, R. R., and Dutta, S. (2009). “Prediction of longitudinal dispersion coefficients in natural rivers using genetic algorithm.” *Hydrology Research*, 40(6), 544–552.

Salamon, P., Fernàndez-Garcia, D., and Gómez-Hernández, J. J. (2006). “Modeling mass transfer processes using random walk particle tracking.” *Water Resources Research*, 42(11).

Schafer-Perini, A.L., Wilson, J.L. (1991). “Efficient and accurate front tracking for two-dimensional groundwater flow models.” *Water Resources Research*, 27, 1471–1485.

Shamskhany, A., Li, Z., Patel, P., and Karimpour, S. (2021). “Evidence of microplastic size impact on mobility and transport in the marine environment: A review and synthesis of recent research.” *Frontiers in Marine Science*, 8.

Shi, H., and Yu, X. (2015). “An effective Euler–Lagrange model for suspended sediment transport by open channel flows.” *International Journal of Sediment Research*, 30(4), 361–370.

Spivakovskaya, D., Heemink, A. W., and Schoenmakers, J. G. M. (2007). “Two-particle models for the estimation of the mean and standard deviation of concentrations in coastal waters.” *Stochastic Environmental Research and Risk Assessment*, 21(3), 235–251.

Taghvaei, P. (2013). “Simulating Transport and Deposition of Non-Cohesive Sediments by Applying Particle Tracking Method.” *MSc Thesis*. University of Tehran.

Taylor, K. E. (2001). “Summarizing multiple aspects of model performance in a single diagram.” *Journal of Geophysical Research: Atmospheres*, 106(D7), 7183–7192.

Tropea, C., Yarin, A. L., and Foss, J. F. (Eds.). (2007). Springer Handbook of Experimental Fluid Mechanics. Springer Berlin Heidelberg, Berlin, Heidelberg.

Tsai, C. W., Hung, S. Y., and Oh, J. (2018). “A stochastic framework for modeling random-sized batch arrivals of sediment particles into open channel flows.” *Stochastic Environmental Research and Risk Assessment*, 32(7), 1939–1954.

Tsai, C. W., Hung, S. Y., and Wu, T.-H. (2020). “Stochastic sediment transport: Anomalous diffusions and random movement.” *Stochastic Environmental Research and Risk Assessment*, 34(2), 397–413.

Tsai, C. W., Man, C., and Oh, J. (2014). “Stochastic particle-based models for suspended particle movement in surface flows.” *International Journal of Sediment Research*, 29(2), 195–207.

Van Rijn, L.C., (1987). “Mathematical modelling of morphological processes in the case of suspended sediment transport.” Waterloopkundig Lab., Delft Hydraulics Comm-382.

Van Rijn, Leo. C. (1993). “Principles of sediment transport in rivers, estuaries and coastal seas.” *Aqua Publications*, Amsterdam, The Netherlands.

Warner, J. C., Sherwood, C. R., Signell, R. P., Harris, C. K., and Arango, H. G. (2008). “Development of a three-dimensional, regional, coupled wave, current, and sediment-transport model.” *Computers & Geosciences*, 34(10), 1284–1306.

Wu, W. (2004). “Depth-averaged two-dimensional numerical modeling of unsteady flow and nonuniform sediment transport in open channels.” *Journal of Hydraulic Engineering*, 130(10), 1013–1024.

# CHAPTER 3

# MODELING NON-COHESIVE SEDIMENT TRANSPORT IN NATURAL STREAMS USING A LAGRANGIAN APPROACH

# CASE STUDY: WILSON CREEK, MCKINNEY, TEXAS, USA


## ABSTRACT

The present study aims to develop and assess the performance of a Lagrangian particle tracking model (PTM) in simulating sediment transport in natural streams. To achieve this goal, a field monitoring program was conducted while a bridge was being built over Wilson Creek, in McKinney, Texas. The field monitoring included collecting total suspended solids (TSS), bedload material, and substrate; assessing the turbidity (Tu); and surveying depositional areas in the creek. The PTM outputs included changes in the creek's sediment regime, i.e., suspended sediment concentration and depositional areas. A comparison between the model results and field data showed that the PTM predicted suspended sediment concentrations during high and low flow scenarios with acceptable accuracy and predicted the depositional areas as well as the field observation and measurements. Overall, the PTM showed an acceptable performance in simulating sediment transport in a natural stream. It also showed that the eroded particles that entered the creek from the construction site elevated the sediment concentrations in the creek and changed the bed morphology, which could have short- and long-term effects on aquatic habitats.



**Author Keywords:** Sediment transport, Suspended sediment concentrations Particle tracking model, Stochastic approach, Natural streams

## INTRODUCTION

Effluent discharge and anthropogenic activities have increasingly polluted and contaminated natural rivers over the past few decades, while rainfall, channel scouring, dam breaks, and landslides have generated a random quantity of sediment (Bennett et al., 2014). In addition to these events that have the potential to produce a significant amount of sediment yield, most construction activities near waterbodies increase overland erosion and add additional sediment load to streams (Ahmari et al., 2021; Sulaiman et al., 2021). Sediment particles are first eroded and then transported by water in the form of suspended loads, bedloads, or both, and are eventually deposited in streams, lakes, and reservoirs (Malmon et al., 2003), where they may impact aquatic habitats and water quality (Bilotta and Brazier 2008; Hall et al., 2019; Tao et al., 2019). Due to the significant role of sedimentation in the health of a river system, empirical and numerical approaches are used to assess the sediment transport in waterbodies, and numerical and empirical models are used to evaluate changes in sediment regime, i.e., suspended sediment transport, bedload transport, or deposition/resuspension of sediment particles (Pinto et al., 2006) and to predict the effect of added sediment particles on water quality and aquatic habitats (Bilotta and Brazier 2008; Hall et al., 2019).

The complex behavior of sediment particles in waterways makes it challenging to fully understand the mechanics of sediment transport (Tsai et al., 2018; Safari et al., 2016; Muste et al., 2009), but several researchers have developed empirical approaches and formulas that can be used to predict it in natural streams (Sulaiman et al., 2021; Priya et al., 2016; Lopez et al., 2014). These formulas are drastically different from one another (Pinto et al., 2006), however, which means that there is no way to select the most accurate empirical equation for a specific problem (Huntley and Bowen 1989). The source of the inaccuracy of empirical models has been studied by various researchers,

such as Camenen and Larroudé (2003), who showed that empirical models are sensitive to small variations in sediment gradations and flow conditions and that the different variables entered into empirical sediment transport models can result in inaccuracy. Empirical models are only viable within the geographical area from which their relationships are derived (Hajigholizadeh et al., 2018). Empirical sediment transport modeling can be performed using deterministic or stochastic approaches. Deterministic sediment transport models treat the sediment as a continuum, and suspended particles are represented by solving the concentration equation (Kiat et al., 2008; Amoudry and Souza 2011). Stochastic sediment transport models consider the randomness of the data and generate a stochastic result for a given input parameter set, which can increase the reliability of the model since it mimics the random behavior of sediment particles in natural streams. The majority of stochastic sediment transport models are based on Lagrangian approaches (Oh 2011) and model sediment particles as a dispersed phase (Ji et al., 2013; Shi and Yu 2015).

It should be noted that numerical modeling of sediment transport, using either a deterministic or stochastic approach, has some uncertainties that could be due to dimensionality simplification for 1D, 2D, or 3D models or stream-specific coefficients such as Shields' critical shear stress and bedload/suspended load parameters, among others (Beckers et al., 2018). Hantush and Kalin (2004) mentioned that deterministic and stochastic approaches (numerical models) can result in less uncertainty than empirical approaches.

Sediment transport deterministic models use conservation of mass and momentum principles and produce the exact results for a particular set of inputs. They usually require a longer simulation period than stochastic approaches. Deterministic approaches have been employed in various studies to model sediment transport in rivers (Wu 2004; Fang and Rodi 2003; Liu et al., 2002) and coastal areas (Mengual et al., 2021; Warner et al., 2008). Wu (2004) developed a coupled

deterministic model based on a finite volume approach for solving equations for 2D depth-averaged, unsteady, open channel flow and sediment transport. Sediment transport equations were solved using an iteration approach that accounted for a coupling procedure among sediment transport, bed change, and bed material. Periáñez et al. (2013) assessed sediment transport in Cádiz Bay, Spain, using an explicit finite difference method to solve a transport equation on a spatial flow domain with a 200 m mesh grid size and developed suspended sediment concentration contour maps for the inner bay area.

Einstein (1950) pioneered using stochastic approaches to simulate bedload transport, as they present data and predict outcomes that account for a certain level of unpredictability or randomness within a short period of simulation. Lagrangian stochastic sediment transport models consider a group of particles as mass transport elements in the flow domain to solve transport equations, using advection and dispersion. Several researchers have shown the performance of Lagrangian stochastic approaches in modeling sediment transport (Baharvand et al., 2022; Ahmari et al., 2021; Allison et al., 2017; Dunn et al., 2015; Liu et al., 2007; De Baas et al., 1986; Ley 1982). Lackey and Smith (2008) used a PTM to predict the fate of dredged sediment in the Willamette River, near the confluence of the Willamette and Columbia Rivers in Oregon. They coupled the EFDC (Estuarine Fluid Dynamics Code) with a particle tracking model and showed that sediment particles settled quickly in two areas where dredging operations were taking place. Oh (2011) investigated the performance of a particle-based sediment transport model using the stochastic diffusion particle tracking model (SD-PTM) and the stochastic jump-diffusion particle tracking model (SJD-PTM). The SJD-PTM was developed to reflect the effect of extreme flows on particle movement, using a jump term added to the stochastic dispersion term. Tsai et al. (2014) used various mathematical forms of particle tracking models, such as the gambler ruin problem and the

multi-state discrete-time Markov chain. Zhao et al. (2018) developed a Lagrangian particle tracking model to simulate contaminant transport in Tangdao Bay, in China and found that the pollution was mainly caused by the low water exchange capability and long residence time. Hache et al. (2021) used a PTM to investigate accumulated sediment in an inundated anthropogenic marshland in the southeastern North Sea and the impact of coastal protection measures on sediment transport. Baharvand et al. (2022) developed a Lagrangian particle tracking model to simulate sediment transport in prismatic open channels. They assessed the accuracy of different empirical dispersion terms with a random walk stochastic approach in the PTM, using laboratory data and analytical solution of the advection-dispersion equation.

Lagrangian particle tracking models have not been used to simulate the effects of road and bridge construction on sediment transport in natural streams. However, in some studies PTMs have been used to assess the effect of dredging operations on sediment regions in rivers (e.g., Lackey and Smith 2008; Lackey et al., 2020). In the present study, the PTM developed by Baharvand (2022) was adopted to simulate sediment transport in natural streams and to study the potential of the model to simulate sediment transport in a creek downstream of a bridge construction site. The model uses empirical dispersion equations and the random walk approach to simulate sediment transport. Unlike most the PTMs coupled with internal deterministic hydrodynamic solvers that may not be applicable to different flow and sediment environment, the PTM used in this study was coupled with the HEC-RAS 2D (version 5.0.7) and used Python-based packages as an external hydrodynamic model. This widely used hydraulic model can be employed in different study areas, using limited geographical and hydrological information. The model output includes heat maps of suspended sediment distribution and depositional areas in the river channel. The model's

performance was assessed using field data. The methodology and validation processes of the PTM are discussed in the following sections.

## METHODOLOGY

### 3.1.1 Case Study

The field study took place from December 2020 to December 2021 in Wilson Creek near Highway FM 2478 in McKinney, Texas (Figure 3.1). Wilson Creek was selected because of a road and bridge expansion project that was likely to cause increased sedimentation to the creek during the construction period, and the PTM was used to predict changes in suspended sediment concentrations and sediment depositions. The bridge construction site was located downstream of the existing bridge on the north and south sides of the creek. The bridge location and footprints of the construction site are shown in Figure 3.1.

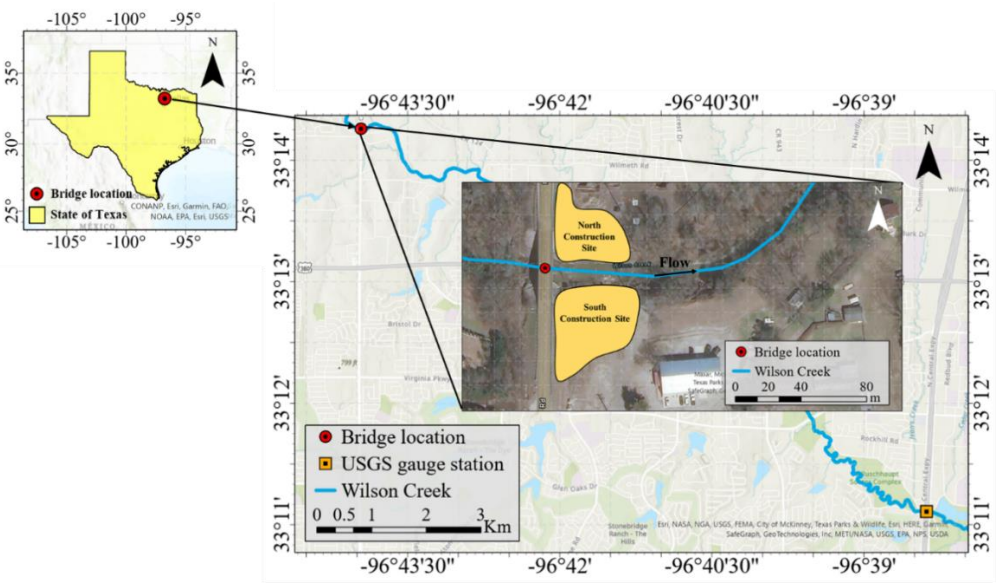


**Figure 3.1** Wilson Creek study area near Highway FM 2478, McKinney, Texas

The 196.8 km$^2$Wilson Creek watershed originates in Collin County, approximately 3.2 km east of Celina, Texas. The creek is 46.6 km long and discharges into Lavon Lake, which is located on the

east fork of the Trinity River. The bedrock in the Wilson Creek watershed consists of Austin chalk (Ferring 1994). The creek lies within the Blackland Prairie, which expands through North Texas to an area southwest of San Antonio (Moring 2009) and is dominated by swelling clay soils that are prone to widescale surficial erosion (Harmel et al., 2006). Adjacent land use in the basin is primarily residential and undeveloped agricultural areas. Flow in the upper part of the basin is intermittent but becomes more perennial in its lower reaches, due in part to runoff from municipal water (Maier and Dunkin, 1988).

The Wilson Creek streamflow is recorded at the USGS 08059590 gauge station, 11.2 km downstream of the bridge (Figure 3.1). Historical data shows that the average daily minimum, mean, and maximum discharges at the site are 0.18, 2.2, and 149.5 $m^3/s$, respectively. The 2-year and 10-year peak discharges at the bridge site are estimated as 98.4 and 210.7 $m^3/s$ (JMT 2019), respectively, representing the average and high flow conditions at this location. The minimum, mean, and maximum daily discharges recorded at this station from December 2020 to December 2021 are shown in Figure 3.2. In 2021, the minimum and maximum daily discharges were 0 and 74.5 $m^3/s$, respectively. The mean daily flow varied between 0 and 37.4 $m^3/s$ with an average of 1.98 $m^3/s$.

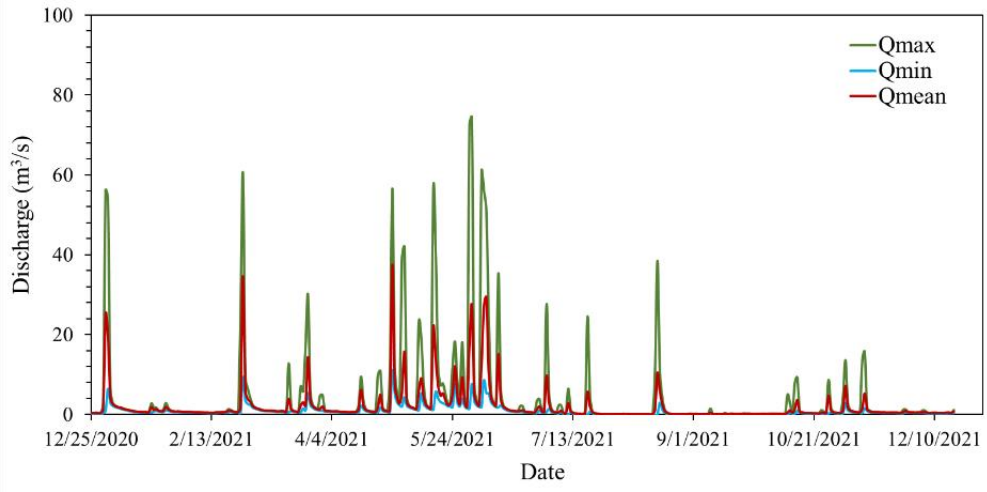


**Figure 3.2** Wilson Creek minimum, mean, and maximum daily streamflow recorded from December 2020 to December 2021 at the USGS gauge station in McKinny, Texas

### 3.1.2 Developing a Lagrangian Particle Tracking Model for Natural Streams

A Lagrangian-based particle tracking model (PTM) developed by Baharvand (2022) was coupled with the HEC-RAS 2D and adopted and modified by this research to simulate sediment transport in natural streams. A continuous sediment source was considered in the model to simulate the particles' pathways along the stream. Advection and dispersion displacement equations were solved in the PTM for each sediment particle in the flow domain. For advection, the displacement of the particle was based on the interpolated velocity estimated by the HEC-RAS 2D model developed for Wilson Creek, at the position of the particle in the flow domain. However, the dispersion term generates the stochastic movement of the particles in a three-dimensional space, using the random walk method. The model structure and governing equations of the PTM were based on a particle-based sediment transport model that was developed for prismatic open channels (Baharvand et al., 2022). Equation 3.1 shows the three-dimensional Lagrangian transport equation used in the PTM to estimate the displacement of the particles on each mesh cell in the flow domain.

$$\underbrace{\begin{bmatrix} x_p^{t+1} \\ y_p^{t+1} \\ z_p^{t+1} \end{bmatrix}}_{\text{Particle location at "}t+1\text{"}} = \underbrace{\begin{bmatrix} V_{x_p} & 0 & 0 \\ 0 & V_{y_p} & 0 \\ 0 & 0 & -w_s \end{bmatrix} \times \Delta t}_{\text{Advection term}} + \underbrace{\begin{bmatrix} N(0,1) \times \sigma_x \\ N(0,1) \times \sigma_y \\ N(0,1) \times \sigma_z \end{bmatrix}}_{\text{Diffusion term}} + \underbrace{\begin{bmatrix} x_p^t \\ y_p^t \\ z_p^t \end{bmatrix}}_{\text{Particle location at "}t\text{"}} \quad (3.1)$$

where ($x_p{}^t$, $y_p{}^t$, $z_p{}^t$) and ($x_p{}^{t+1}$, $y_p{}^{t+1}$, $z_p{}^{t+1}$) are the particle locations before and after one computational time step ($dt$) in the flow domain. $V_{x_p}$ and $V_{y_p}$ are the linearly interpolated velocity components in streamwise and transverse directions at the particle location, respectively. $N$ (0,1) represents the stochastic term with normal distribution, mean of 0, and standard deviation of 1. Equation 3.2 is used to estimate the fall velocity of sediment particles (Van Rijn, 1993).

$$W_s = \begin{cases} \frac{(S\text{-}1)\, g d^2}{18\nu} & 1 < d \leq 100\ \mu\text{m} \\ \frac{10\,\nu}{\mathrm{d}} \left[ \left( 1 + \frac{(S-1) g d^3}{100\,\nu^2} \right)^{0.5} \text{-}1 \right] & 100 < d \leq 1000\ \mu\text{m} \\ 1.1[(S\text{-}1) g d]^{0.5} & d \geq 100\ \mu\text{m} \end{cases} \quad (3.2)$$

where $w_s$ is the particle fall velocity, $\nu$ is the kinematic viscosity of water, $d$ is the particle diameter, and $S$ refers to the particle specific gravity.

The dispersion term ($\sigma$) was computed using Equation 3.3. In this equation, $D$ represents the dispersion coefficient. Baharvand et al. (2022) showed the superiority of the Elder (1959) equation over other widely used longitudinal dispersion equations to simulate longitudinal dispersion; therefore, Equation 3.4 was used to calculate the longitudinal dispersion term in the present model. Equation 3.5, proposed by Gualtieri and Mucherino (2008), was used to estimate the transverse dispersion coefficient, and the vertical dispersion coefficient was estimated using Equation 3.6 proposed by Van Rijn (1987).

$$\sigma = \sqrt{2Ddt} \quad (3.3)$$

$$D_x = 5.93Hu_* \tag{3.4}$$

$$D_y = 0.166Hu_* \tag{3.5}$$

$$D_z = \begin{cases} D_{zm} - D_{zm}\left(1 - \frac{2z}{H}\right)^2 & ; \quad \frac{z}{H} < 0.5 \\ D_{zm} & ; \quad \frac{z}{H} \geq 0.5 \end{cases} \tag{3.6}$$

In these equations, $H$ represents flow depth, $z$ is the vertical elevation of particle, and $D_{zm}$ is the maximum vertical dispersion coefficient. As can be seen in Equation 3.6, the vertical dispersion for $z/H < 0.5$ is described with a parabolic distribution over the flow depth, and for $z/H > 0.5$, it is considered equal to the maximum vertical dispersion. Equation 3.7 was used to calculate the maximum vertical dispersion term.

$$D_{zm} = \frac{\kappa u_* H}{4} \tag{3.7}$$

where $\kappa$ refers to the von Kármán constant ($\kappa = 0.4$), and $u_*$ is the shear velocity.

According to Shields diagram, if the critical shear stress ($\tau_{cr}$) of a particle is greater than the shear stress ($\tau_{app}$), the particle will deposit; otherwise, it stays in suspension. Previous studies used the Shields criterion to determine the initiation of motion of bed materials in stochastic sediment transport models (e.g., MacDonald et al., 2006). The PTM uses the dimensionless mobility number $M$, expressed by Equation 3.8 to determine whether the particle stays in suspension or gets deposited on the streambed.

$$M = \frac{\tau_{cr}}{\tau_{app}} \tag{3.8}$$

If $M > 1$, the particle will deposit on the streambed. When $M < 1$, a vertical resuspension movement using the pure dispersion term will be applied to the particle centroid elevation to keep it in suspension mode. The critical shear stress for different sediment classes (e.g., fine stilt, fine sand,

etc.) obtained from Berenbrock and Tranmer (2008) is used to produce the critical shear stress for sediment particles with a certain diameter, using the cubic interpolation technique (Baharvand et al., 2022). The PTM calculates the mobility number for each particle reaching the zero-velocity layer (Figure 3.3). Equation 3.9 was used to calculate the elevation of the zero-velocity layer for each sediment particle (Van Rijn, 1993).

$$z_0 = \begin{cases} 0.11\frac{\nu}{u_*} & \beta \leq 5 \\ 0.033\, k_s & \beta \geq 70 \\ 0.11\frac{\nu}{u_*} + 0.033\, k_s & 5 < \beta < 70 \end{cases} \quad (3.9)$$

where $k_s$ is bed roughness height, and $\beta$ is the boundary Reynolds number ($\beta = \frac{u_* k_s}{\nu}$).

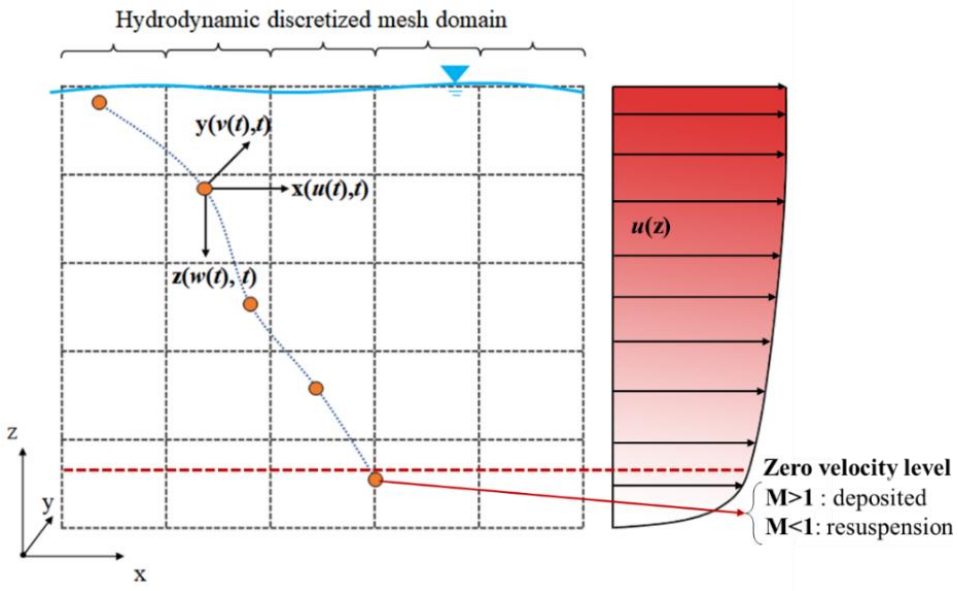


**Figure 3.3** Sediment particle movement in a discretized flow domain

### 3.1.3 Developing HEC-RAS 2D Model for Wilson Creek

Geo-spatial velocity, shear stress, and flow depth are the required hydrodynamic inputs to the developed PTM to model sediment transport in natural streams. These parameters were obtained from the HEC-RAS 2D model developed for Wilson Creek. HEC-RAS 2D is a more highly

developed version of the HEC-RAS 1D, with a 2D structured and unstructured mesh grid and an implicit finite volume solver, combined with computational cells involving a digital terrain map (Brunner 2016). The computational mesh grid assessment, boundary conditions, and model validation are discussed in the following section.

*3.1.3.1 Hydrodynamic Model Preparation and Validation Processes*

The digital elevation model (DEM) with 10-meter resolution, exported from the USGS National Dataset, was used as a three-dimensional terrain model of Wilson Creek in the present study, but was modified, based on the cross sections used in a calibrated HEC-RAS 1D model developed by JMT (2019) for Wilson Creek at the bridge site. Figure 3.4 depicts the extent of the structured mesh plain of Wilson Creek and the boundary conditions used for the hydrodynamic modeling. A steady-state flow condition was used at the upstream section, and the downstream boundary condition was set to normal depth.

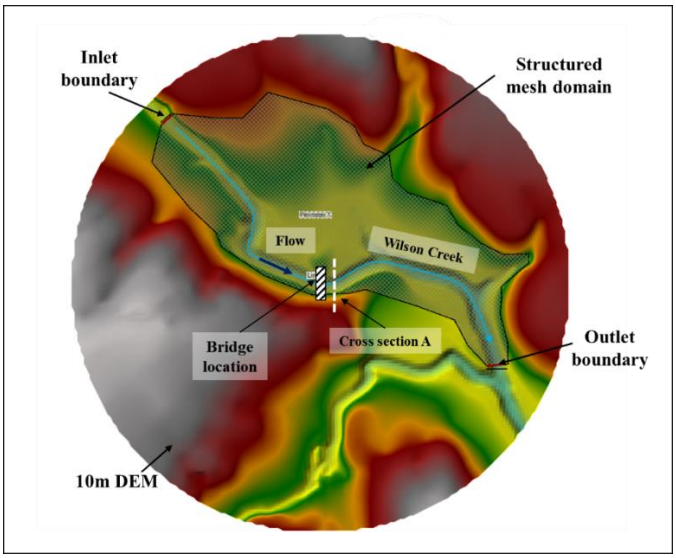


**Figure 3.4** Mesh plain and boundary condition used in the Wilson Creek HEC-RAS 2D model

The accuracy of 2D hydrodynamic models may be affected directly by the generation of computational grids and the selected boundary conditions (Kim et al., 2014). Very fine mesh grids

increase the simulation time; however, coarse mesh grids can reduce the accuracy of the hydrodynamic solver in detecting the features of the terrain geometry. Coarse mesh grid dimensions up to 10 m do not impact the geomorphologic indices such as flow patterns and basin hydrologic responses (Zhang and Montgomery 1994).

A structured rectangular mesh domain with different mesh grid sizes was developed to determine the optimal mesh grid dimensions and assess the impact of the mesh size on flow characteristics. The 2-year and 10-year flows were used as the steady-state flow conditions in the HEC-RAS 2D model. The average flow velocity for the 2-year and 10-year discharges at a section 28 m downstream of the bridge location (cross section A in Figure 3.4) was estimated by the HEC-RAS 1D model as 1.01 and 1.73 m/s, respectively (JMT 2019). The average flow velocity calculated by the HEC-RAS 2D model at this section of the creek was used to determine the optimal mesh size. Table 3.1 shows the number and sizes of mesh cells used in this study, as well as the corresponding average flow velocity at cross section A, for comparison of the average flow velocity estimated by the HEC-RAS 1D and HEC-RAS 2D models.

**Table 3.1** Mesh Grid Size and Corresponding Average Velocity in Wilson Creek at Cross Section A

| No. | Discharge ($m^3/s$) | Mesh cell size (m) | Number of mesh cells | Calculated average velocity (m/s) |
|---|---|---|---|---|
| 1 | 98.4 | 2 | 132587 | 1.18 |
| 2 | 98.4 | 5 | 21482 | 1.19 |
| 3 | 98.4 | 10 | 5492 | 1.12 |
| 4 | 210.7 | 2 | 132587 | 1.24 |
| 5 | 210.7 | 5 | 21482 | 1.23 |
| 6 | 210.7 | 10 | 5492 | 1.16 |

As shown in Table 3.1, the average velocity for both flow scenarios changed marginally when the mesh cell size decreased from 5 m to 2 m; however, the simulation time increased notably. Figures

3.5a and 3.5b show the velocity distribution across Wilson Creek at cross section A for the 2-year and 10-year flow scenarios, respectively. According to these figures, it can be argued that the 10 m mesh resolution did not detect the creek geometry effectively, especially near the banks. For the 2-year flood scenario (Figure 3.5a), the model with 10 m mesh grids overestimated the maximum velocity compared to the models with mesh grids of 2 m and 5 m. The variations in the velocity from the center to the north side of the channel were underestimated by the model with coarser mesh. For the 10-year flood scenario (Figure 3.5b), however, the model with 10 m mesh estimated the velocity relatively close to the result of the models with finer mesh cells. As a result, a mesh resolution of 5 m with a total number of 21,482 mesh cells was considered for the HEC-RAS 2D model. For the 2-year and 10-year flow scenarios, the flow depth at cross section A was estimated as 3.65 m and 5.78 m by the HEC-RAS 1D and 3.32 m and 5.48 m by the HEC-RAS 2D.

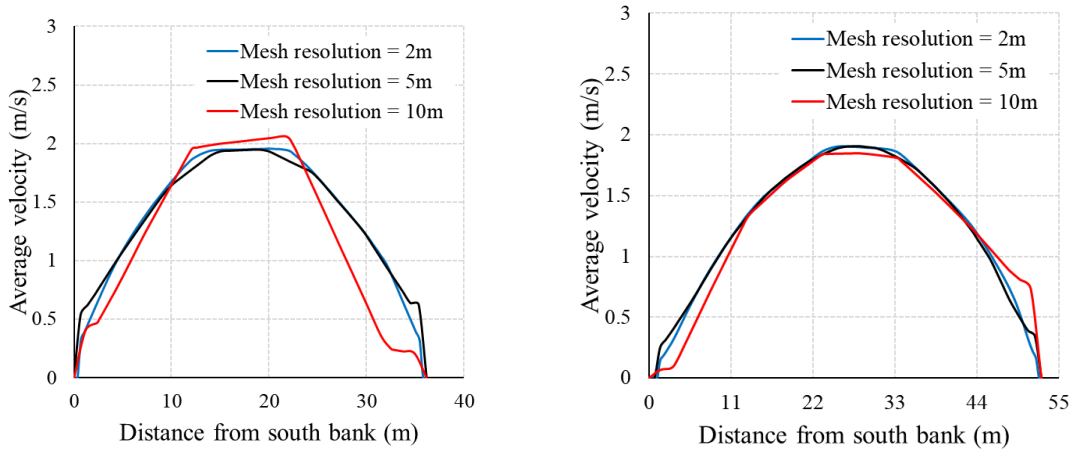


**Figure 3.5** Velocity distribution across Wilson Creek at cross section A downstream of the bridge (shown in Figure 3.4) for different mesh grid sizes: a) 2-year flow with $Q$ = 98.4 $m^3/s$, and b) 10-year flow with $Q$ = 210.7 $m^3/s$

### 3.1.4 Developing A PTM For Wilson Creek

A particle tracking model (PTM) was developed to assess changes in the sediment regime in Wilson Creek caused by overland erosion at the bridge construction site. The PTM requires the

creek flow parameters and information on the overland erosion, including daily sediment yield and gradation of eroded materials entering the creek. The flow parameters were extracted from the HEC-RAS 2D model developed for Wilson Creek, and the daily sediment load entering the creek and its gradation were obtained from an overland erosion model developed by Ahmari et al. (2022).

The PTM performance was evaluated for storm events that occurred on April 29 and November 3, 2021. The daily rainfall in these two days was recorded as 70.1 mm (the highest recorded precipitation in 2021) and 35.6 mm at the Frisco Station, located 7 km southwest of the study area. The storm on April 29 was selected since it produced the highest sediment yield during the study period due to overland erosion (Section 3.2.4.2). The storm on November 3 was selected since it was the only day that the TSS concentration was concurrently measured upstream and downstream of the bridge.

Two 12.8 m long line sources were considered: one along the north water's edge and one along the south water's edge, to replicate sediment entering the creek from construction areas. Using line sources instead of point sources simulated the sediment release to the creek more realistically. Once the diameters and percentages of the sediment particles were determined, the model simulation time was set to 1800 seconds to ensure that the PTM considered the entire study area for sediment transport modeling. Sediment discharge at the sediment sources was set to 100 particles per second for three different sediment classes (Section 3.2.5.3).

*3.1.4.1 Hydrodynamic Flow Parameters*

After validating the hydrodynamic model, the recorded mean daily flows at the USGS gauge in McKinney on April 29, 2021 ($Q$ = 37.4 $m^3/s$) and November 3, 2021 ($Q$ = 7.4 $m^3/s$) were used for hydrodynamic modeling of Wilson Creek. The raster-based hydrodynamic parameters, including water depth ($d$) and shear stress ($\tau$), were exported from the creek's HEC-RAS 2D model to the

PTM. The 2D velocity outputs ($v_x$, $v_y$) were also introduced to the PTM from a binary file written in an HDF-5 file format from the HEC-RAS 2D model. Figure 3.6 shows the spatial distribution of the depth-averaged flow velocity, flow depth, and shear stress for the April 29, 2021 storm.

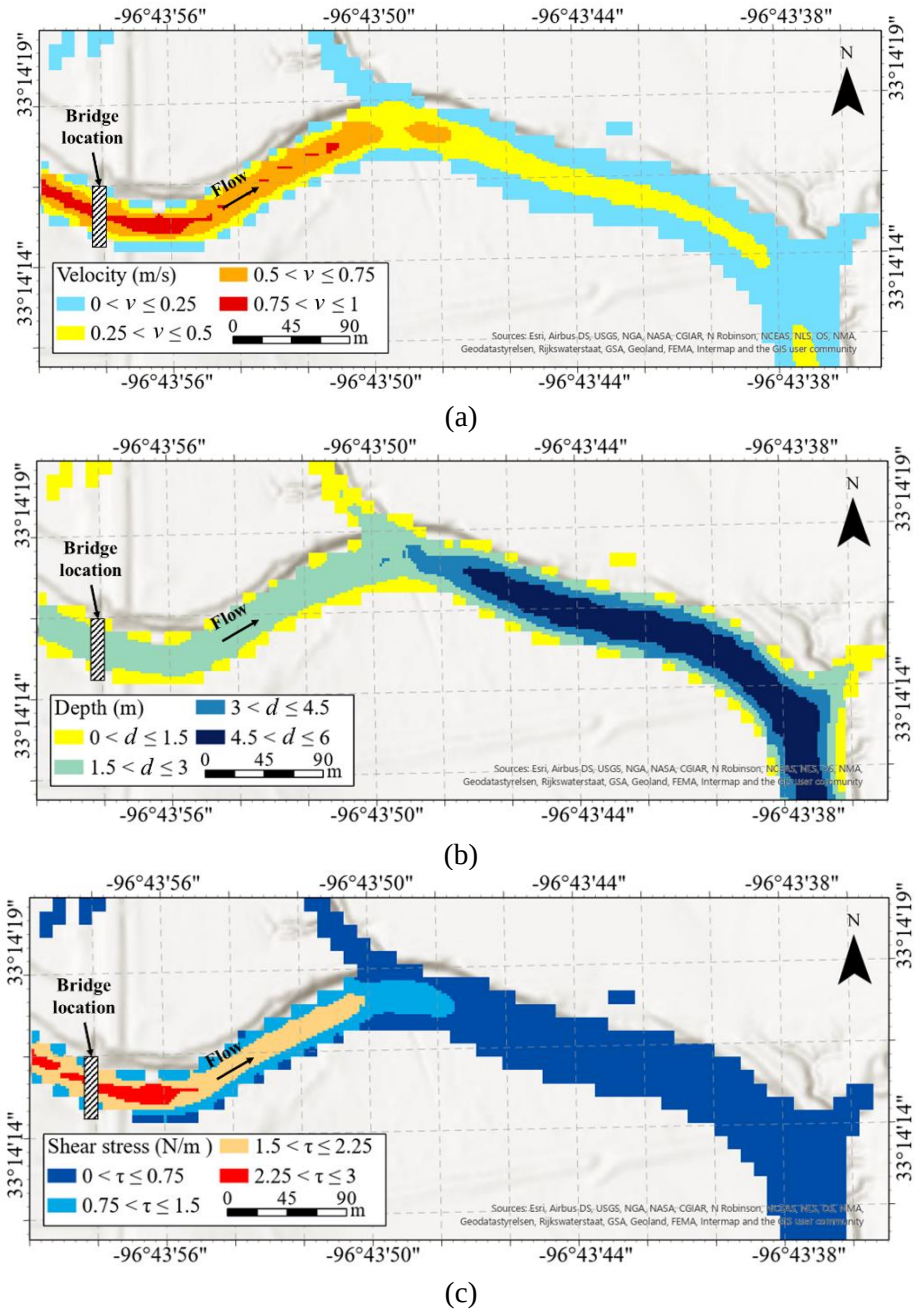


**Figure 3.6** Hydrodynamic parameters of Wilson Creek produced by the HEC-RAS 2D model for the April 29, 2021 storm: a) depth-averaged flow velocity, b) flow depth, and c) shear stress

*3.1.4.2 Overland Erosion and Sediment Yield*

In addition to hydrodynamic flow parameters, the PTM requires sediment data from the sediment source to simulate sediment transport in Wilson Creek. Ahmari et al. (2022) developed a predictive overland erosion model based on the SCS curve number method and modified universal soil erosion loss equation (MUSLE) to determine overland erosion and sediment yield for the study area. The MUSLE model relates soil erosivity to both runoff volume ($Q$) and peak flow $q_p$ and is produced by the SCS curve number method. The development of the overland erosion model is discussed in detail by Ahmari et al. (2022). Equation 3.10 shows the MUSLE model that was used to estimate the sediment yield in the study area.

$$Q_s = 11.6\,(Q \times q_p)^{0.56} K \times LS \times C \times P \tag{3.10}$$

where $Q_s$ represents sediment yield (tonnes), $Q$ is the runoff volume ($m^3$), $q_p$ refers to the runoff peak flow rate ($m^3/s$), $K$ is soil erosivity, $LS$ is slope length factor, $C$ is management practice factor, and $P$ shows the erosion control factor.

Total runoff volume and peak flow rate were estimated using the SCS method. Equations 3.11 to 3.12 (in imperial system of units) were used to calculate the runoff depth $P_e$ (in) and peak flow rate $q_p$ ($ft^3/s$) (Mays 2010).

$$P_e = \frac{(P - 0.2S)^2}{(P + 0.8S)} \tag{3.11}$$

$$q_p = \frac{484\,A\,P_e}{0.67\,t_c} \tag{3.12}$$

where $P$ is total rainfall (in), $S$ is potential maximum retention (in), $A$ is the watershed area ($mi^2$), and $t_c$ represents the time of concentration (hr). $S$ and $t_c$ are calculated using Equations 3.13 and 3.14.

$$S = \frac{1000}{CN} - 10 \tag{3.13}$$

$$t_c = \frac{L^{0.8}(Y+1)^{0.7}}{1140\, Y^{0.5}} \tag{3.14}$$

In these equations $CN$ is the curve number, $L$ is flow length (ft), and $Y$ is average slope along the flow path (%). The runoff volume is calculated as $Q = P_e\, A$.

The performance of the overland erosion model for Wilson Creek was evaluated using field data collected from the erosion plots that were installed during bridge construction activities. Four 3 m × 3 m erosion plots were constructed on slopes with different soil conditions and surface covers, based on the available space near the bridge construction site, and were installed on the north and south sides of the creek downstream of the bridge to collect eroded sediment particles during storm events. Sediment deposited in the storage tank of each plot was collected after each storm, from March to December 2021, and was sent to the lab to be weighed, to provide an estimate of the amount of soil lost from the bounded area of each plot during each storm and for the particle sizes to be analyzed. (Ahmari et al. 2022). Figure 3.7 illustrates the location of the erosion plots.

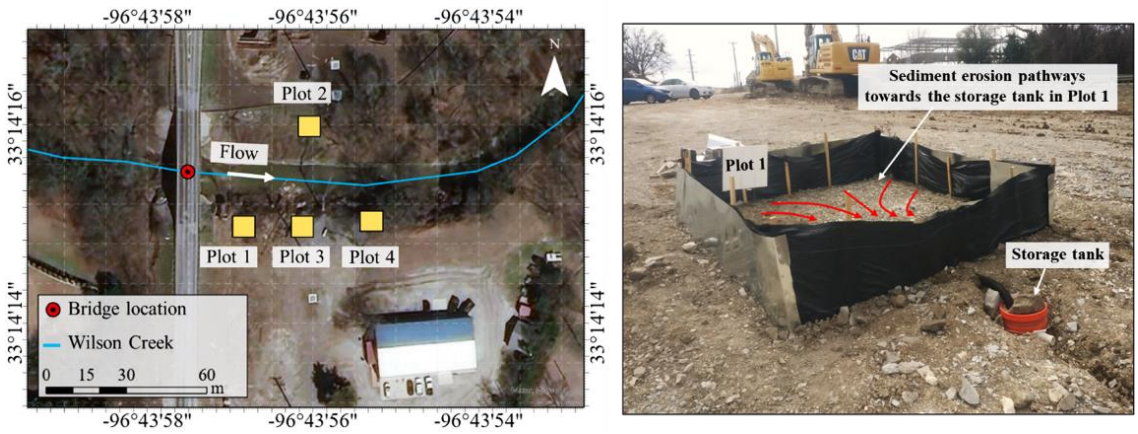


(a) (b)

**Figure 3.7** a) Location of erosion plots on the north and south sides of Wilson Creek downstream of the bridge location, and b) Erosion Plot No.1 (Ahmari et al. (2022)

The outputs of the overland erosion model were used as the sediment load for the PTM to evaluate its performance in natural streams with local sediment sources. Figure 3.8 shows the daily sediment yield produced by the predictive overland erosion model at the Wilson Creek bridge site during construction activities in 2021. The activities that exacerbated overland erosion included site clearing, grading, temporary access roads, drilled shafts, construction and installation of foundations and abutments, backfilling, slope formation, and superstructure construction.

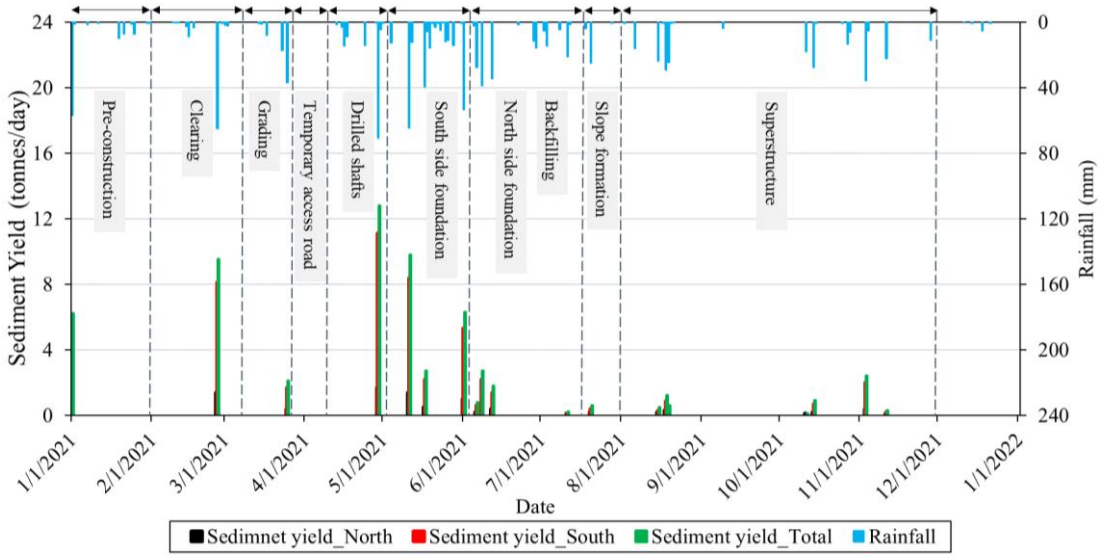


**Figure 3.8** Sediment yield at the Wilson Creek bridge site due to overland erosion in the north and south construction areas, and daily rainfall records at the Frisco station, Frisco, Texas (Ahmari et al. 2022)

### 3.1.5 Field Measurements

In 2021, the sediment characteristics were monitored at the Wilson Creek bridge site for one year. The bridge construction site was visited an average of two to four times per month after each storm event, depending upon the rainfall and streamflow conditions. The field monitoring included collecting total suspended solids (TSS) and bedload material, monitoring the turbidity (Tu), typing the substrate, and surveying depositional areas. Bridge construction activities and best management practices (BMPs) were also documented throughout the monitoring program. It

should be noted that the monitoring program was conducted only during the construction of Phase I of the Wilson Creek bridge replacement project (northbound bridge) in 2021.

*3.1.5.1 Total Suspended Sediment Solids (TSS) and Turbidity (Tu)*

The present study aims to model sediment transport in Wilson Creek using sediment yield from local sediment sources, i.e., overland erosion in the north and south construction areas (Figure 3.9a). Nevertheless, sediment particles could be also added to the creek from the upstream watershed area. Therefore, two automated water sampler units (ISCO 6712, Teledyne) were installed upstream and downstream of the bridge location to collect water samples during storm-based events for lab analysis of the concentration of the suspended sediment. Figure 3.9a illustrates the location of the automated water samplers upstream (Section 1) and downstream of the bridge (Section 3). Figure 3.9b shows the downstream water sampler unit and the solar panel installed on the north bank, with its sampling line placed in the middle of the creek. The upstream sampler collected water samples upstream of the bridges where the sediment load in the creek was not impacted by the local overland erosion in the construction areas. The water samples collected by the downstream sampler represented the cumulative effect of sediment inflow from upstream and the sediment load entering the creek from the north and south sides of the bridge due to overland erosion. Comparing the TSS data from the upstream and downstream units made it possible to estimate the elevated TSS in the creek due to overland erosion.

Streamflow sampling was triggered both upstream and downstream when the flow reached 30 cm above the sampler's inlet. Sampling took place at 10-minute intervals during storm events and stopped when the flow was reduced to below the trigger threshold. Discrete TSS and turbidity (Tu) samples (Figure 3.9c) were also obtained at the location of the automated water samplers, as well as the area between the bridge and the downstream water sampler unit (Section 2 in Figure 3.9a).

The TSS and turbidity discrete data were collected mainly during low flow conditions to complement sediment data collected by the automated water samplers during storms.

The turbidity of the samples was measured in NTU units, using a Hach 2100Q portable turbidimeter. The discrete data collected in Section 2 represents the area subject to local overland erosion, where the sediment plume was not fully mixed with the creek flow. Water samples collected by the automated samplers and grab samples were sent to the lab for TSS analysis using EPA method 160.2 (U.S. Environmental Protection Agency 2017).

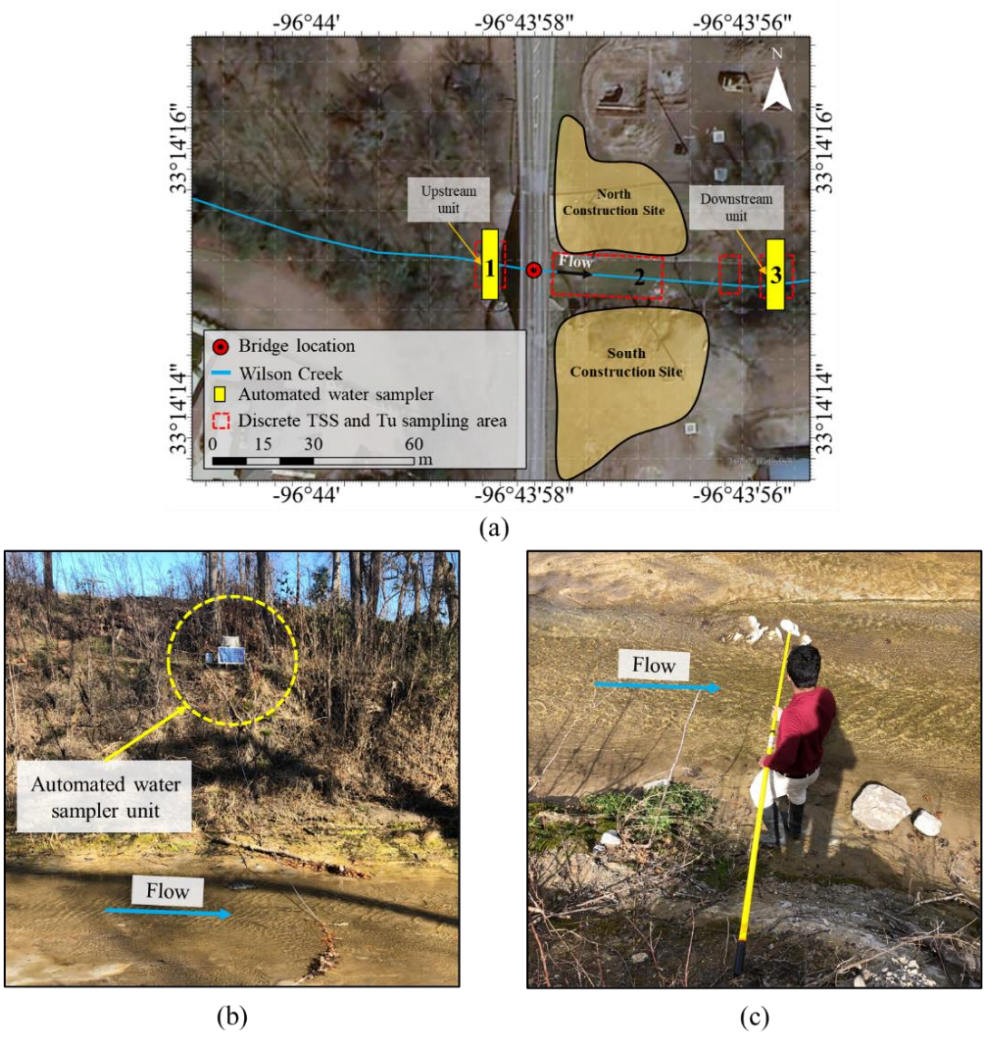


**Figure 3.9** Total suspended solids (TSS) and turbidity (Tu) sampling in Wilson Creek: a) Location of automated water sampler units installed upstream and downstream of the bridge and discrete sampling

areas, b) Automated water sampler installed downstream of the bridge, and c) Discrete TSS and Tu sampling

Over the study period, between March 24 and November 8, 2021, 27 water samples were collected from Sections 1 and 3. Six were collected by automated water samplers during periods of high flows; 21 were grab samples. The TSS measured downstream and upstream of the bridge site and average daily discharge recorded at the USGS stream gauge in McKinney, Texas are depicted in Figure 3.10.

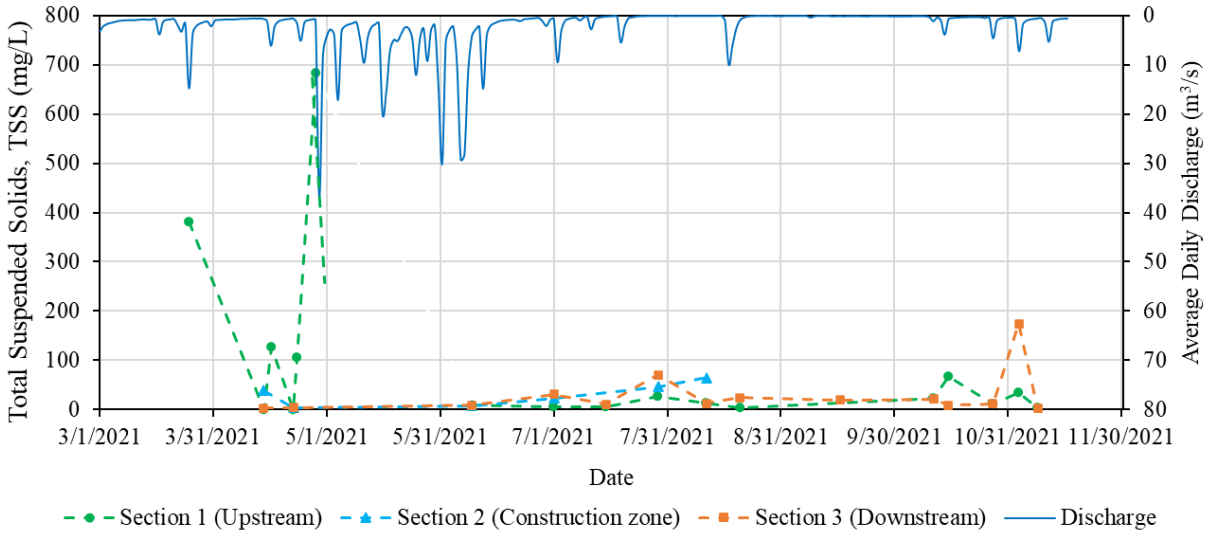


**Figure 3.10** TSS variations in Wilson Creek upstream of the bridge (Section 1), in the construction zone (Section 2), and downstream of the construction area (Section 3), and average daily discharge at the USGS stream gauge in McKinney (Sections 1 to 3) are shown in Figure 3.9a.

All samples collected in Section 1 before June 9, 2021, were associated with high flow events and captured by the upstream water sampler. For the downstream water sampler, mechanical issues prevented sampling, except on November 3, 2021. Therefore, the downstream samples were generally collected by hand during baseflows and following storm events. Based on these collections, the TSS increased with storm events, peaking at 684 ± 301 mg/L (mean ± SE) on April 29, 2021 for the upstream site and at 174 ± 83 mg/L (mean ± SE) on November 3, 2021 for the downstream site. Finally, a storm event that occurred both upstream and downstream was captured

by water samplers on November 3, 2021 which allowed comparing the TSS at the two sites. The TSS at the downstream location was 174 mg/L and at the upstream location was 35 mg/L, which indicates that the TSS levels downstream of the construction site were significantly higher than the TSS levels upstream during the storm event.

During low flow events, the TSS concentration was also higher downstream of the construction site except on October 15, 2021, when the average TSS at the upstream and downstream sites were 17 and 20 mg/L, respectively. This shows the effect of construction activities on local overland erosion that increases the TSS in the creek.

A limited number of water samples was also collected in the vicinity of the construction site (Section 2), and a comparison of the TSS concentration in this zone with the TSS values collected upstream and downstream of the construction site shows higher sediment concentration in the construction site area due to local overland erosion (Figure 3.10). This issue is also evident in Figure 3.11, which shows turbidity measurements in this area, along with the upstream and downstream Tu values. Similar to the variation of the TSS concentration from upstream to downstream (Figure 3.10), the turbidity values were always higher downstream of the construction site, except on August 11, 2021. From July 15 to December 4, 2021, the average Tu upstream and downstream of the site was 13 and 17 NTU, respectively. The Tu values were much higher in the construction zone (Section 2), with a maximum value of 85 NTU. The average Tu in this area was 38 NTU. Since sediment plumes from construction activities became diluted as they moved further downstream, smaller values of TSS and Tu were measured in Section 3.

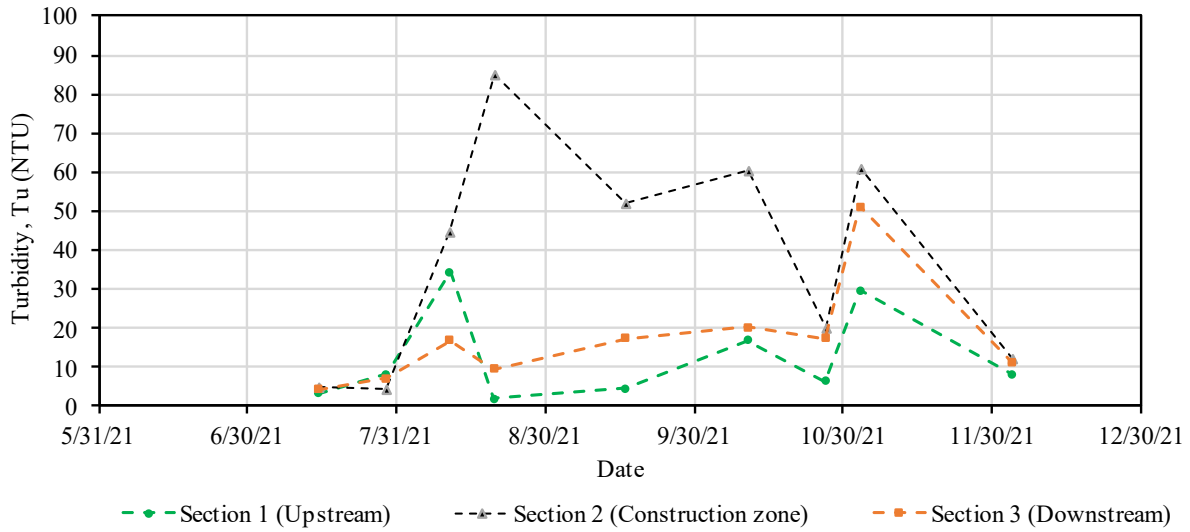


**Figure 3.11** Comparison of Tu in Wilson Creek upstream of the bridge (Section 1), in the construction zone (Section 2), and downstream of the construction site (Section 3) from July 15 to December 4, 2021

*3.1.5.2 TSS -Tu Relationship*

Available data from water samplers and discrete sampling were used to develop relationships between total suspended solids (TSS) and turbidity (Tu) for Wilson Creek, upstream of the bridge (Section 1 in Figure 3.9a) and downstream of the construction site (Section 3 in Figure 3.9a). These relationships are expressed by Equations 3.15 and 3.16 and are shown in Figure 3.12. Both relationships have a relatively high correlation coefficient ($R^2$ = 0.70 and 0.78), considering the dependency of TSS and Tu on many factors, including flow and environmental effects. Due to technical problems with the water sampler units, and therefore lack of TSS measurements for some days of the study period, Equation 3.16 was used to estimate the TSS downstream of the bridge location and validate the performance of the PTM in predicting the suspended sediment load in Wilson Creek.

TSS (mg/L)= 0.88 Tu (NTU) (Section 1) (3.15)

TSS (mg/L)= 2.66 Tu (NTU) (Section 3) (3.16)

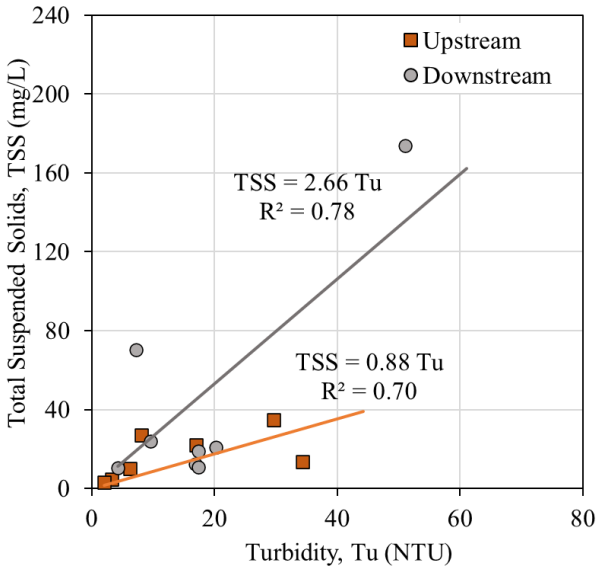


**Figure 3.12** Relationship between total suspended solids (TSS) and turbidity (Tu) in Wilson Creek upstream and downstream of the construction site

*3.1.5.3 Substrate Sampling and Delineation of Depositional Areas*

The changes in the Wilson Creek substrate were monitored downstream of the bridge site by visual inspection and the grab sampling method. The delineation of depositional areas and grab sampling were conducted in the vicinity of the bridge construction site, as well as the downstream areas, for both pre-construction and construction periods (Figure 3.13a). Before the bridge construction activities started, the creek bed was bedrock in most parts with a few patches of depositional areas (Figure 3.13b). During the construction period, more sediment was deposited along the creek. The depositional areas were delineated during each site visit, and a minimum of 500 grams of samples were collected from each area. Figure 3.13c shows grab sampling activities from the depositional areas marked in Figure 3.13a. An example of delineation of depositional areas downstream of the bridge location is shown in Figure 3.13d. Grab samples were sent to the lab, and the content of the gravel, sand, silt, and clay in the samples was measured by sieve analysis and hydrometry tests after removing debris and other objects.

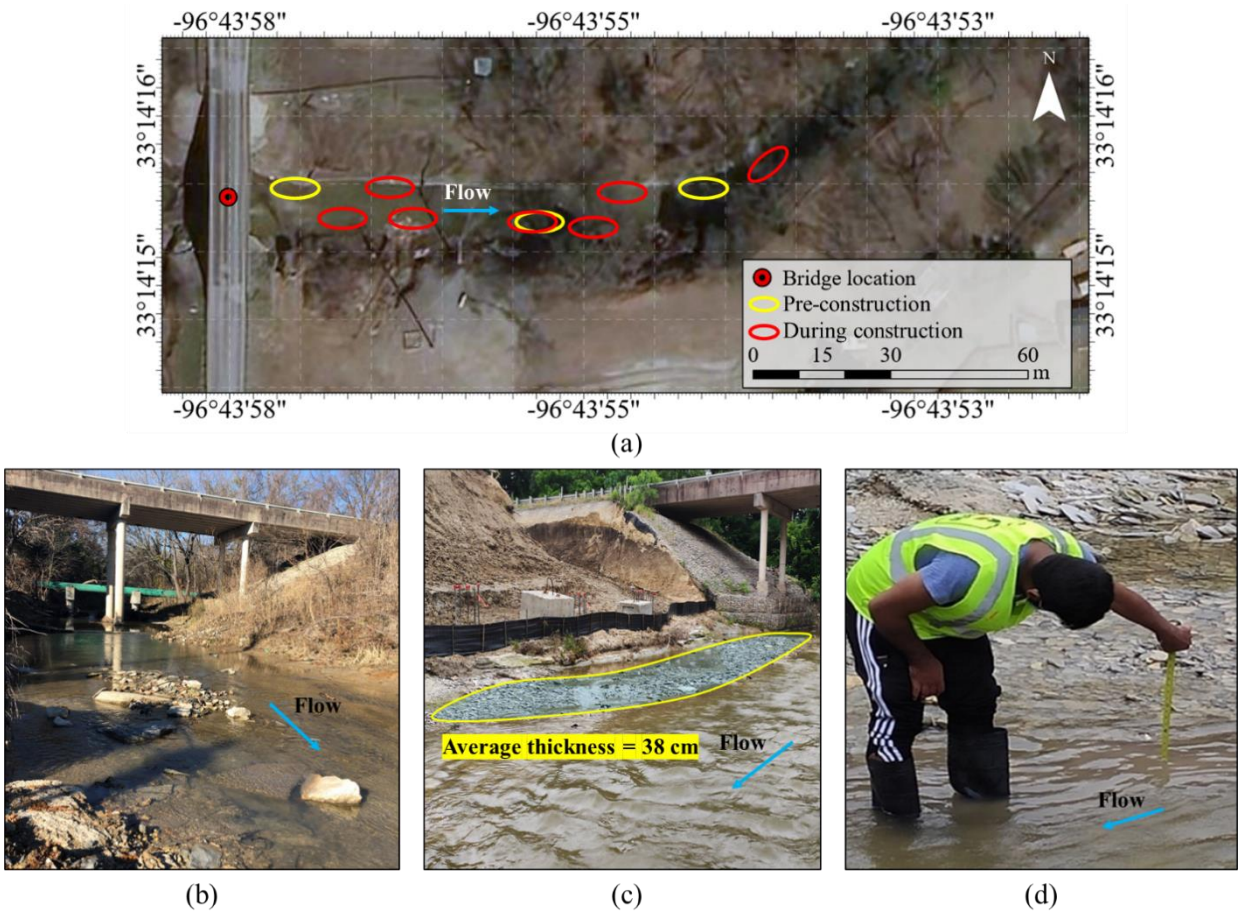


**Figure 3.13** Wilson Creek substrate monitoring program: a) Area of visual inspection and delineation and sampling locations, b) Wilson creek substrate (bedrock) downstream of the bridge before construction, c) Wilson creek depositional area downstream of the bridge during construction, and d) Delineating depositional areas

A gradation analysis of the sediment samples from the depositional areas and eroded materials from the construction sites on the north and south sides of the creek allowed estimation of the percentage of clay/silt, sand, and gravel contributing to the total sediment load entering Wilson Creek, which was used in the PTM model. The fraction and average diameter of soil particles are presented in Table 3.2. Figure 3.14 illustrates the location of the sediment sources on the south and north sides of the creek.

**Table 3.2** Fraction and Average Diameter of Sediment Particles Used in the PTM for the North and South Sediment Sources Downstream of the Bridge Location at Wilson Creek

| Sediment Class | Ave. Diameter (mm) | Fraction (%) | |
|---|---|---|---|
| | | North | South |
| Gravel | 4 | 15 | 15 |
| Sand | 0.32 | 75 | 75 |
| Silt/Clay | 0.032 | 10 | 10 |

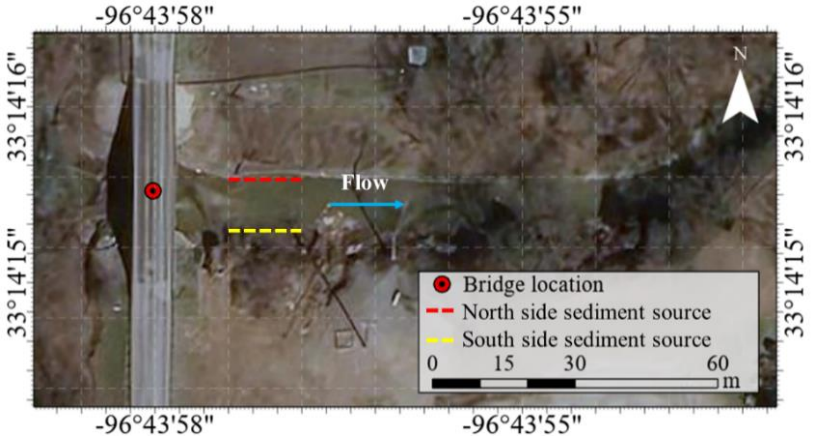


**Figure 3.14** North and south sediment sources downstream of the Wilson Creek bridge

## RESULTS AND DISCUSSION

The performance of the PTM was assessed under two flow conditions with the mean daily discharge of 37.4 $m^3/s$ and 7.4 $m^3/s$ corresponding to the April 29 and November 3, 2021 storm events. The outputs of the PTM that show changes in the sediment regime in Wilson Creek, including suspended sediment concentration and depositional areas for two storm events, are presented in the following. The sediment concentrations predicted by the PTM were compared with the historical TSS data and the results from discrete and automated water sampling during the study period. The predicted depositional areas were also compared with the field observations and measurements.

### 3.1.6 Suspended Sediment Concentration

#### *3.1.6.1 Increase in Suspended Sediment Concentration in Fully Mixed Areas*

The eroded soil from the bridge construction areas on the north and south sides (Figure 3.9a) contributed to the sediment load in Wilson Creek, and the fine particles (clay and silt) increased the TSS concentration. The increase in TSS was estimated for each day of construction using sediment yields from the north and south sides (Figure 3.8), percentage of silt/clay (Table 3.2), and mean daily discharge measured by the USGG gauge in McKinney (Figure 3.3). The added total suspended solids from the construction areas to Wilson Creek were computed and are presented in Figure 3.15. The largest daily sediment yield from both sides of the creek was estimated as 12.8 tonnes/day (April 29, 2021; Figure 3.8), which would elevate the TSS by 0.4 mg/L in the fully mixed area in the creek. The mean discharge on this day was 37.4 $m^3$/s. The second-largest sediment yields were calculated for February 26 and May 11, 2021, with a total of 9.5 and 9.8 tonnes/day, respectively. The mean streamflow during these two days was 37.4 and 9 $m^3$/s. The elevated TSS concentrations in Wilson Creek during the storm events were estimated as 0.3 and 1.3 mg/L, respectively (Figure 3.15). Despite the smaller sediment load entering the creek, the smaller streamflow on May 11, 2021 resulted in a higher TSS than that of the sediment load on April 29, 2021.

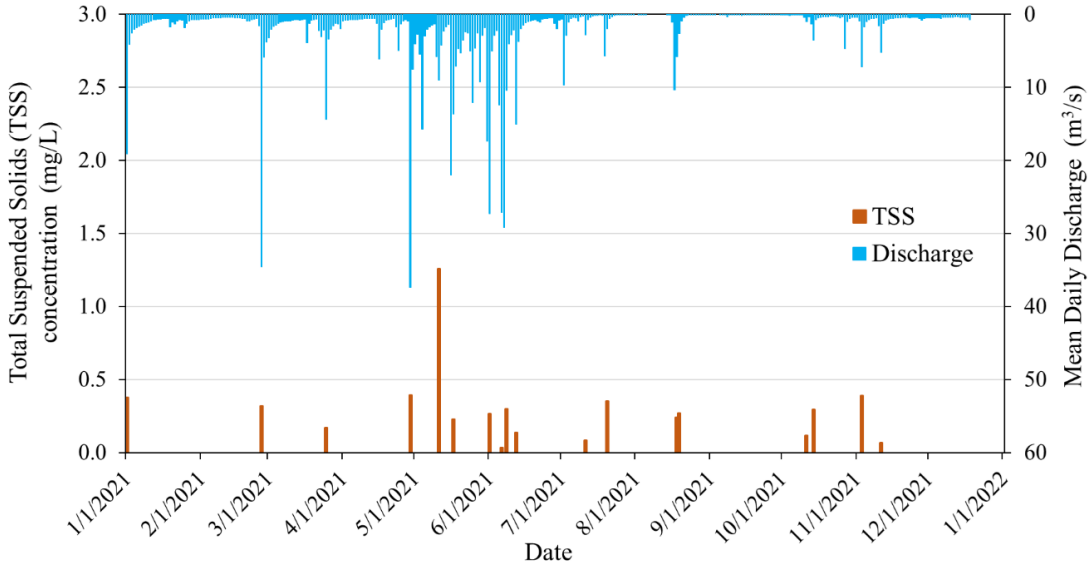


**Figure 3.15** Elevated suspended sediment concentrations in Wilson Creek due to overland erosion in north and south construction areas (Figure 3.9a), and mean daily discharge at the USGS gauge in McKinney

The estimated increase in TSS in Wilson Creek, due to local overland erosion in the construction site and the measured TSS upstream of the bridge from January 1 to December 22, 2021, is shown in Figure 3.16. During high flow events on March 25 and April 29, 2021 that had mean daily discharges of 34.5 and 37.4 $m^3/s$, the TSS in Wilson Creek upstream of the bridge was measured as 381 mg/L and 683 mg/L and was estimated to be elevated downstream of the construction area in fully mixed areas by 0.2 mg/L and 0.4 mg/L, respectively. The small contribution to Wilson Creek's suspended sediment load from the overland erosion in construction areas is justifiable, considering that the surface area of the construction site (3884 $m^2$) is only 0.012% of the Wilson Creek watershed area at the bridge site (32.3 $km^2$) (JMT 2019). The suspended sediment concentration was locally elevated during low-to-medium flows at the bridge site, even in smaller amounts (up to 0.1 mg/L). This increase is insignificant compared to the ambient TSS.

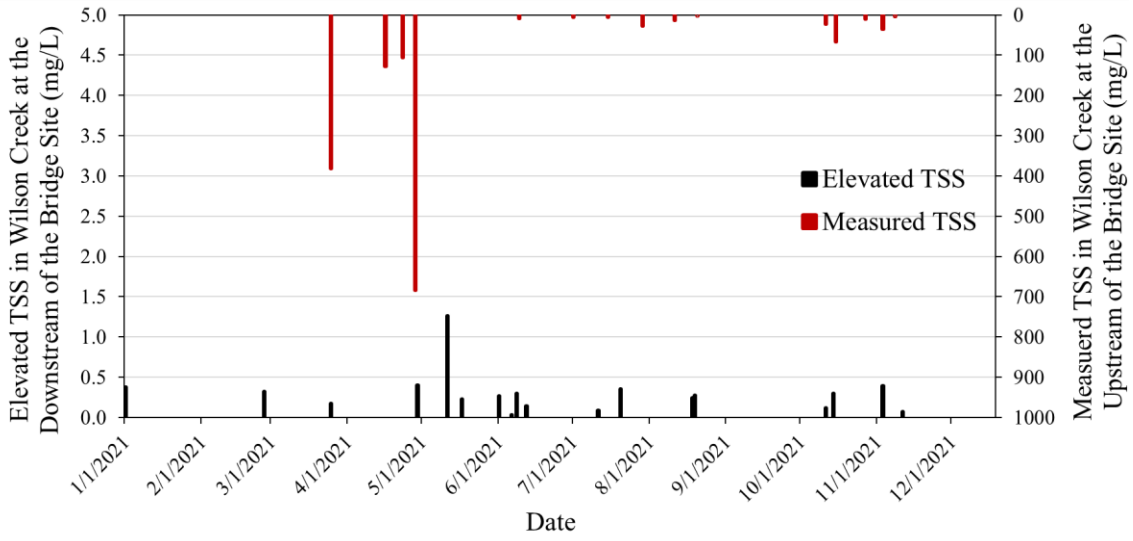


**Figure 3.16** Estimated increase in TSS in the fully mixed zone downstream of the Wilson Creek bridge due to overland erosion in construction areas, and measured TSS upstream of the bridge for the period of January 1 to December 22, 2021

The TSS in Wilson Creek was also measured sporadically between 1988 and 2019 and varied between 2 and 140 mg/L at the TCEQMAIN-10777 station, located approximately 4 km downstream of the bridge site. The streamflow for the same period varied between 0 and 3.8 $m^3/s$. The estimated increase in TSS due to local overland erosion for the period of January to December 2021 is insignificant compared to the range of TSS recorded between 1988 and 2019.

*3.1.6.2 Increase in Suspended Sediment Concentration Predicted by PTM*

In the following sections, the results of the PTM are presented for two flow scenarios ($Q$ = 37.4 $m^3/s$ on April 29, 2021, and $Q$ = 7.4 $m^3/s$ on November 3, 2021).

***Suspended Sediment Concentration Resulting from April 29, 2021 Storm***

The increase in the suspended sediment concentration in Wilson Creek estimated by the PTM for the April 29, 2021 storm is presented in Figure 3.17. The total sediment yield from the north and south sides for this day was 12.8 tonnes, larger than usual; the increase was due to the overland erosion in construction areas downstream of the bridge location (Figure 3.8). Five cross sections

(CS-1 to CS-5) were used to assess the distribution of the suspended sediment along and across the creek. As can be seen in Figure 3.9a, CS-1 and CS-2 are located in the TSS measuring areas (Sections 2 and 3 in Figure 3.9a). The TSS measurements from these two areas were used to assess the performance of the PTM in estimating the distribution of suspended sediment in Wilson Creek. Figure 3.17 shows that the increase in the suspended sediment concentration was larger along the north and south banks, where the sediment entered the creek; the maximum values were estimated as 161 and 192 mg/L, respectively. High sediment concentrations at the toes of banks are not expected, as the concentration of suspended sediment in surface runoff can be high.

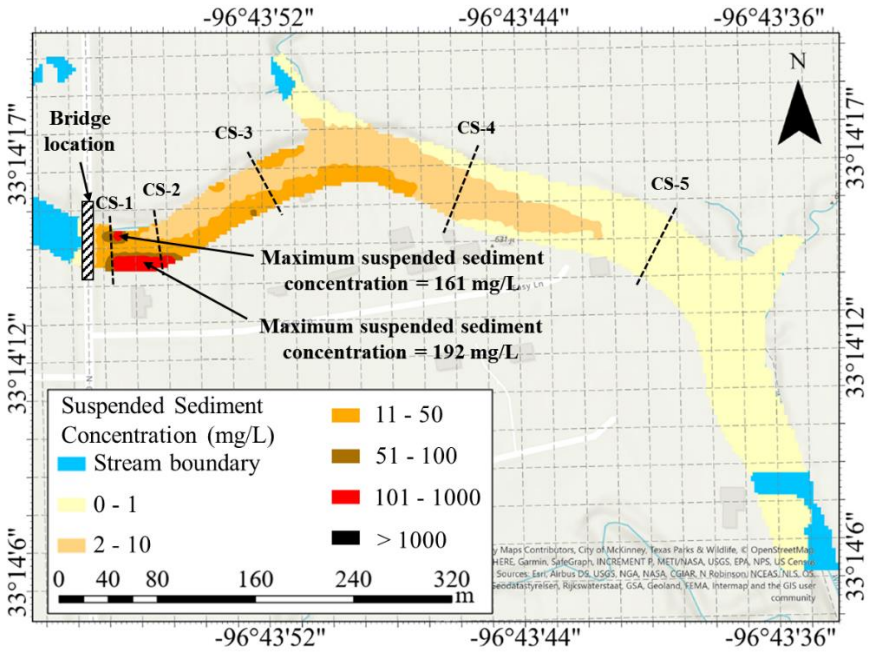


**Figure 3.17** Estimated elevated suspended sediment concentration in Wilson Creek due to overland erosion corresponding to the April 29, 2021 storm ($Q$ = 37.4 $m^3/s$ and sediment yield = 12.8 tonnes/day)

The elevated suspended sediment concentrations across CS-1 and CS-2 varied across CS-1 with two peak values of 121 and 130 mg/L corresponding to the sediment loads entering the creek from the north and south sides (Figure 3.18a). The maximum elevated sediment concentration across CS-2 was 146 mg/L near the south bank (Figure 3.18b). The high concentration values in the construction zone, where the sediment was not fully mixed with ambient, were expected. Due to

the lack of direct measurement of TSS on April 29, 2021, the suspended sediment concentration was estimated using the TSS-Tu relationship (Equation 3.16). Using this relationship and the turbidity measurements in the construction zone on 8/11, 8/20, 9/16, and 10/11/2021 revealed TSS values ranging between 120 and 226 mg/L. Considering the estimated values of TSS in Wilson Creek, the PTM predicted the suspended sediment concentrations in CS-1 and CS-2 within an acceptable range.

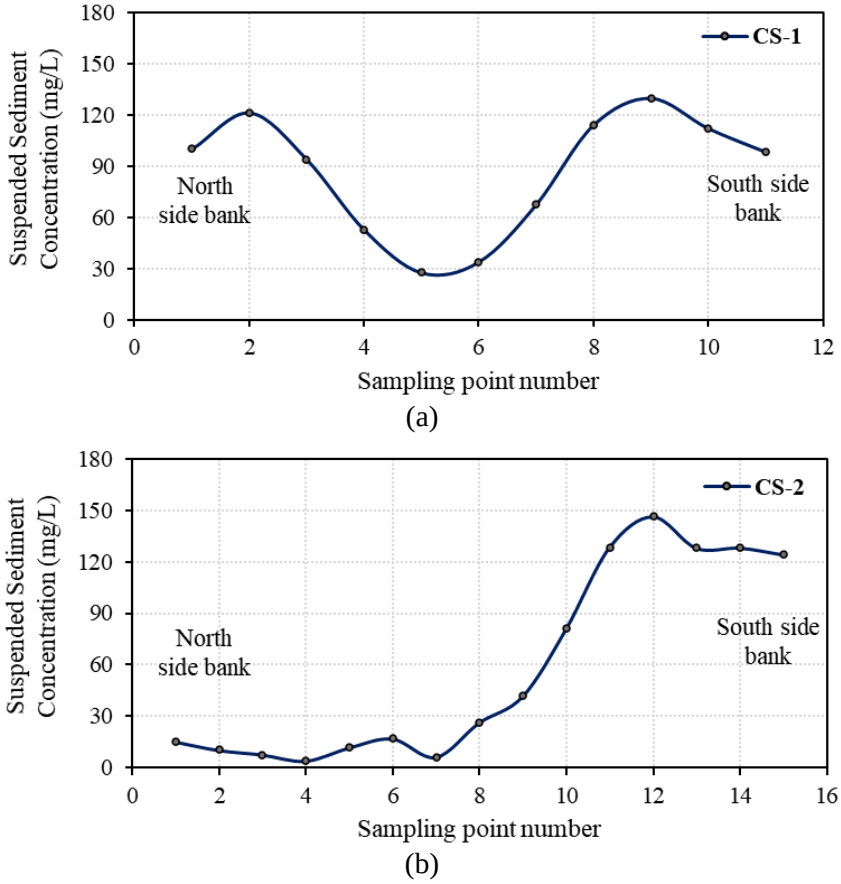


**Figure 3.18** Elevated suspended sediment concentration across Wilson Creek due to overland erosion from north and south sides corresponding to April 29, 2021, storm ($Q$ = 37.4 $m^3$/s and sediment yield = 12.8 tonnes/day): a) Cross section CS-1, b) Cross section CS-2. Cross sections are shown in Figure 3.17.

Elevated suspended sediment concentrations across Wilson Creek at cross sections CS-3 to CS-5 are depicted in Figure 3.19. As the sediment plumes originating from the north and south banks traveled downstream, they became diluted. The maximum elevated sediment concentrations across

CS-3, CS-4, and CS-5 (152, 335, and 503 m downstream of the bridge site) were estimated as 25, 3, and 0.27 mg/L, respectively. This shows that the sediment concentration decreased by 99% from CS-3 to CS-5. The cross-sectional average of elevated sediment concentration in the cross sections was estimated as 10.25, 1.2, and 0.1 mg/L.

The sediment plume was fully mixed downstream of CS-5 with negligible changes across and along the creek. The maximum elevated suspended sediment load of 0.27 mg/L in the fully mixed area (CS-5) is comparable to the result presented in Figure 3.16 that shows an elevated TSS of 0.4 mg/L on April 29, 2021.

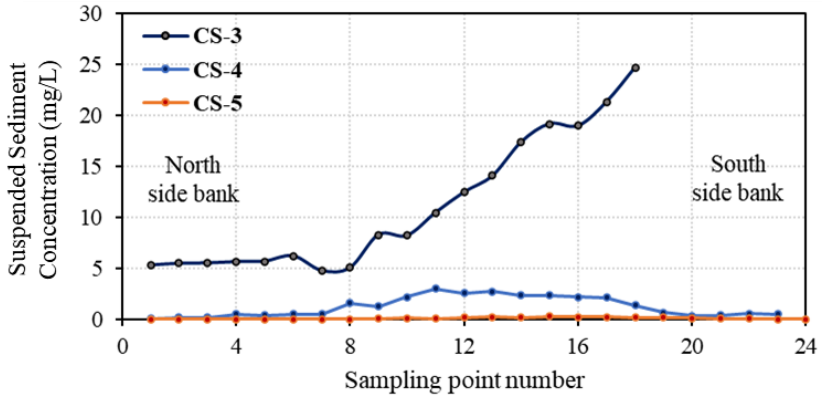


**Figure 3.19** Elevated suspended sediment concentration across Wilson Creek due to overland erosion in constructing areas corresponding to April 29, 2021 storm ($Q$ = 37.4 $m^3$/s and sediment yield = 12.8 tonnes/day) across CS-3 to CS-5. Cross sections are shown in Figure 3.17.

***Suspended Sediment Concentration - November 3, 2021 Storm***

The estimated increase in the suspended sediment concentration in Wilson Creek on November 3, 2021 was due to the overland erosion from the north and south construction areas downstream of the bridge location (Figure 3.2). The total sediment yield from the north and south sides on November 3, 2021 was 2.4 tonnes (Figure 3.8). The same cross sections (CS-1 to CS-5) were used to present the distribution of suspended sediment along and across the creek. As shown in Figure 3.20, the suspended sediment concentration increased in larger magnitudes between the bridge site

and upstream of cross section CS-4. The maximum values of elevated suspended sediment concentration in the vicinity of the north and south sides, where the sediment yield from the local areas enter the creek, were 327 and 374 mg/L, respectively.

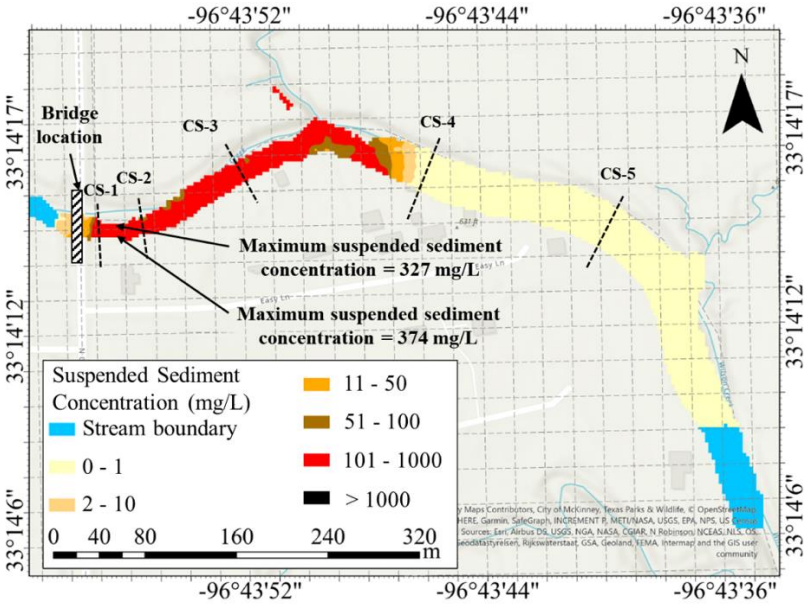


**Figure 3.20** Estimated elevated suspended sediment concentration in Wilson Creek due to overland erosion corresponding to November 3, 2021 storm ($Q$ = 7.4 $m^3/s$ and sediment yield = 2.4 tonnes/day)

The variations of suspended sediment concentration along the five cross sections shown in Figure 3.20 were used to assess changes in sediment concentration as the sediment particles moved downstream of the bridge. The changes across CS-1 and CS-2 are depicted in Figure 3.21. The location of CS-2 coincides with the location of the downstream automated water sampler installed in Wilson Creek. Figure 3.21a shows the suspended sediment concentration across CS-1 with a maximum of 415 mg/L; the corresponding value at CS-2 was 325 mg/L. The TSS was measured on November 3, 2021 at Sections 1 and 3 upstream and downstream of the bridge with two automated water samplers (Figure 3.9a). The average TSS was elevated by 139 mg/L from Section 1, located upstream of the bridge (35 mg/L), to Section 3, located downstream of the bridge (174 mg/L). The samples were taken from the center of the channel, and the PTM estimated the average elevated suspended sediment concentration as 201 mg/L (Figure 3.21b). Comparing the elevated

suspended sediment concentration estimated by PTM with the average elevated TSS recorded by the water samplers (139 mg/L) shows that the PTM overestimated the sediment concentration. However, considering the many uncertainties in modeling sediment transport and measuring it in the field, the PTM predicted the impact of the local overland erosion on the suspended sediment load in Wilson Creek with acceptable accuracy.

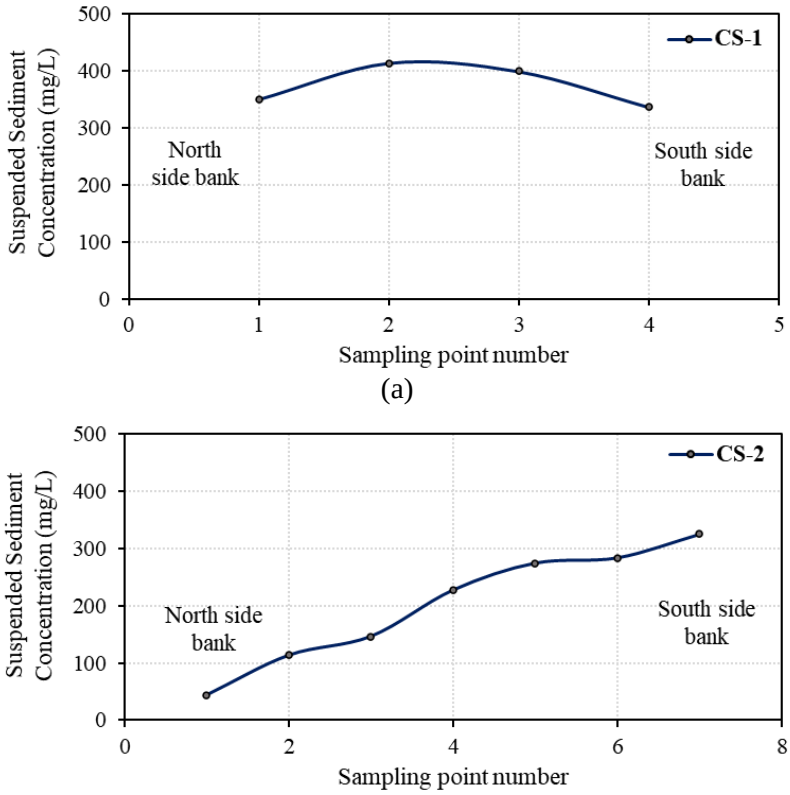


**Figure 3.21** Elevated suspended sediment concentration across Wilson Creek due to overland erosion corresponding to November 3, 2021 storm ($Q$ = 7.4 $m^3$/s and sediment yield = 2.4 tonnes/day): a) Cross section CS-1, and b) Cross section CS-2. Cross sections are shown in Figure 3.20

The sediment concentration values changed slightly across CS-3, CS-4, and CS-5 (Figure 3.22), but as the sediment plumes passed CS-3, the elevated concentration values dropped rapidly, reducing the cross-sectional average sediment concentration from 145 mg/L at CS-3 to almost zero at CS-4 and CS-5. The sediment plume was fully mixed at CS-3, with negligible changes across the creek.

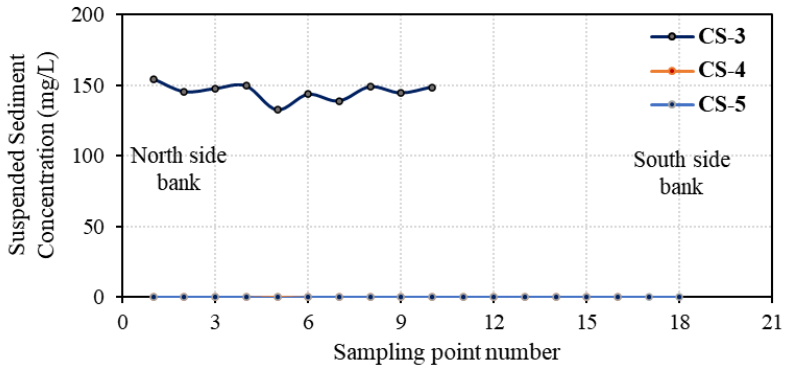


**Figure 3.22** Elevated suspended sediment concentration across Wilson Creek due to overland erosion corresponding to November 3, 2021 storm ($Q$ = 7.4 $m^3/s$ and sediment yield = 2.4 tonnes/day. Cross sections are shown in Figure 3.20

### 3.1.7 Depositional Areas

Predicted depositional areas along Wilson Creek downstream of the bridge site corresponding to April 29, 2021 ($Q$ = 37.4 $m^3/s$) and November 3, 2021 ($Q$ = 7.4 $m^3/s$) storm events are shown in Figure 3.23. As can be seen, the gravel particles that entered the creek from the north and south banks deposited very quickly on the edge of the water on both sides downstream of the bridge location (S1 and S2). During the high flow condition (April 29, 2021), most of the sand particles moved along the north and south sides of the channel and were deposited further downstream in an area that started 216 m downstream of the bridge and extended 542 m along the length of the creek (Figure 3.23a). During the low flow on November 3, most of the sand materials were moved by the flow and deposited in a limited area 300 m downstream of the bridge (Figure 3.23b). Silt and clay particles were deposited during both flow scenarios; however, the silt and clay depositional areas for $Q$ = 7.4 $m^3/s$ (Figure 3.23b) were significantly larger than those of the flow with $Q$ = 37.4 $m^3/s$ (Figure 3.23a). These results show that larger flows potentially transport sand and silt/clay particles further downstream in Wilson Creek.

Predicted depositional areas S1 to S4 match with the field observations. Figures 3.24a and b show two gravel depositional areas downstream of the bridge along the north and south banks that were delineated on June 2021, after the creek experienced several high flow events, including the April 29, 2021 storm. Samples taken from these areas were mainly composed of gravel and coarse materials. Sand and depositional areas were also found at S3 and S4 during the field visits (Figures 3.24c and d); no sediment was deposited in the area between S1-S2 and S3-S4, as predicted by the PTM and observed in the field (Figure 3.24e).

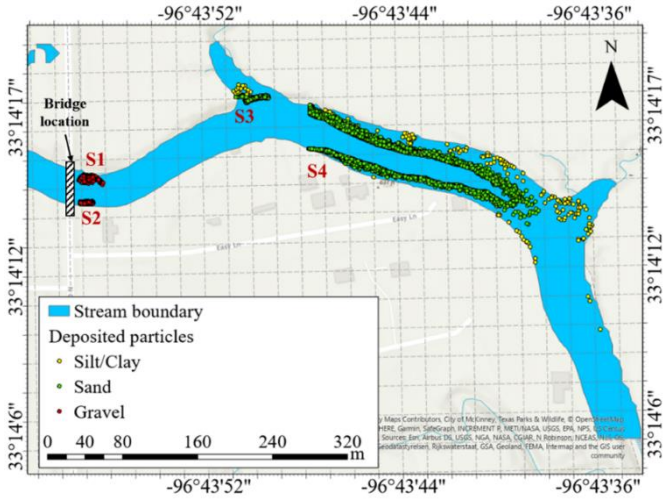


(a)

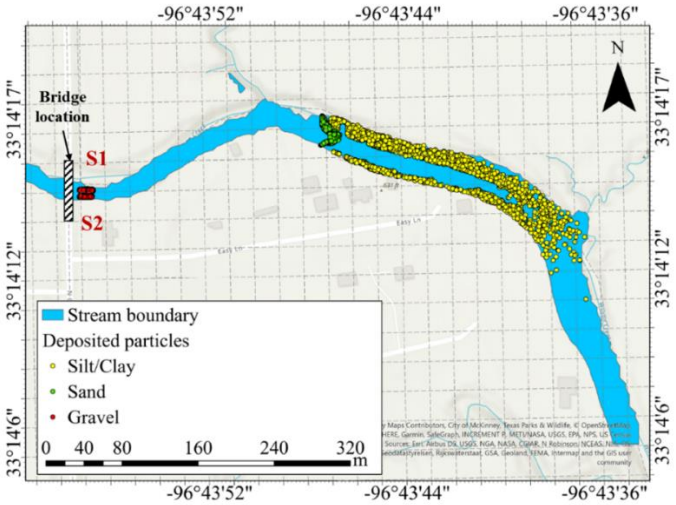


(b)

**Figure 3.23** Depositional areas in Wilson Creek predicted by the PTM, due to overland erosion materials entering the creek from north and south construction areas corresponding to: a) April 29, 2021 storm ($Q$ = 37.4 $m^3/s$), and b) November 3, 2021 storm ($Q$ = 7.4 $m^3/s$)

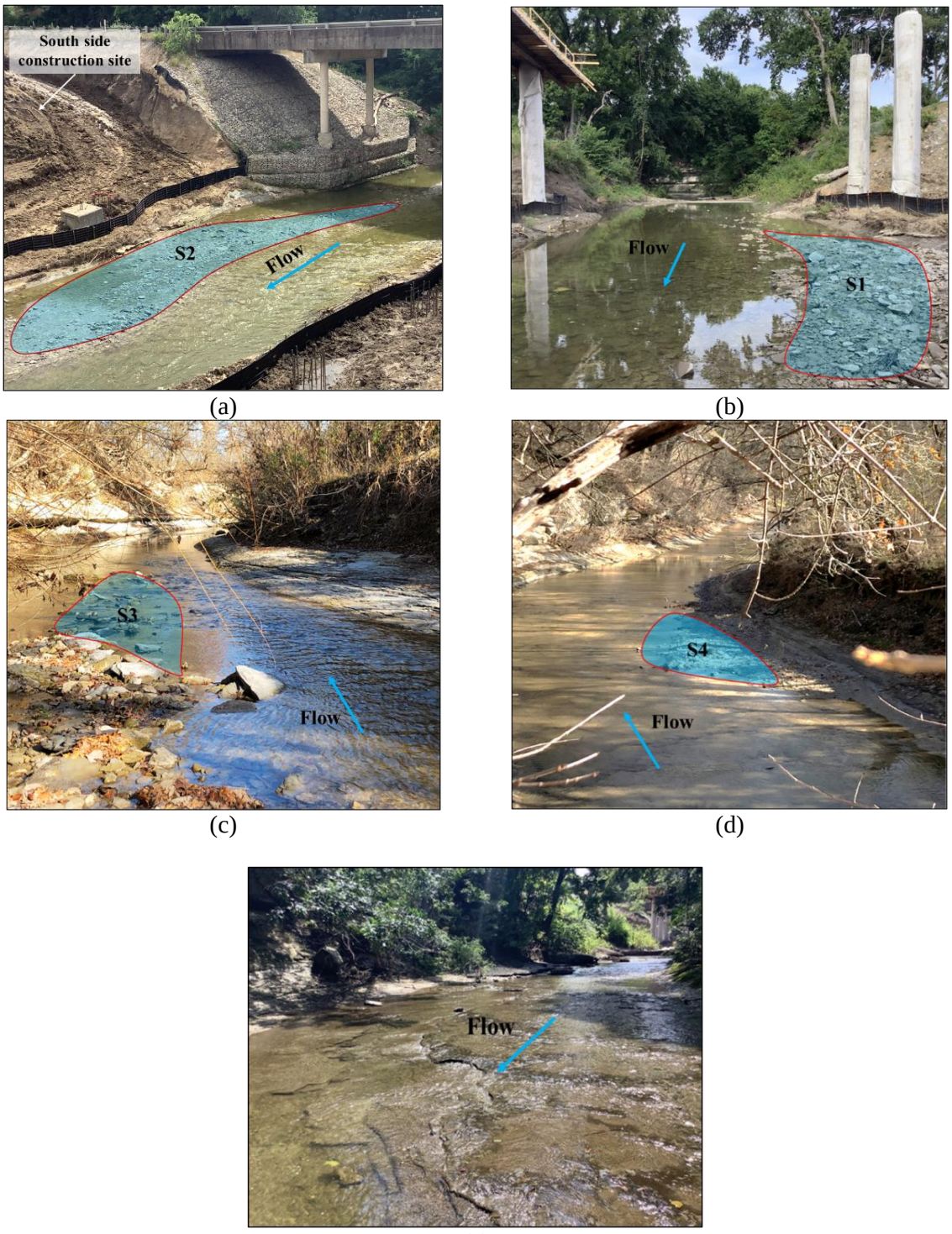


**Figure 3.24** Delineated depositional and non-depositional areas in Wilson Creek: a) to d) S1 to S4 depositional areas, and e) non-depositional area

## CONCLUSIONS AND RECOMMENDATIONS FOR FUTURE RESEARCH

The particle tracking model developed by Baharvand et al. (2022) for open channel flows was adopted and modified for this study to simulate sediment transport in natural streams. It considers advection and dispersion transport equations for sediment particles in a two-dimensional flow domain simulated by the HEC-RAS 2D model developed for the study area. The geospatial information, including velocity, shear stress, and flow depth, were extracted from the HEC-RAS model and introduced to the PTM.

The performance of the PTM was evaluated using field data. A section of Wilson Creek near Highway FM 2478 in McKinney, Texas was selected as the study area, as the road and bridge expansion project were expected to introduce additional sediment loads to the creek during the construction period. The PTM was used to simulate sediment transport in the creek during construction activities. The sediment yield from local sediment sources, i.e., overland erosion in the construction area, was obtained from previous studies. The field monitoring program conducted during the construction period included collecting data on TSS, Tu, bedload material, substrate type, and depositional areas.

The performance of the PTM was assessed under two flow conditions, with the mean daily discharge of 37.4 $m^3/s$ and 7.4 $m^3/s$ corresponding to the April 29 and November 3, 2021 storm events, respectively. The outputs of the PTM showed changes in the Wilson Creek sediment regime in the vicinity of the bridge, including an increase in the suspended sediment concentration and sediment deposition. In both flow scenarios, the PTM predicted the depositional areas in locations similar to those where the sediment deposition had been observed. The predicted increase in suspended sediment concentration in Wilson Creek was comparable to the expected values and field data.

Since the model's performance was promising, it is recommended that it be used by river authorities and other agencies to simulate sediment transport in natural streams for project planning and management purposes. It may also be utilized to assess the effect of construction activities in or near waterbodies on water quality and stream geomorphology, the information that is required for predicting the short- and long-term impacts of construction activities on stream health.

The present model simulates suspended sediment loads under a steady-state flow condition. Further research is needed to determine whether adding the unsteady flow condition and bedload transport would enhance the capabilities of the PTM. Due to the important role of dispersion coefficients in sediment transport modeling, it is also suggested that the impact of different dispersion modeling techniques on sediment transport be evaluated, using the PTM in natural streams.

**Acknowledgment**

The present study was supported by the Texas Department of Transportation (TxDOT) under project Number 0-7023.

**Conflict of Interest** The authors declare no conflict of interest.

## REFERENCES


Ahmari, H., Baharvand, S., Pebworth, M. (2021). "Developing an ArcGIS Pro Toolkit for assessing bridge construction effects on sediment regime and aquatic habitat." 20th *Iranian Hydraulic Conference*, Gorgan University of Agricultural Sciences and Natural Resources, Gorgan, Iran.

Ahmari, H., Randklev, C. R., Jaber, F., Yu, X., Baharvand, S., Pebworth, M., Kandel, S., and Goldsmith, A. M. (2022). "Determining downstream ecological impacts of sediment derived from bridge construction." TxDOT Report No. 0-7023.

Allison, M. A., Yuill, B. T., Meselhe, E. A., Marsh, J. K., Kolker, A. S., and Ameen, A. D. (2017). "Observational and numerical particle tracking to examine sediment dynamics in a Mississippi River delta diversion." *Estuarine, Coastal and Shelf Science*, 194, 97–108.

Amoudry, L. O., and Souza, A. J. (2011). "Deterministic coastal morphological and sediment transport modeling: A review and discussion." *Reviews of Geophysics*, 49(2), RG2002.

Baharvand, S., Ahmari, H., Taghvaei, P. (2022). "Developing a three-dimensional Lagrangian sediment transport model For open channel flows." *International Journal of Sediment Research*, Elsevier, (submitted).

Beckers, F., Noack, M., and Wieprecht, S. (2018). "Uncertainty analysis of a 2D sediment transport model: an example of the Lower River Salzach." *Journal of Soils and Sediments*, 18(10), 3133–3144.

Bennett, G., Molnar, P., McArdell, B., Burlando, P. (2014). "A probabilistic sediment cascade model of sediment transfer in the Illgraben." *Water Resource Research*, 50(2):1225–1244.

Berenbrock, C., and Tranmer, A.W., (2008). "Simulation of flow, sediment transport, and sediment mobility of the Lower Coeur d'Alene River, Idaho." U.S. Geological Survey Scientific Investigations Report 2008–5093, 164 p.

Bilotta, G. S., and Brazier, R. E. (2008). "Understanding the influence of suspended solids on water quality and aquatic biota." *Water Research*, 42(12), 2849–2861.

Brunner, G. W. (2016). "HEC-RAS River Analysis System - Hydraulic Reference Manual, Version 5.0." Hydrologic Engineering Centre (HEC), U. S. Army Corps of Engineers.

Camenen, B., and Larroudé, P. (2003). "Comparison of sediment transport formulae for the coastal environment." *Coastal Engineering*, 48(2), 111–132.

De Baas, A. F., Van Dop, H., and Nieuwstadt, F. T. M. (1986). "An application of the Langevin equation for inhomogeneous conditions to dispersion in a convective boundary layer." *Quarterly Journal of the Royal Meteorological Society*, 112(471), 165–180.

Dunn, R., Zigic, S., Burling, M., and Lin, H.-H. (2015). "Hydrodynamic and sediment modelling within a macro tidal estuary: Port Curtis Estuary, Australia." *Journal of Marine Science and Engineering*, 3(3), 720–744.

Einstein, H. A. (1950). "The bed-load function for sediment transportation in open channel flows." vol 1026. United States Department of Agriculture, U.S. Government Printing Office, Washington, D.C.

Elder, J. W. (1959). "The dispersion of marked fluid in turbulent shear flow." *Journal of Fluid*

*Mechanics*, 5(4), 544–560.

United States Environmental Protection Agency (2017). "EnviroAtlas. Total Suspended Solids (TSS)-EPA Method160.2." Retrieved: 01,19,2017, from https://19january2017snapshot.epa.gov/sites/production/files/2015-06/documents/160_2.pdf.

Fang, H.W., and Rodi, W. (2003). "Three-dimensional calculations of flow and suspended sediment transport in the neighborhood of the dam for the Three Gorges Project (TGP) reservoir in the Yangtze River." *Journal of Hydraulic Research*, 41(4), 379–394.

Ferring, C. R. (1994). "Late Quaternary geology of the upper Trinity River basin, Texas." Doctoral dissertation, The University of Texas at Dallas.

Gualtieri, C., and Mucherino, C. (2008). "Comments on 'Development of an empirical equation for the transverse dispersion coefficient in natural streams' by Tae Myoung Jeon, Kyong Oh Baek and Il Won Seo." *Environmental Fluid Mechanics*, 8(1), 97–100.

Hache, I., Niehüser, S., Karius, V., Arns, A., and von Eynatten, H. (2021). "Assessing sediment accumulation at inundated anthropogenic marshland in the southeastern North Sea: Using particle tracking on modified coastal protection structures." *Ocean & Coastal Management*, 208, 105631.

Hajigholizadeh, M., Melesse, A., and Fuentes, H. (2018). "Erosion and sediment transport modelling in shallowwWaters: A review on approaches, models and applications." *International Journal of Environmental Research and Public Health*, 15(3), 518.

Hall, E. S., Hall, R. K., Aron, J. L., Swanson, S., Philbin, M. J., Schafer, R. J., Jones-Lepp, T., Heggem, D. T., Lin, J., Wilson, E., and Kahan, H. (2019). "An ecological function approach to managing harmful Cyanobacteria in three Oregon lakes: Beyond water quality advisories and total maximum daily loads (TMDLs)." *Water*, 11(6), 1125.

Harmel, R. D., Richardson, C. W., King, K. W., and Allen, P. M. (2006). "Runoff and soil loss relationships for the Texas Blackland Prairies ecoregion." *Journal of Hydrology*, 331(3-4), 471-483.

Havens, H., Luther, M. E., Meyers, S. D., and Heil, C. A. (2010). "Lagrangian particle tracking of a toxic dinoflagellate bloom within the Tampa Bay estuary." *Marine Pollution Bulletin*, 60(12), 2233–2241.

Hantush, M. M., and Kalin, L. (2004). "Evaluation of Sediment Transport Models and Comparative Application of Two Watershed Models." Environmental Protection Agency Report, Washington, DC.

Huntley, D.A., Bowen, A.J. (1989). "Modeling sand transport on continental shelves." In: Davies, A.M. (Ed.), Modeling Marine Systems. CRC Press, Boca Raton, pp. 221–254.

Ji, C., Munjiza, A., Avital, E., Ma, J., and Williams, J. J. R. (2013). "Direct numerical simulation of sediment entrainment in turbulent channel flow." *Physics of Fluids*, 25(5), 056601.

JMT (2019). "Drainage Study for the Proposed FM 2478 (Custer Road) Structures at Rutherford Branch and Wilson Creek." TxDOT report.

Kiat, C. C., Ghani, A. A., Abdullah, R., and Zakaria, N. A. (2008). "Sediment transport modeling

for Kulim River – A case study." *Journal of Hydro-environment Research,* 2(1), 47–59.

Kim, B., Sanders, B. F., Schubert, J. E., and Famiglietti, J. S. (2014). "Mesh type tradeoffs in 2D hydrodynamic modeling of flooding with a Godunov-based flow solver." *Advances in Water Resources,* 68, 42–61.

Lackey, T., and Smith, S. (2008). "Application of the Particle Tracking Model To Predict the fate of Dredged Suspended Sediment at the Willamette River." *Proceedings Western Dredging Association Twenty-Eighth Annual Technical Conference.*

Lackey, T. C., Bailey, S. E., Gailani, J. Z., Kim, S. C., and Schroeder, P. R. (2020). "Hydrodynamic and Sediment Transport Modeling for James River Dredged Material Management." Engineer Research and Development Center Vicksburg.

Ley, A. J. (1982). "A random walk simulation of two-dimensional turbulent diffusion in the neutral surface layer." *Atmospheric Environment,* 16(12), 2799–2808.

Liu, W.-C., Chen, W. B., Cheng, R. T., Hsu, M. H., and Kuo, A. Y. (2007). "Modeling the influence of river discharge on salt intrusion and residual circulation in Danshuei River estuary, Taiwan." *Continental Shelf Research,* 27(7), 900–921.

Liu, W.-C., Hsu, M.-H., and Kuo, A. Y. (2002). "Modelling of hydrodynamics and cohesive sediment transport in Tanshui River estuarine system, Taiwan." *Marine Pollution Bulletin,* 44(10), 1076–1088.

Lopez, R., Vericat, D., Batalla, R. J. (2014). "Evaluation of bed load transport formulae in a large regulated gravel bed river: the lower Ebro (NE Iberian Peninsula)." *Journal of Hydrology,* 510:164–181.

MacDonald, N. J., Davies, M. H., Zundel, A. K., Howlett, J. D., Demirbilek, Z., Gailani, J. Z., ... & Smith, J. (2006). "PTM: particle tracking model. Report 1: Model theory, implementation, and example applications." Engineering Research and Development Center, Vicksburg MS Coastal and Hydraulic Lab.

Maier, N.D., and Dunkin, J.T. (1988). "McKinney Floodplain Management Study: Wilson Creek, Franklin Branch, Stover Creek, Honey Creek." Prepared for City of McKinney, Texas.

Malmon, D. V., Dunne, T., Reneau, S. L. (2003). "Stochastic theory of particle trajectories through alluvial valley floors." *Journal of Geology,* 111(5):525–542.

Mengual, B., Le Hir, P., Rivier, A., Caillaud, M., and Grasso, F. (2021). "Numerical modeling of bedload and suspended load contributions to morphological evolution of the Seine Estuary (France)." *International Journal of Sediment Research*, 36(6), 723–735.

Muste, M., Yu, K., Fujita, I., and Ettema, R. (2009). "Two-phase flow insights into open-channel flows with suspended particles of different densities." *Environ Fluid Mech,* 9(2):161–186.

Moring, J. B. (2009). "Effects of urbanization on the chemical, physical, and biological characteristics of small Blackland prairie streams in and near the Dallas-Fort Worth metropolitan area, Texas." Chapter C in effects of urbanization on stream ecosystems in six metropolitan areas of the United States (No. 2006-5101-C). US Geological Survey.

Oh, J. (2011). "Stochastic particle tracking modeling for sediment transport in open channel flows." Ph.D. dissertation. State University of New York at Buffalo.

Periáñez, R., Casas-Ruíz, M., and Bolívar, J. P. (2013). “Tidal circulation, sediment and pollutant transport in Cádiz Bay (SW Spain): A modelling study.” *Ocean Engineering*, 69, 60–69.

Pinto, L., Fortunato, A. B., and Freire, P. (2006). “Sensitivity analysis of non-cohesive sediment transport formulae.” *Continental Shelf Research*, 26(15), 1826–1839.

Priya K. L., Jegathambal P., and James, E. J. (2016). “Salinity and suspended sediment transport in a shallow estuary on the east coast of India.” Reg Stud Mar Sci 7:88–99.

Safari M.J.S., Aksoym H., and Mohammadi, M. (2016). “Artificial neural network and regression models for flow velocity at sediment incipient deposition.” *Journal of Hydrology*, 541:1420–1429.

Sulaiman, S. O., Al-Ansari, N., Shahadha, A., Ismaeel, R., and Mohammad, S. (2021). “Evaluation of sediment transport empirical equations: case study of the Euphrates River West Iraq.” *Arabian Journal of Geosciences*, 14(10), 825.

Tao, H., Keshtegar, B., and Yaseen, Z. M. (2019). “The feasibility of integrative radial basis M5tree predictive model for river suspended sediment load simulation.” *Water Resources Management*, 33(13), 4471–4490.

Tsai, C. W., Man, C., and Oh, J. (2014). “Stochastic particle based models for suspended particle movement in surface flows.” *International Journal of Sediment Research*, 29(2), 195–207.

Tsai, C. W., Hung, S. Y., and Oh, J. (2018). “A stochastic framework for modeling random-sized batch arrivals of sediment particles into open channel flows.” *Stochastic Environmental Research and Risk Assessment*, 32(7), 1939–1954.

Van Rijn, L.C., (1987). “Mathematical modelling of morphological processes in the case of suspended sediment transport.” Waterloopkundig Lab., Delft Hydraulics Comm-382.

Van Rijn, L.C. (1993). “Principles of Sediment Transport in Rivers, Estuaries and Coastal Seas.” Aqua Publications, Amsterdam, The Netherlands.

Warner, J. C., Sherwood, C. R., Signell, R. P., Harris, C. K., and Arango, H. G. (2008). “Development of a three-dimensional, regional, coupled wave, current, and sediment-transport model.” *Computers & Geosciences*, 34(10), 1284–1306.

Wu, W. (2004). “Depth-averaged two-dimensional numerical modeling of unsteady flow and non-uniform sediment transport in open channels.” *Journal of Hydraulic Engineering*, 130(10), 1013–1024.

Zhang, W., and Montgomery, D. R. (1994). “Digital elevation model grid size, landscape representation, and hydrologic simulations.” *Water Resources Research*, 30(4), 1019–1028.

Zhao, E., Mu, L., Qu, K., Shi, B., Ren, X., and Jiang, C. (2018). “Numerical investigation of pollution transport and environmental improvement measures in a tidal bay based on a Lagrangian particle-tracking model.” *Water Science and Engineering*, 11(1), 23–38.

# CHAPTER 4

# APPLICATION OF MACHINE LEARNING APPROACHES TO PARTICLE TRACKING MODEL TO ESTIMATE SEDIMENT TRANSPORT IN NATURAL STREAMS


## ABSTRACT

Longitudinal and transverse dispersion coefficients are important parameters for modeling sediment transport in natural streams. Several empirical equations and machine learning approaches have been developed to predict these two dispersion coefficients in open channels; however, the ability of some learning-based models to predict dispersion coefficients has not yet been evaluated and the direct application of machine learning-based dispersion coefficients to Lagrangian sediment transport models has not yet been studied. In this research, data from previous studies is used to evaluate the ability of two ensemble machine learning models, random forest regression and gradient boosting regression, to predict longitudinal and transverse dispersion in natural streams. The optimal principal parameters of ensemble models were adjusted using the grid-search cross-validation (GridsearchCV) technique, and the ML-based dispersion models were integrated with a Lagrangian particle tracking model (PTM) to simulate suspended sediment concentration in natural streams. The resulting suspended sediment concentration distribution was compared with water samples from different hydraulic scenarios that were collected from a field monitoring program during construction activities at Wilson Creek in McKinney, Texas. The study showed that the GBR model, with a coefficient of determination ($R^2$) of 0.95, performed better than the RFR model, with a coefficient of determination of 0.9, in predicting the longitudinal

dispersion coefficients in a natural stream in both the training and testing stages. However, the RFR model ($R^2$ = 0.94) performed better than the GBR in predicting the transverse dispersion in testing stage. Both models underestimated the dispersion coefficients in the training and testing stages. Comparison between the PTM with ensemble dispersion coefficients and empirical-based dispersion relationships revealed the better performance of the GBR model compared to the other two methods. However, all the models showed acceptable accuracy in predicting the suspended sediment concentration distribution in natural streams.

**Author Keywords:** sediment transport, natural streams, particle tracking model, ensemble models, machine learning.

## INTRODUCTION

The sediment regime in natural streams can be altered by anthropogenic activities such as agriculture (Peacock et al., 2005), logging (Beschta 1978), mining (Seakem Group et al., 1992), urbanization (Guy and Ferguson 1963), bridge and dam constructions (Ahmari et al., 2021; Ahmari et al., 2013a and 2013b), and hydrological alteration (Black 1995; Hastie et al., 2001), as the eroded material from these activities adds to the sediment load, which can significantly impact water quality and threaten the lives and abodes of aquatic species (Tao et al., 2019; Ahmari et al., 2021; Sulaiman et al., 2021). Numerical models have been utilized to assess sediment transport in natural streams (Wu 2004; Fang and Rodi 2003) and estuaries (Tu et al., 2019; Ouda and Toorman 2019); however, the mechanisms of sediment movements in a flow domain are not well understood (Shi and Yu 2015). In recent decades, advancements in computer technology have significantly improved hydraulic and sediment transport numerical models that use computational techniques to solve mathematical equations governing flow and sediment movements in open channels. The choice of a model for each specific problem depends on the project's requirements, availability of data, and knowledge about the physical processes that determine the system's behavior.

There are two approaches to modelling sediment transport in streams: Eulerian-Eulerian and Eulerian-Lagrangian (Shi and Yu 2015). Eulerian-Eulerian models simulate sediment movement as a continuous phase and consider the statistical properties of the sediment cloud, while Eulerian-Lagrangian models consider sediment particles as a dispersed phase and the movement of individual sediment particles is tracked in the flow domain.

Eulerian-Eulerian sediment transport models determine sediment concentrations within a control volume, using deterministic differential equations to solve flow and sediment transport equations (Oh 2011). The models require very small grid spacing to provide reasonable solutions in

environments with a sudden change in suspended solids concentration, such as sediment plumes downstream of a construction site or accidental spills. This method requires significantly less computational effort than is needed for the Eulerian-Lagrangian models (Shi and Yu 2015), but the computation time and modeling cost  is usually greater (MacDonald et al., 2006). Several studies have shown the applicability of stochastic models that consider random movements of particles for modelling sediment motion behavior (Tsai et al., 2020; Park and Seo, 2018; Oh and Tsai 2018; Fan et al., 2016; Tsai et al., 2014; Macdonald et al., 2006; Niño and García 1998). The majority of stochastic models are Lagrangian models that simulate natural processes such as sediment entrainment or deposition (Oh 2011). Lagrangian stochastic models have proven to be accurate methods for tracking sediment particles in turbulent flows (Ley and Thomson 1983; De Baas et al., 1986). In this method, a particle tracking model (PTM) tracks individual sediment particles in the flow domain, using discretized advection and dispersion terms. Therefore, any changes in advection and dispersion terms have the potential to directly affect the movement of sediment particles.

Advection shows the effect of flow velocity on the movement of particles, and the dispersion coefficient shows the diffusivity effect. The longitudinal and transverse dispersion coefficients address variations of suspended sediment concentration along and across a stream channel. Figure 4.1 shows the results of sediment transport modeling in a prismatic open channel and the temporal and spatial distribution of suspended sediment concentration in the longitudinal and transverse directions (Baharvand et al., 2022a).

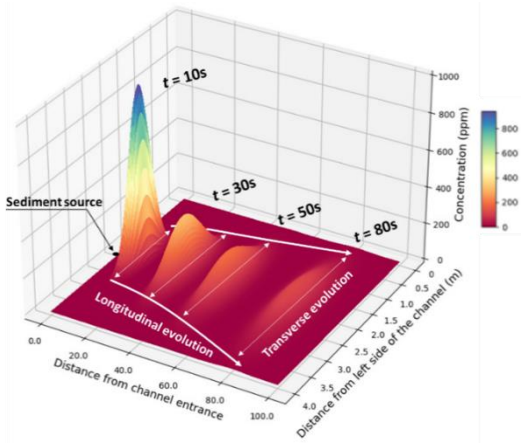


**Figure 4.1** Temporal and spatial evolution of suspended sediment concentration in longitudinal and transverse directions of a prismatic rectangular open channel (Baharvand et al., 2022a)

Despite studies on modeling sediment transport in waterbodies, the effects of several parameters of sediment transport are not well understood (Lick 2009). The dispersion coefficient is one of the essential parameters in modeling sediment transport in natural streams, and several empirical equations, shown in Table 4.1, have been developed to estimate longitudinal ($D_x$) and transverse ($D_y$) dispersion coefficients. In these equations, $H$ is water depth, $u$ is depth-average velocity, $u_*$ is shear velocity, $W$ is stream width, and $S_n$ is stream sinuosity coefficient.

**Table 4.1** Commonly Used Longitudinal and Transverse Dispersion Empirical Equations

| Dispersion term | Equation | Reference | Equation No. |
|---|---|---|---|
| Longitudinal | $D_x = 5.93\, Hu_*$ | Elder (1959) | (4.1) |
| Longitudinal | $D_x = 5.92\, Hu_* \left(\frac{u}{u_*}\right)^{1.43} \left(\frac{W}{H}\right)^{0.62}$ | Seo and Cheong (1998) | (4.2) |
| Longitudinal | $D_x = 10.612\, Hu \left(\frac{u}{u_*}\right)$ | Kashefipour and Falconer (2002) | (4.3) |
| Longitudinal | $D_x = 2\,(Hu_*) \left(\frac{u}{u_*}\right)^{1.25} \left(\frac{W}{H}\right)^{0.96}$ | Sahay and Dutta (2009) | (4.4) |
| Transverse | $D_y = 0.23\, Hu_*$ | Fischer and Park (1967) | (4.5) |
| Transverse | $D_y = 0.291\, Hu_* (\frac{W}{H})^{0.463} \left(\frac{u}{u_*}\right)^{0.299} (S_n)^{0.733}$ | Jeon et al. (2007) | (4.6) |
| Transverse | $D_y = 0.15\, Hu_*$ | Ahmad (2007) | (4.7) |
| Transverse | $D_y = 0.166\, Hu_*$ | Gualtieri and Mucherino (2008) | (4.8) |

In recent years, machine learning (ML) approaches have been used in several studies as an alternative to empirical equations to predict the dispersion coefficient in natural streams. The main advantage of using ML models (also known as soft computing techniques) is their independency from the physics of the problem (Baharvand et al., 2021; Salazar and Crookston 2019). Several studies have examined the ability of these approaches to predict longitudinal dispersion coefficients. For example, Toprak and Savci (2007) compared the performance of a learning-based model, fuzzy logic, with different empirical equations (e.g., an equation proposed by Kashefipour and Falconer 2002), and showed the superiority of fuzzy logic models. Toprak and Cigizoglu (2008) also compared the accuracy of several ML models (i.e., feed-forward back propagation, radial basis function-based neural networks, and generalized regression neural networks) with different widely used empirical longitudinal dispersion coefficient equations and concluded that ML-based models are more reliable and more accurate than empirical equations in predicting longitudinal dispersion coefficients in natural streams. Riahi-Madvar et al. (2009) developed an adaptive neuro-fuzzy inference system (ANFIS) that could predict the longitudinal dispersion coefficient in a natural stream with higher accuracy than empirical-based dispersion model. Azamathulla and Ahmad (2012) used laboratory data in conjunction with a dataset from previous studies to develop functional relations for estimating transverse mixing coefficients in natural streams using a gene expression programming (GEP) model. They compared the accuracy of their model with some commonly used empirical equations, such as Equation 4.5 (Fischer 1967) and Equation 4.7 (Ahmad 2007) and showed the superiority of the GEP model in predicting the transverse dispersion coefficient in natural streams. Antonopoulos et al. (2015) developed an artificial neural network (ANN) and proposed an empirical model to estimate the dispersion coefficient in a section of the Axios River in Greece, under different hydrological and

hydrodynamic scenarios. They compared the accuracy of ANN and their empirical model with Fischer's (1975) empirical equation and found that the ANN model was superior. In addition to these studies, several others, over the past two decades, have shown the advantages of various soft computing models in estimating dispersion coefficients over empirical approaches (Toprak et al., 2004; Toprak and Cigizoglu 2008; Azamathulla and Ghani 2011; Piotrowski et al., 2012; Parsaie and Haghiabi 2015a,b; Zahiri and Nezaratian 2020; Najafzadeh et al., (2021); Nezaratian et al., 2021).

Despite numerous studies that have used ML-based models to predict dispersion coefficients in natural streams, the precision level can vary significantly, even when the MLMs are fed by the same input parameters (Noori et al., 2016). In other words, because the ML-based approaches are data-driven models, a change in the model feed dataset can significantly influence its performance. Therefore, each machine learning method can produce a specific level of accuracy due to the fed dataset.

Although several studies have been conducted on the application and sensitivity analysis of machine learning approaches to predict the dispersion coefficient in natural streams, they have not been used in Lagrangian-based sediment transport models. In addition, the ability of some learning-based models, such as random forest and gradient boosting regression, to predict dispersion coefficients has not been evaluated. In this study, we used data from previous studies to examine the performance of ensemble machine learning models in predicting longitudinal and transverse dispersion in natural streams. The ML-based dispersion models were integrated with a Lagrangian particle-based sediment transport model, and the performance of the PTM–ML-based dispersion models was compared with the result of the PTM–empirical dispersion relationships.

## METHODOLOGY

The two main steps of this study were the development and evaluation of dispersion models for natural streams using soft computing techniques and combining learning-based dispersion models with a particle tracking model developed by Baharvand et al. (2022a). In the first step, field data from previous studies were used to develop machine learning models that could predict longitudinal and transverse dispersion in natural streams, and the dispersion coefficients were coupled with the PTM to simulate sediment transport. Empirical dispersion equations were used in the PTM to evaluate the performance of each technique in generating suspended sediment concentration distribution in a natural stream, using field data collected downstream of a bridge construction site in Wilson Creek in McKinney, Texas. Figure 4.2 illustrates the flowchart of the dispersion models coupled with the PTM.

The model architecture was programmed in Python 3.9.0, a high-level, general-purpose programming language (Rossum 1995) , using several Python-based packages such as *NumPy*, *SciPy*, *Pandas*, *Matplotlib*, *Arcpy*, *Seaborn* (Waskom 2021), and *Scikit-learn*. The following presents a summary of the PTM development process, case study area, field data collection, and development of the dispersion models.

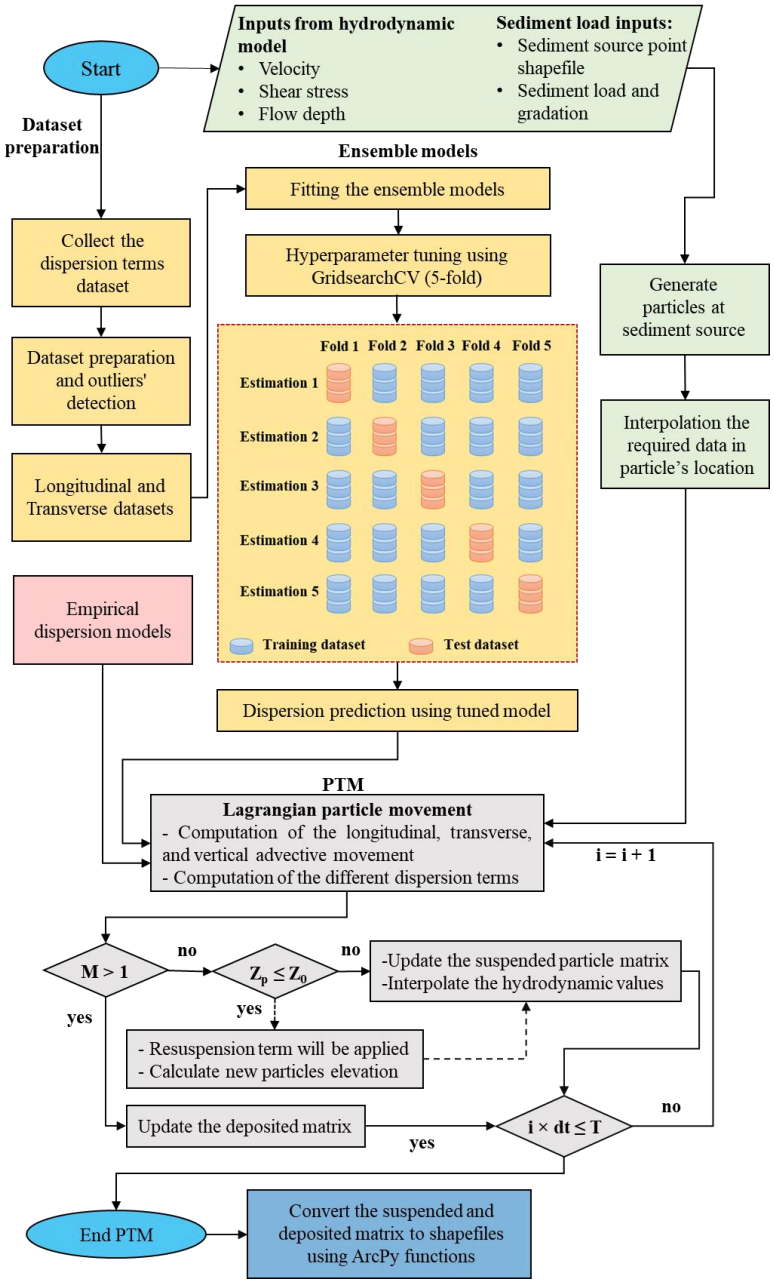


**Figure 4.2** Flowchart of the in-stream sediment transport model with learning-based and empirical dispersion coefficients

### 4.1.1 Particle Tracking Model

The present study utilized a particle tracking model with a continuous sediment source to simulate the added sediment load caused by bridge construction activities in a natural creek. The architecture and governing equations of the PTM are discussed by Baharvand et al. (2022a), and

details of the integration of the PTM with HEC-RAS 2D are presented in Baharvand et al. (2022b). The advection and dispersion terms were considered as displacement equations for individual particles in the flow domain in the PTM. The hydrodynamic parameters were exported from an HEC-RAS 2D model and calculated using a linear interpolation technique in the flow domain to estimate total displacement of the particles caused by the advection term.

The model was developed, based on two-dimensional advection coefficients in longitudinal and transverse directions, to estimate the sediment particles' advection displacement using streamwise ($u$) and transverse ($v$) velocity components. The dispersion coefficients were estimated in three dimensions to address the diffusivity effect on particles in $x$, $y$, and $z$ directions. Different experimental and field studies have reported various values for three-dimensional dispersion coefficients ($D_x$ , $D_y$ , $D_z$). Some of the widely used longitudinal and transverse dispersion coefficients are listed in Table 4.1. In this study, discretized advection and dispersion coefficients were estimated by using the hydrodynamic parameters (flow depth, shear velocity, etc.) at the position of the sediment particle.

The dispersion coefficients in longitudinal and transverse directions were estimated using two methods: 1) empirical equations and 2) ML-based approaches. The performance of the longitudinal dispersion coefficient equation by Elder (1959) (Equation 4.1) and transverse dispersion coefficient by Gualtieri and Mucherino (2008) (Equation 4.8) in a PTM was assessed by Baharvand et al. (2022a). In the present study, these empirical equations were used in the PTM to simulate sediment transport in a natural stream and the results were compared with the PTM coupled with ML-based dispersion coefficients. More information on the development of the PTM with empirical equations may be found in Baharvand et al. (2022a). The following sections discuss

the development of the ensemble ML-based dispersion prediction models, vertical displacement, stochastic term development, and general discretized Lagrangian transport equations.

#### *4.1.1.1 Ensemble Dispersion Prediction Models*

The dispersion coefficients in longitudinal and transverse directions can be predicted using empirical and ML-based models, and several ML approaches have been used to estimate dispersion coefficients in natural streams. For instance, Azamathulla and Wu (2011) used a kernel-based ML support vector regression (SVR) model, Kargar et al. (2020) used random forest regression (RFR), and Tayfur et al. (2005) and Noori et al. (2016) used different types of artificial neural network (ANN) algorithms to predict the longitudinal dispersion coefficient. Nezaratian et al. (2021) and Ahmad et al. (2011) utilized SVR and ANFIS models, respectively, to evaluate the performance of kernel-based and artificial neural network models to predict transverse dispersion coefficients in natural streams.

After initial assessment of different machine learning models, the ensemble ML models in this study were used to predict longitudinal and transverse dispersion coefficients. The advantage of ensemble approaches is that they build a powerful model, using the collection of weak prediction models (Hastie et al., 2009; Shao and Deng 2018). Several types of ensemble approaches (i.e., bagging, stacking, and boosting), RFR (classified as a bagging ensemble model), and gradient boosting regression (GBR) (classified as a boosting ensemble model) were selected as the ensemble tree-based models. The two main reasons for this selection were that both models had demonstrated a high level of accuracy in generating longitudinal dispersion coefficients in previous studies with different input datasets, and the literature lacks adequate information on the use of these two approaches for predicting transverse dispersion coefficients in natural streams.

The RFR and GBR ensemble models were developed using the scikit-learn package (Pedregosa et al., 2011) in *Spyder IDE*, a widely used open-source scientific environment written in Python.

***Natural Stream Dispersion Dataset***

The parameters used to estimate longitudinal and transverse dispersion coefficients in natural streams obtained from previous studies include flow velocity ($u$), flow depth ($H$), and shear velocity ($u_*$). In some of the studies, stream width is also considered an effective parameter for predicting dispersion coefficients (Toprak and Savci 2007; Zeng and Huai 2014; Kargar et al., 2020; Nezaratian et al. 2021). Since the variations in the channel width in the present case study are insignificant (Section 2.2.1), they are not considered an effective parameter. Other parameters, such as longitudinal slope, Froude number, and Reynolds number, were also not included as effective parameters because of their lesser importance (Najafzadeh et al., 2021).

Effective parameters for estimating longitudinal dispersion coefficients were extracted from studies by Fischer (1968), Yotsukura et al. (1970), McQuivey and Keffer (1974), Nordin and Sabol (1974), Rutherford (1994), Graf (1995), and Toprak and Cigizoglu (2008) (Table A-1 in Appendix A). The transverse dispersion coefficient dataset was obtained from Nezaratian et al. (2021) (Table A-2 in Appendix A), which contains data from various studies, including Fischer (1967), Yotsukura et al. (1970), Holley and Abraham (1973), Krishnappan and Lau (1977), Beltaos (1979), Rutherford (1994), Jeon et al. (2007), Baek and Seo (2008), Lee and Seo (2013).

The effective parameters for estimating dispersion coefficients, hereinafter called feature dataset ($H$, $u$, $u_*$), were plotted against the dispersion coefficients with the frequency of each feature dataset in Figures A-1 and A-2 in Appendix A, for longitudinal and transverse directions, respectively. The histogram of dispersion coefficients is shown in Figure A-3 in Appendix A**.**

Table 4.2 shows descriptive statistics of the longitudinal and transverse dispersion database used to develop the dispersion coefficients ensemble prediction models.

**Table 4.2** Descriptive Statistics of the Longitudinal and Transverse Dispersion Database

| Parameter | Dispersion coefficient | Flow depth (m) | Flow velocity (m/s) | Shear velocity (m/s) | Dispersion ($m^2/s$) |
|---|---|---|---|---|---|
| Min | Longitudinal | 0.22 | 0.13 | 0.02 | 1.9 |
| | Transverse | 0.013 | 0.04 | 0.005 | 0.00003 |
| Max | Longitudinal | 8.9 | 1.74 | 0.17 | 1486.45 |
| | Transverse | 5.25 | 1.75 | 0.16 | 0.215 |
| Mean | Longitudinal | 1.4 | 0.53 | 0.071 | 132.14 |
| | Transverse | 0.304 | 0.308 | 0.027 | 0.007 |
| STD* | Longitudinal | 1.39 | 0.37 | 0.032 | 240.83 |
| | Transverse | 0.71 | 0.27 | 0.023 | 0.025 |

* STD: Standard Deviation

### *Development of Ensemble Machine Learning Models*

Each machine learning model has specific hyperparameters (parameters that control the learning process) whose value is highly correlated with the performance of the learning-based model. There is not a way to determine the optimal set of the hyperparameters values in advance, but various methods, such as optimization techniques (genetic algorithm, particle swarm optimization), trial and error, and grid-search cross-validation (GridsearchCV) can be used to find them. None of them are without problems, however. Optimization techniques are usually complex processes with high computation costs that increase the prediction time significantly. GridsearchCV is a method that tunes each hyperparameter in an ML model by performing an exhaustive search of optimal parameters in a grid-wise manner (Alwated and El-Amin 2021). The GridSearchCV technique can perform pairwise computations of the hyperparameters. Pairwise computations are not performed in the trial and error technique, and it could be argued that this method just provides a scenario of the GridSearchCV hyperparameters' tuning technique in each trial. The present study used the GridsearchCV technique's *Scikit-learn* package to assess the

performance of the hyperparameters for the RFR and GBE ensemble models and relied on randomly selected 80% of the collected dataset for each dispersion coefficient.

The tree specific (max feature, min sample leaf, min sample split) and boosting (number of estimators) hyperparameters are considered in the GridsearchCV method to find the optimal combination for both ensemble models. In this technique, 5-fold cross-validation is employed, which splits the dataset into five random subsets (Figure 4.2).

In tree specific hyperparameters, the max feature hyperparameter represents the number of features that will be considered for the best randomly splitting scenario. In most cases, the higher values of the max feature result in an over-fitting problem. Min sample leaf determines the minimum required data in a leaf that controls the model overfitting. Min sample split refers to the minimum number of observation data needed for splitting in the tree-based model. The number of estimators is a boosting hyperparameter that controls the number of trees in the modeling. Once the optimal hyperparameter combination is defined, the model's accuracy in both training (with randomly selected 80% of the dataset) and testing stages (remaining 20% of dataset) will be tested, using different statistical measures. After ensuring the performance of the models, the tuned ensemble models will be used as ML-based dispersion estimators in the PTM to calculate the longitudinal and transverse dispersion coefficients in natural stream.

***Random Forest Regression***

Random forests (RF) are bagging ensemble machine learning algorithms developed by Breiman (2001). This approach is a meta estimator that fits many prediction decision trees created by the bootstrapping technique on various sub-samples of the dataset (Pedregosa et al., 2011). The random forest classification and prediction problems are comparable to the learning-based

approaches such as boosting methods (Breiman 2001) and support vector machines (Zhu 2007). This method controls the overfitting of the model and increases the prediction performance by using an averaging method (Pedregosa et al., 2011).

The RF method uses the measure of importance to rank the input variables and increase the prediction's accuracy. The importance of the variables is estimated by comparing the prediction's error metrics of out-of-bag (OOB) samples, which provides an opportunity to estimate the unbiased prediction error in the training stage's random forest construction phase, with in-bag-samples (IBS). The RF model's flowchart is illustrated in Figure 4.3, and detailed information on random forest governing equations may be found in Breiman (2001).

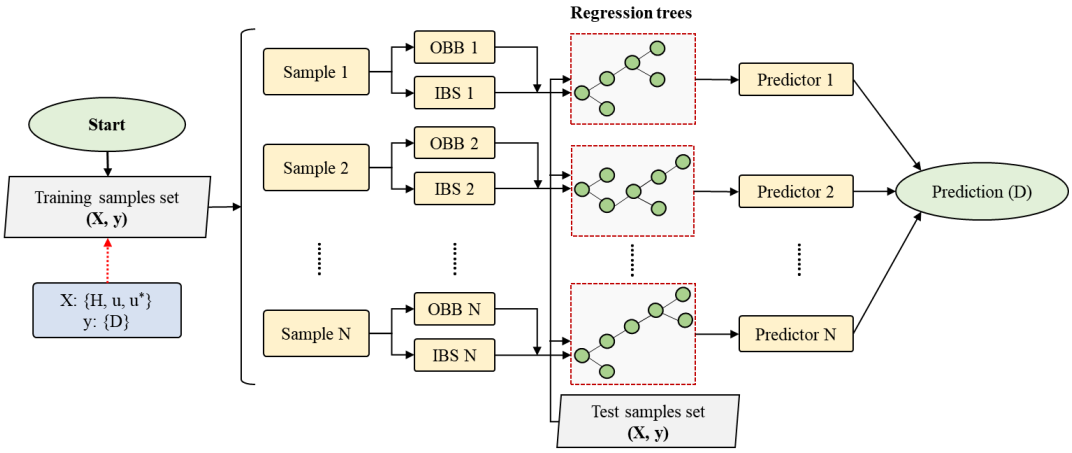


**Figure 4.3** Random forest regression model flowchart (Baharvand et al., 2022c)

***Gradient Boosting Regression (GBR)***

Some boosting ensemble models can predict target values using weak classifiers generated by feature data samples. Gradient boosting is a popular algorithm that, unlike the random forest algorithms that use independent regression trees, builds an ensemble of regression trees in sequence, with each tree using the previous tree to learn and improve the prediction accuracy. In essence, the boosting attacks the bias-variance tradeoff, using weak decision tree models, and

boosts the model accuracy using sequential trees. New weak models concentrate on the training rows of the weighted datasets with less prediction accuracy in the previous step. Figure 4.4 shows the gradient boosting regression flowchart.

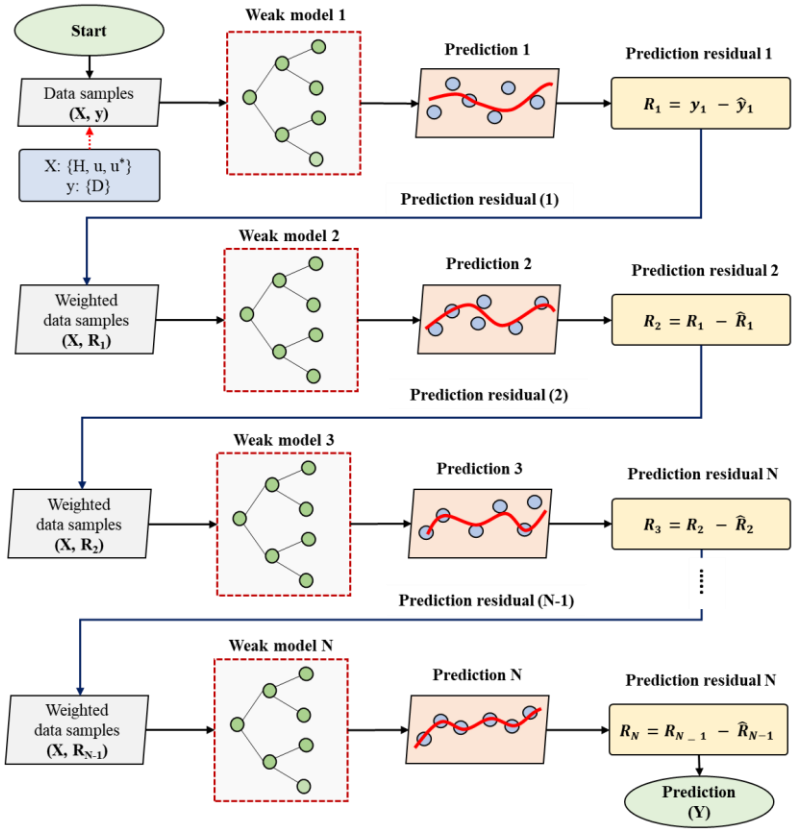


**Figure 4.4** Flow chart of gradient boosting regression model

As shown in Figure 4.4, the GBR is trained using *N* regression trees (weak models). In the first step, the weak model is trained using the feature matrix *X* (a matrix of *H*, *u*, $u_*$); the target value is *y* (dispersion terms $D_x$ and $D_y$). The prediction residual error is estimated for the first step ($R_1$) using the observed ($y_1$) and predicted ($\hat{y}_1$) target values. Once the residual of the first step has been determined, the second weak model is trained using the feature matrix *X*, and the residual errors that are calculated from step 1 ($R_1$) are considered the target values for the second step. The step 2 prediction residual error ($R - \hat{R}_1$) is used as the target value for the next step, and this

sequential prediction process is repeated until the ensemble tree-based gradient boosting model is trained.

The shrinkage factor is an essential variable in GBR that describes the portion of each weak model in the prediction method after multiplying the prediction residual of each tree in the ensemble model. The shrinkage factor (also known as learning rate) ranges from 0 to 1. After all the weak models are trained in the GBR, the prediction is obtained by using Equation 4.9.

$$Y = y_1 + \nu R_1 + \nu R_2 + \nu R_3 + \cdots + \nu R_N \quad (4.9)$$

where $Y$ is the prediction of the GBR, $y_1$ is the observed target values from the first step of the model (observed dispersion coefficients), $\nu$ is the shrinkage factor, and $R$ refers to the prediction residuals that come from each weak model. After using different values for the shrinkage factor in the trial-and-error process in this study, it was set at 0.1 to develop the GBR model.

***Performance Standards***

Three statistical measures were utilized to assess the accuracy of predicted values: coefficient of determination ($R^2$), root mean square error (RMSE), and mean absolute error (MAE). The total discrepancy ratio ($DR_s$) was also used to evaluate the performance of ensemble models adopted in the present study. The $DR_s$ is a statistical measure that was used in several studies to assess the accuracy of ML-based models in predicting the dispersion coefficient in natural streams (e.g., Kashefipour and Falconer, 2002; Zeng and Huai 2014; Nezaratian et al., 2021). Equations 4.10 to 4.13 show $R^2$, RMSE, MAE, and $DR_s$ relationships, respectively.

$$R^2 = \frac{\sum_{i=1}^{N}(x_i - \bar{x})(\hat{x}_i - \bar{x})}{\sqrt{\sum_{i=1}^{N}(x_i - \bar{x})^2 \times \sum_{i=1}^{N}(\hat{x}_i - \bar{x})^2}} \quad (4.10)$$

$$\mathrm{RMSE} = \sqrt{\sum_{i=1}^{N} \frac{(\hat{x}_i - x_i)^2}{N}} \tag{4.11}$$

$$\mathrm{MAE} = \frac{1}{N}\sum_{i=1}^{N}(\hat{x}_i - x_i) \tag{4.12}$$

$$\mathrm{DR_s} = \frac{\sum_{i=1}^{N} \log\left(\frac{\hat{x}_i}{x_i}\right)}{N} \tag{4.13}$$

where $x_i$ is i[th] observed dispersion coefficient, $\hat{x}_i$ is i[th] predicted dispersion coefficient, $\bar{x}$ refers to the mean dispersion coefficient, and N refers to the amount of data.

*4.1.1.2 Particles Vertical Displacement Computation*

The PTM does not consider the effects of the vertical advection term, and vertical displacement of particles is calculated by considering the vertical dispersion coefficient and settling velocity that are due to gravitational forces acting on suspended particles. Therefore, the Van Rijn (1993) particle settling velocity equation was used to compute the temporal vertical displacement of each particle. Equation 4.14 shows the settling velocity of sediment particles.

$$w_s = \begin{cases} \frac{(S-1)gd^2}{18\nu} & 1 < d \leq 100\ \mu m \\ \frac{10\nu}{d}\left[\left(1 + \frac{(S-1)gd^3}{100\nu^2}\right)^{\frac{1}{2}} - 1\right] & 100 < d \leq 1000\ \mu m \\ 1.1[(S-1)gd]^{\frac{1}{2}} & d \geq 100\ \mu m \end{cases} \tag{4.14}$$

where $w_s$ is particle settling velocity, $\nu$ is the kinematic viscosity of water, $S$ is ratio of particle density to fluid density, and $d$ is the particle diameter.

Unlike longitudinal and transverse dispersion coefficients, which are computed based on both empirical and ML-based approaches discussed in previous sections, the vertical dispersion coefficient is computed using Equation 4.15 proposed by Von Rijn (1987).

$$D_z = \begin{cases} D_{zm} - D_{zm}\left(1 - \frac{2z}{H}\right)^2 & \frac{z}{H} < 0.5 \\ D_{zm} & \frac{z}{H} \geq 0.5 \end{cases} \quad (4.15)$$

where $H$ represents flow depth, $z$ is the vertical elevation of particles, and $D_{zm}$ is the maximum vertical dispersion coefficient. $D_{zm}$ is maximum vertical dispersion term ($D_{zm} = \frac{\kappa u_* H}{4}$) in which $u_*$ is shear velocity, and $\kappa$ refers to the von Kármán constant ($\kappa$ = 0.4).

*4.1.1.3 Stochastic Random Walk Method*

Random behavior of sediment particles in natural streams can be modeled using different stochastic approaches, such as the stochastic jump diffusion model (Oh 2011) and the random walk method. Due to the acceptable performance of the random walk method, various studies have used this method to calculate the random motion of sediment particles in turbulent flows (Lane and Prandle 2006; Taghvayi 2013; Shi and Yu 2015). In the present study, the random walk method was used to generate the stochastic term, i.e., $N(\mu, \sigma)$, using a normal distribution probability function (Equation 4.16) with a mean of $\mu$ = 0, and a standard deviation of $\sigma$ = 1.

$$f(x) = \frac{1}{\sigma\sqrt{2\pi}}\, \mathrm{e}^{-0.5\left(\frac{x-\mu}{\sigma}\right)^2} \quad (4.16)$$

*4.1.1.4 Discretized Particle Tracking Equations*

Once the dispersion coefficients are estimated based on an empirical equation and machine learning approaches, advection and dispersion displacement equations are solved for each particle in the flow domain. Equations 4.17 to 4.19 show the displacement of a particle in a three-dimensional space of the flow domain.

$$\Delta x_p = u_p\, \Delta t + N(\mu, \sigma)\sqrt{2D_x \Delta t} \quad (4.17)$$

$$\Delta y_p = v_\mathrm{p}\, \Delta t + N(\mu, \sigma)\sqrt{2D_y \Delta t} \quad (4.18)$$

$$\Delta z_p = -w_s \Delta t + N(\mu, \sigma)\sqrt{2D_z \Delta t} \quad (4.19)$$

where $\Delta x_p, \Delta y_p$, and $\Delta z_p$ are the total particle displacement in streamwise, transverse, and vertical directions after one computational time step ($\Delta t$). $u_p$ and $v_{\mathrm{p}}$ are the linearly interpolated velocity components in streamwise and transverse directions at the particle location, respectively.

### 4.1.2 Case Study

#### *4.1.2.1 Study Area*

A section of Wilson Creek near Highway FM 2478 in McKinney, Texas was selected as the study area (Figure 4.5), as road expansion and bridge replacement projects were expected to add sediment load to the creek. The bridge location and construction site footprints on the south and north sides of the Wilson Creek are shown in Figure 4.5. The sediment regime in the creek was monitored during the construction period in 2021. According to the historical flow data at the USGS 08059590 gauge station (11.2 km downstream of the bridge location), the mean daily flow varied between 0 and 37.4 $m^3/s$, with an average of 1.98 $m^3/s$. Two storm events, on April 29 and November 3, 2022, with an average daily discharge of 37.4 $m^3/s$ and 7.4 $m^3/s$, were considered, and it was estimated that during these events a total of 12.8 and 2.4 tonnes/day of sediment entered the creek from the construction sites, respectively. The daily overland erosion from the construction sites was predicted using a predictive overland erosion GIS-based toolkit developed by Ahmari et al. (2022).

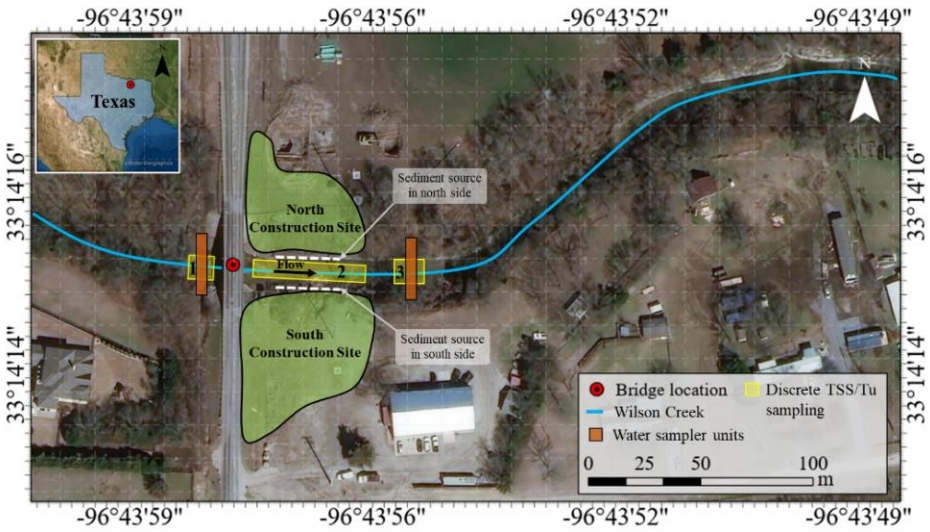


**Figure 4.5** Wilson Creek study area near Highway FM 2478, McKinney, Texas

*4.1.2.2 Field Measurements*

Flow and sediment characteristics were monitored at the Wilson Creek bridge site from December 2020 to December 2021. The monitoring site was extended from upstream of the bridge to downstream of the impacted area by construction activities and was visited after each storm event, with an average of 2 to 4 visits per month, depending upon the rainfall and streamflow conditions. The field program included monitoring total suspended solids (TSS), turbidity (Tu), bedload material, substrate type, and depositional areas. Two ISCO 6712 Teledyne water sampler units were installed upstream and downstream of the bridge location to collect samples during storm-based events for lab analysis of the concentration of the suspended sediment (Figure 4.5). The upstream unit collected water samples before the bridges, where the sediment load in the creek was not impacted by the local overland erosion in the construction areas. The samples collected by the downstream sampler represented the cumulative effect of the sediment load from upstream and the sediment load entering the creek from the bridge construction areas. The TSS data from the upstream and downstream units were compared to estimate the elevated suspended sediment in the creek due to the overland erosion.

Discrete TSS and turbidity (Tu) samples were collected at the location of the automated water samplers, as well as from the area between the bridge location and the downstream water sampler unit, where the sediment regime in the creek was impacted by the construction activities (Section 2 in Figure 4.5). The turbidity of the samples was measured in the NTU unit, using a Hach 2100Q portable turbidimeter. The TSS and turbidity discrete data were collected mainly during low flow conditions to complement the sediment data collected by the automated water samplers during storms. Water samples collected by the automated samplers and grab samples were sent to the lab for TSS analysis, using EPA method 160.2 (United States Environmental Protection Agency, 2017). More information on the field monitoring program can be found by researching in Baharvand et al. (2022b).

Due to the lack of direct measurement of TSS on April 29, 2021, the suspended sediment concentration was estimated using the TSS-Tu relationships (Equation 4.20) that was developed based on the data collected by water samplers and discrete data collected upstream and downstream of the bridge.

$$TSS = 0{,}88\,Tu \qquad \text{Upstream of the bridge} \qquad (4.20a)$$

$$TSS = 2{,}66\,Tu \qquad \text{Downstream of the bridge} \qquad (4.20b)$$

Grab samples were collected from the eroded materials at the construction site and depositional areas in the creek to determine the sediment gradations contributing to the total sediment load. A minimum of 500 grams of samples were collected from each area and sent to the lab for gradations tests. The content of gravel, sand, silt, and clay in the samples was measured by sieve analysis and hydrometry tests after debris and other objects were removed. Based on this analysis, the average fraction of the clay/silt, sand, and gravel was estimated as 10%, 75%, and 15%, respectively

(Baharvand et al., 2022b). These values were used in the PTM as the gradation of the sediment load entering the creek from the north and south construction areas.

#### *4.1.2.3 Wilson Creek Particle Tracking Model*

A particle tracking model developed by Baharvand et al. (2022a) to simulate sediment transport in natural streams and estimate dispersion coefficients by employing empirical equations was adopted for this study. A calibrated HEC-RAS 2D model for the study area was coupled with the PTM to provide hydrodynamic parameters. Two storm events, on April 29 and November 3, 2022, with an average daily discharge of 37.4 $m^3/s$ and 7.4 $m^3/s$, respectively, were considered. The PTM was used to predict the suspended sediment concentration variations in different sections of the creek downstream of the bridge location, and its performance was evaluated by using field data collected from the bridge construction site in Wilson Creek (Baharvand et al., 2022b). The dispersion coefficients that were estimated using ML methods were used in the Wilson Creek PTM. The distributions of the suspended sediment in the creek were estimated by the PTM, using empirical and ML-based methods, and the results were compared with the field data.

## RESULTS AND DISCUSSION

### 4.1.3 Prediction of Longitudinal Dispersion Coefficient

This section presents the longitudinal dispersion coefficient prediction that was obtained by using random forest (RFR) and gradient boosting regression (GBR) models. The accuracy of each model is discussed in the following for several hyperparameter tuning scenarios, using GridsearchCV.

#### *4.1.3.1 RFR and GBR Ensemble Prediction Models*

Comparisons of the observed and estimated longitudinal dispersion coefficients, using the RFR and GBR models in the training and testing stages, are shown in Figures 4.6 and 4.7. As can be

seen, the RFR model predicted the longitudinal dispersion coefficient with $R^2 = 0.93$ in the training stage (Figure 4.6a); however, the GBR model showed more accuracy with a coefficient of determination of $R^2 = 0.95$ (Figure 4.6b). RMSE and MAE of the GBR model were smaller than that of the RFR model for the training stage (Table 4.3), which means that the GBR model estimated $D_x$ more accurately. The total discrepancy ratios of the RFR and GBR models for the training stage were estimated as $DR_s = -0.16$ and -0.07, respectively. The negative $DR_s$ values show the underestimation of both ensemble models in predicting $D_x$ although the total discrepancy ratio of the GBR was closer to zero, indicating that the GBR model predicted $D_x$ more precisely than the RFR. The confidence intervals shown in Figures 4.6a and b represent the upper and lower bounds of the estimates with a 90% confidence level for the training stage, using RFR and GBR, respectively.

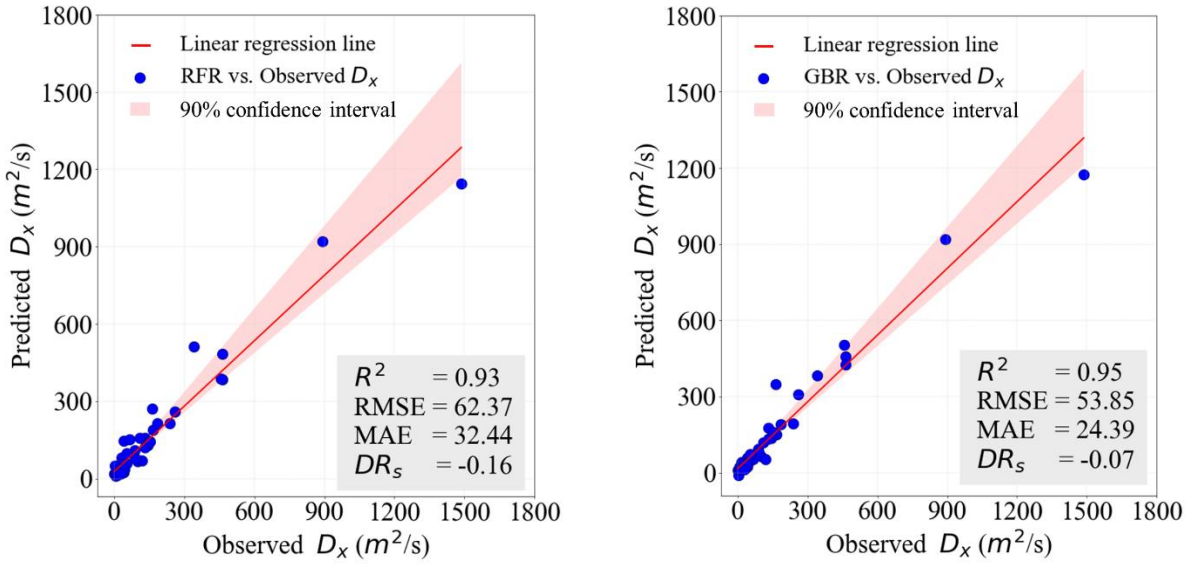


**Figure 4.6** Comparison between the observed and predicted longitudinal dispersion coefficient ($D_x$) by a) RFR, and b) GBR in the training stage

Figure 4.7 compares the $D_x$ that was observed and predicted by the RFR and GBR in the testing stage. As shown, the GBR model more accurately predicted the longitudinal dispersion coefficient in the testing stage ($R^2$ = 0.9) than the RFR model ($R^2$ = 0.86). The RMSE of the RFR model was determined as 79.1 $m^2/s$ in the testing stage, which is higher than the RMSE of the GBR model (66.1 $m^2/s$). Considering the negative $DR_s$ of both models in the testing stage, it could be argued that both models underestimated $D_x$ in the testing stage, as they did in the training stage. Figures 4.8 and 9 illustrate the overestimations and underestimations of the RFR and GBR for each observation in the dataset in the training and testing stages.

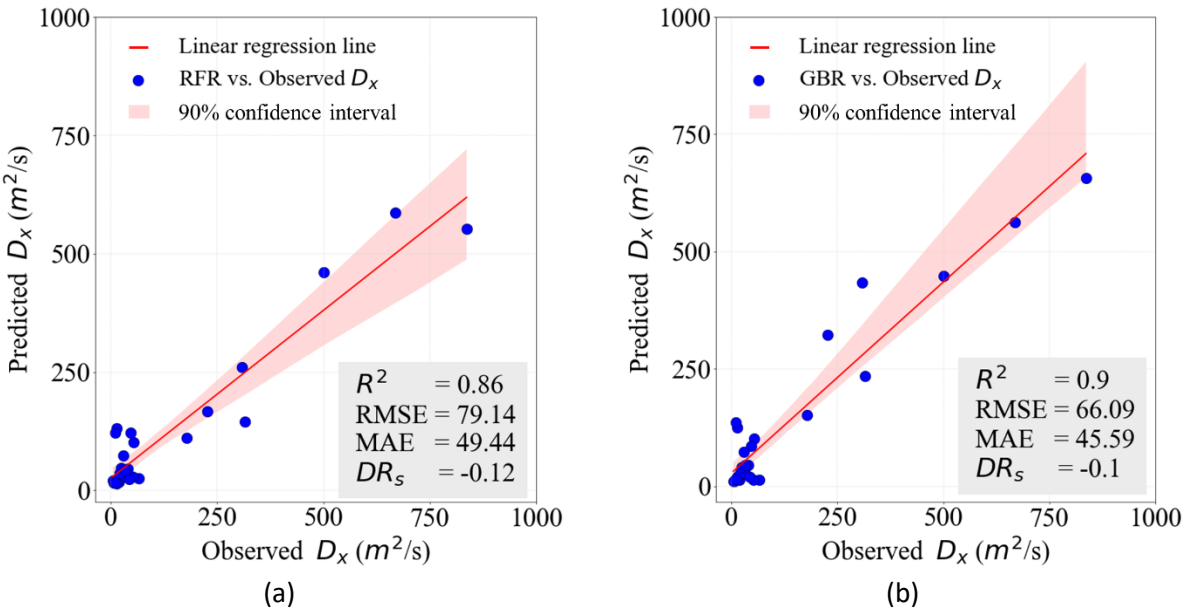


**Figure 4.7** Comparison between the observed and predicted longitudinal dispersion coefficient ($D_x$) by a) RFR and b) GBR in the testing stage

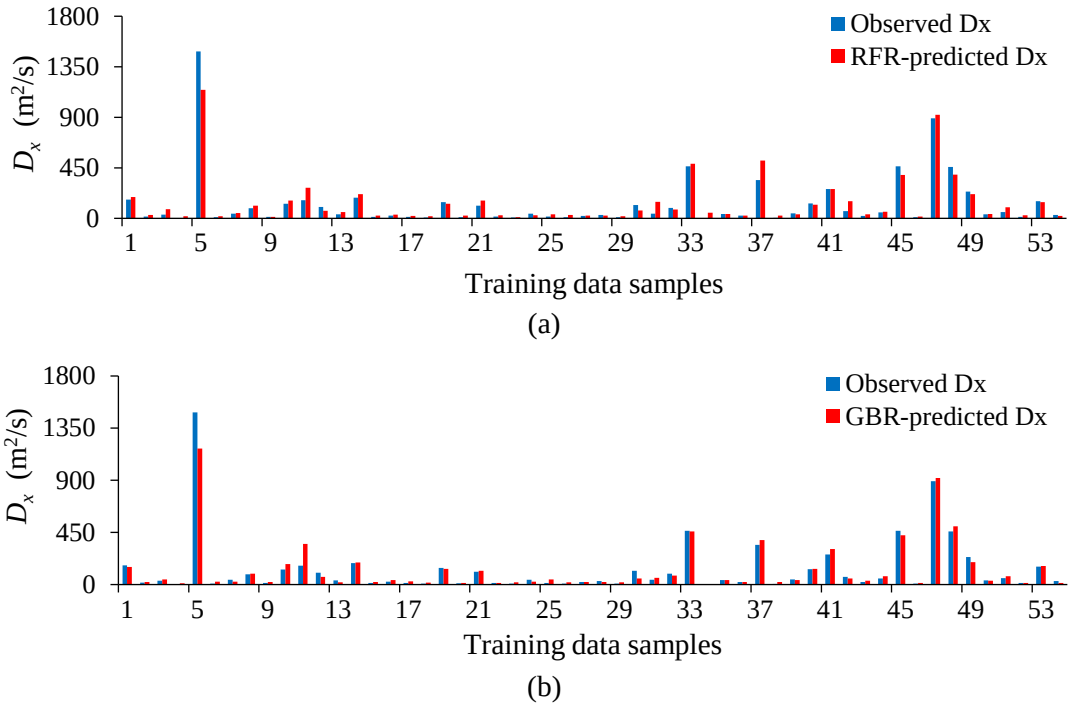


**Figure 4.8** Observed and predicted longitudinal dispersion coefficient ($D_x$) for each data sample by a) RFR and b) GBR in the training stage

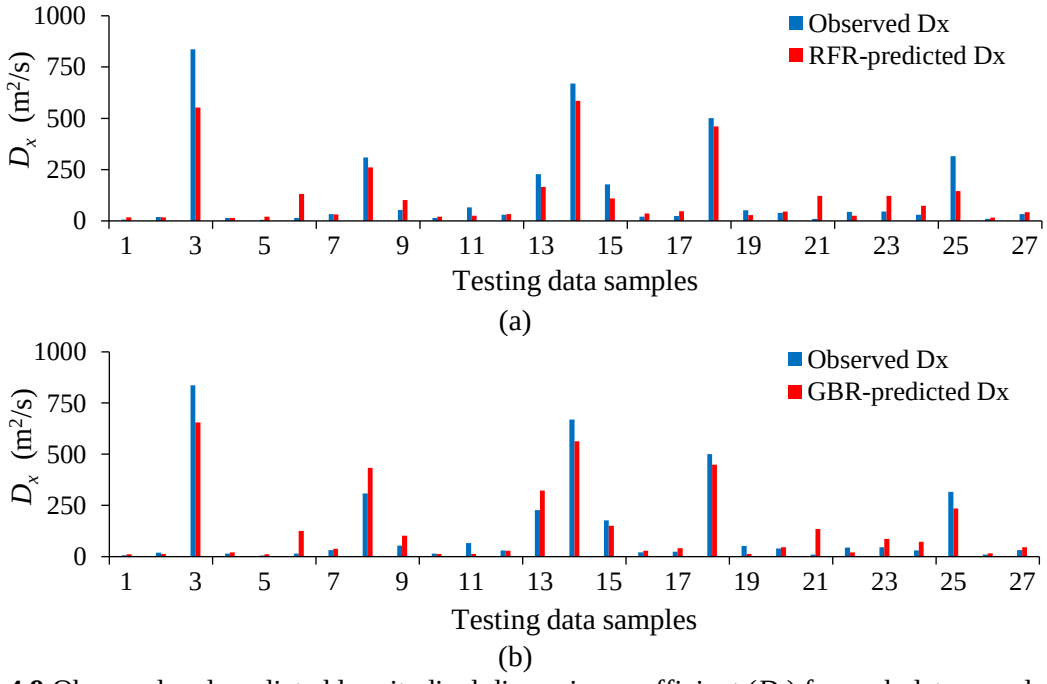


**Figure 4.9** Observed and predicted longitudinal dispersion coefficient ($D_x$) for each data sample by a) RFR and b) GBR in the testing stage

The RFR and GBR models' predictions of the longitudinal dispersion show that the GBR model has advantages over the RFR in both the training and testing stages. As discussed in Section 4.2.1.1, the hyperparameter values for both stages of both models were determined through the GridsearchCV approach. Table 4.3 summarizes the values and shows that by performing the GridsearchCV technique, the optimal values for the RFR hyperparameters (max feature, min sample leaf, min sample split, and number of estimators) to predict longitudinal dispersion were estimated as 3, 3, 2, and 200, respectively. The optimal max feature, min sample leaf, min sample split, and number of estimators hyperparameters of the GBR model were estimated as 3, 5, 4, and 250, respectively.

**Table 4.3** Hyperparameter Tuning Scenarios of Longitudinal Dispersion Coefficients ($D_x$)

(The ideal parameters are shown in bold type.)

| Emulator | Hyperparameter | Interrogated Values | Stage | Statistical Measures | | | |
|---|---|---|---|---|---|---|---|
| | | | | $R^2$ | RMSE ($m^2/s$) | MAE ($m^2/s$) | $DR_s$ |
| RFR | Max feature | 2, **3**, 5,10 | Training | 0.93 | 62.4 | 32.4 | -0.16 |
| | Min sample leaf | **3**, 5, 8, 10, 20 | | | | | |
| | Min sample split | **2**, 4, 6, 8,10, 20 | Testing | 0.86 | 79.1 | 49.4 | -0.12 |
| | Number of estimators | 100, 150, **200**, 250, 300 | | | | | |
| GBR | Max feature | 2, **3**, 5,10 | Training | 0.95 | 53.9 | 24.4 | -0.07 |
| | Min sample leaf | 3, **5**, 8, 10, 20 | | | | | |
| | Min sample split | 2, **4**, 6, 8,10, 20 | Testing | 0.9 | 66.1 | 45.6 | -0.1 |
| | Number of estimators | 100, 150, 200, **250**, 300 | | | | | |

**Prediction of Transverse Dispersion Coefficient**

The results of estimating the transverse dispersion coefficient ($D_y$) using the random forest and gradient boosting regression approaches are discussed in this section. Figure 4.10 shows a comparison of the observed and predicted transverse dispersion coefficients, using the RFR and

GBR in the training stage. The coefficient of determination of the RFR model for the training stage was calculated as $R^2 = 0.92$, and the RMSE was determined as 0.007 $m^2/s$. The discrepancy ratio in the RFR in the training stage was $DR_s = -0.071$ and reveals that the RFR underestimated the transverse dispersion coefficient. Comparing the statistical measure of the GBR model shown in Figure 4.10b ($R^2 = 0.94$, RMSE = 0.006) with that of the RFR model confirms the higher accuracy of the GBR model in predicting $D_y$ in the training stage; however, the GBR model's discrepancy ratio was estimated as -0.27, indicating that it also underestimated the transverse dispersion coefficient.

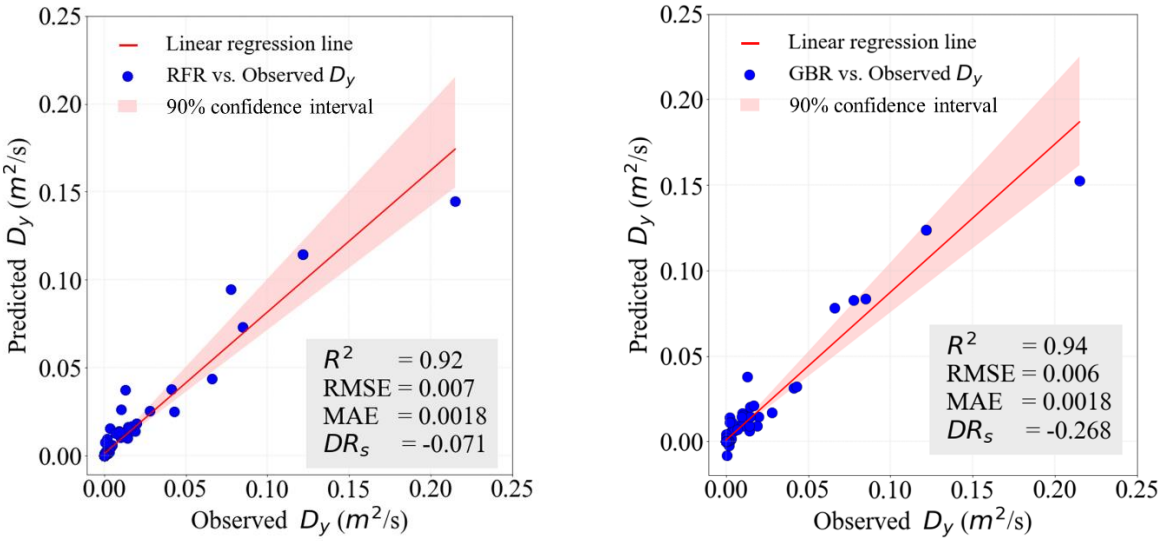


**Figure 4.10** Comparison between the observed and predicted transverse dispersion coefficients ($D_y$) by a) RFR, and b) GBR in the training stage

The results of the RFR and GBR models in predicting the transverse dispersion coefficient were compared with the observed values shown in Figure 4.11 for the testing stage. The RFR model showed a higher coefficient of determination ($R^2 = 0.94$) than the GBR model ($R^2 = 0.91$) in the testing stage. The RSME and MAE of the RFR and GBR models were similar. Moreover, according to the estimated total discrepancy ratio of the RFR ($DR_s = -0.118$), it more accurately

predicted $D_y$ in the testing stage. The discrepancy ratio of the GBR model was determined as $DR_s$ = -0.282.

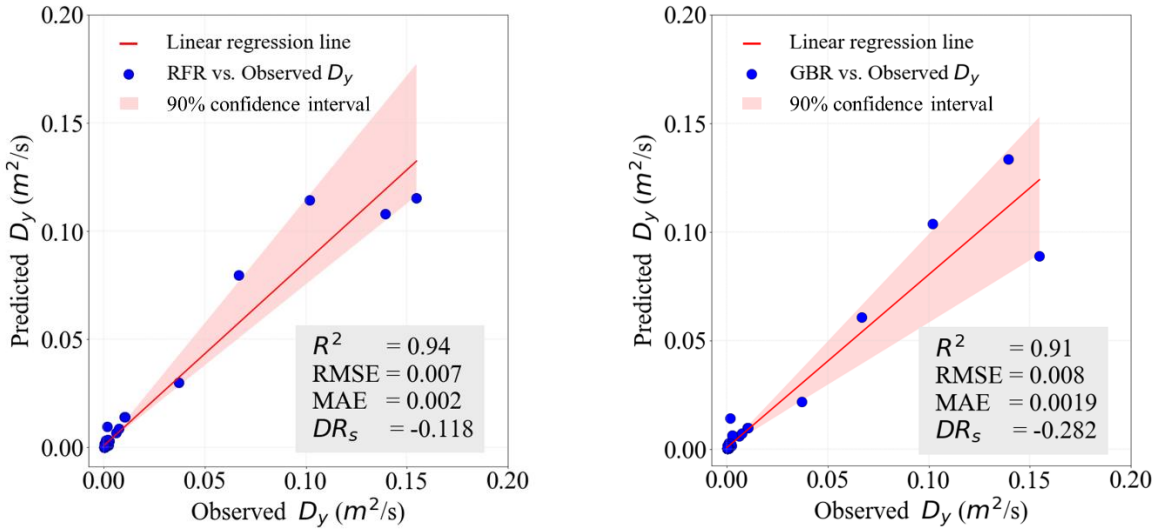


(a) (b)

**Figure 4.11** Comparison between observed and predicted transverse dispersion coefficients ($D_y$) by a) RFR, and b) GBR in the testing stage

Figures 4.12 and 4.13 were used to assess the RFR and GBR models' underestimation and overestimation of each observation value in the dataset in the training and testing stages, respectively. Due to the negative $DR_s$ for both models, an underestimation was expected for most of the data samples in both models.

Table 4.4 summarizes the statistical measures for the optimal hyperparameter interrogated values for the RFR and GBR models in the training and testing stages. The optimal values for the RFR hyperparameters, i.e., max feature, min sample leaf, min sample split, and number of estimators, for predicting the transverse dispersion coefficient are estimated as 3, 5, 2, and 250, respectively. However, the optimal max feature, min sample leaf, min sample split, and number of estimators hyperparameters of the GBR model are estimated as 3, 10, 2, and 250, respectively.

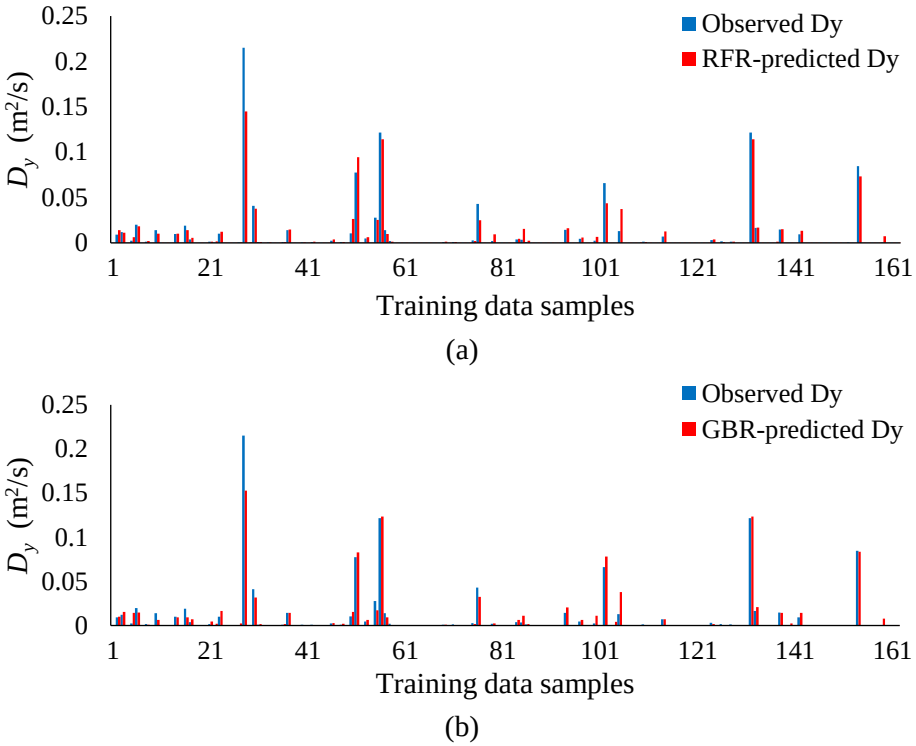


**Figure 4.12** Observed and predicted transverse dispersion coefficient ($D_y$) for each data sample by a) RFR, and b) GBR in training stage

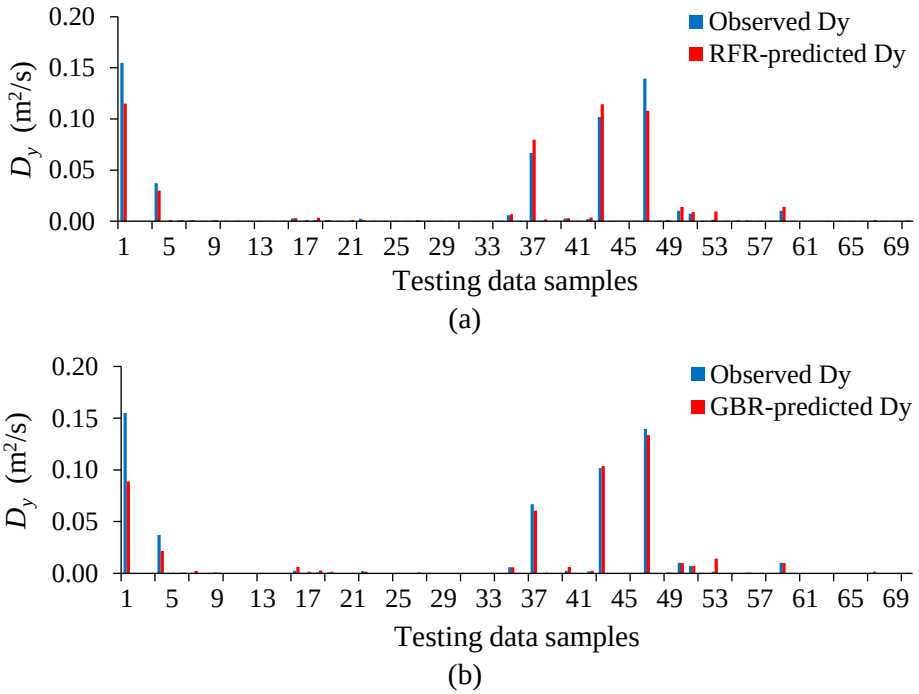


**Figure 4.13** Observed and predicted transverse dispersion coefficient ($D_y$) for each data sample by a) RFR, and b) GBR in testing stage

**Table 4.4** Hyperparameter Tuning Scenarios of Longitudinal Dispersion Coefficients ($D_y$).

(The ideal hyperparameters are shown in bold type.)

| Emulator | Hyperparameter | Interrogated Values | Stage | Statistical Measures | | | |
|---|---|---|---|---|---|---|---|
| | | | | $R^2$ | RMSE ($m^2/s$) | MAE ($m^2/s$) | $DR_s$ |
| RFR | Max feature | 2, **3**, 5,10 | Training | 0.92 | 0.007 | 0.0018 | -0.071 |
| | Min sample leaf | 3, **5**, 8, 10, 20 | | | | | |
| | Min sample split | **2**, 4, 6, 8,10, 20 | Testing | 0.94 | 0.007 | 0.002 | -0.118 |
| | Number of estimators | 100, 150, 200, **250**, 300 | | | | | |
| GBR | Max feature | 2, **3**, 5,10 | Training | 0.94 | 0.006 | 0.0018 | -0.268 |
| | Min sample leaf | 3, 5, 8, **10**, 20 | | | | | |
| | Min sample split | **2**, 4, 6, 8,10, 20 | Testing | 0.91 | 0.008 | 0.0019 | -0.282 |
| | Number of estimators | 100, 150, 200, **250**, 300 | | | | | |

The results of the statistical measures for the RFR and GBR models with optimized hyperparameters using the GridsearchCV technique showed that the GBR model more accurately predicted the transverse dispersion coefficient in the training stage. Both models underestimated $D_y$ during the training and testing stages; however, the accuracy of both in predicting the transverse and longitudinal dispersion coefficients was acceptable.

### 4.1.4 Simulating Suspended Sediment Concentration in Wilson Creek

The following sections present the machine learning and empirical dispersion models' results for two flow scenarios, $Q$ = 37.4 $m^3/s$ on April 29, 2021 and $Q$ = 7.4 $m^3/s$ on November 3, 2021. The simulation time was determined based on each dispersion model to ensure that all the particles injected at the sediment sources exited the downstream boundary of the model.

***Suspended Sediment Concentration - April 29, 2021 Storm***

The increase in suspended sediment concentration in Wilson Creek due to the overland erosion in the construction site was estimated using ensemble learning-based and empirical dispersion models and is presented in Figure 4.14. As mentioned in Section 4.2.2.1, the construction activities produced 12.8 tonnes/day of sediment yield on April 29, 2021, which elevated the sediment concentration downstream of the bridge location. The suspended sediment concentrations estimated by the PTM with the RFR and GBR models were compared at four cross sections downstream of the bridge location. The suspended sediment concentration cross section CS-1 (27 m downstream of the bridge site) was compared with the TSS values estimated from Equation 4.20b downstream of the bridge.

The maximum increase in suspended sediment concentrations (SSC) on the north side of the creek were estimated as 146, 105, and 153 mg/L by the PTM with the empirical dispersion equation, RFR, and GBR (Figures 4.14 a-c). The values for the south side of the creek were 201, 216, and 287 mg/L, respectively. The PTM with the RFR dispersion model predicted the maximum SSC on the north and south sides 24% lower than the GBR and 7% higher than the estimated values by the empirical dispersion model. The maximum SSC predicted by the PTM with the GBR was 40% higher for the south side and 5% higher for the north side compared to the estimates by the PTM using the empirical dispersion equation.

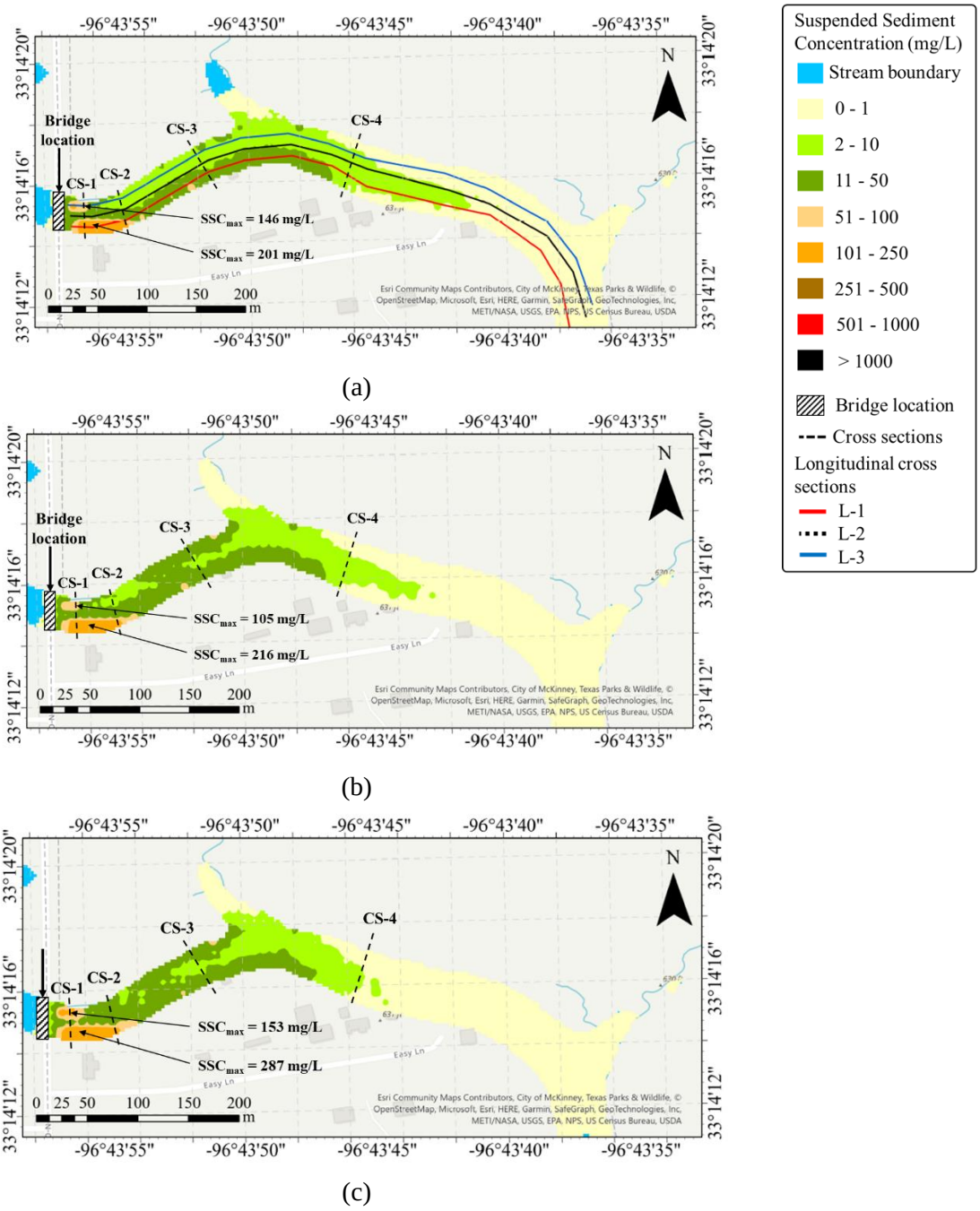


**Figure 4.14** Increase in suspended sediment concentration in Wilson Creek due to overland erosion corresponding to the April 29, 2021 storm estimated by the PTM with using different dispersion coefficients: a) Empirical equation, b) RFR model, and c) GBR model

The elevated suspended sediment concentration across CS-1 to CS-4 is depicted in Figure 4.15. The maximum elevated SSC across CS-1 was estimated as 160, 198, and 229 mg/L by the PTM with the empirical equation, RFR, and GBR, respectively (Figure 4.15a). The estimated TSS using

the TSS-Tu relationship (Equation 4.20b) and the turbidity measurements in the construction zone for different days of field measurement showed the TSS values ranging from 120 to 226 mg/L (Baharvand et al., 2022b). As shown in Figure 4.15a, the PTM models with the empirical equation and the RFR model estimated the maximum suspended sediment concentrations in section CS-1 within an acceptable range, showing the applicability of these PTMs. The PTM with the empirical equation and the RFR model underestimated the SSC, compared to the maximum measured TSS during field measurement, by about 29% and 12%, respectively; however, the difference in the maximum dispersion estimated by the PTM with the GBR dispersion model and the TSS range predicted using Equation 4.20b was negligible.

The elevated suspended sediment concentrations across Wilson Creek at cross sections CS-2, CS-3, and CS-4, located 67, 163, and 335 m downstream of the bridge site are shown in Figures 4.15b-d. The maximum elevated sediment concentrations across CS-3 were estimated as 28, 19, and 23 mg/L for the PTMs with the empirical equation, RFR, and GBR, respectively. As the sediment plume traveled downstream, it became diluted, and the suspended sediment concentration decreased. Unlike the suspended sediment concentration distribution in CS-2 (Figure 4.15b), the maximum sediment concentration estimated by the PTM with ensemble dispersion models was higher than the results from the PTM with an empirical dispersion model (Figures 4.15c and d). According to these figures, the PTM with the empirical dispersion model overestimated the sediment concentration compared to the other two dispersion models in CS-3 and CS-4, especially from the center towards the south side of the creek.

The RFR and GBR models in CS-1 and CS-2 showed higher SSC on the south side of the creek (Figures 4.15a and b). However, in downstream sections (CS-3 and CS-4), the sediment concentration estimated by the PTM with the empirical model was higher than that of the ensemble

models, especially from the center to the south side of the creek. These differences could be due to the underestimation of the empirical dispersion coefficients that results in less displacement of particles and an increase in sediment concentrations.

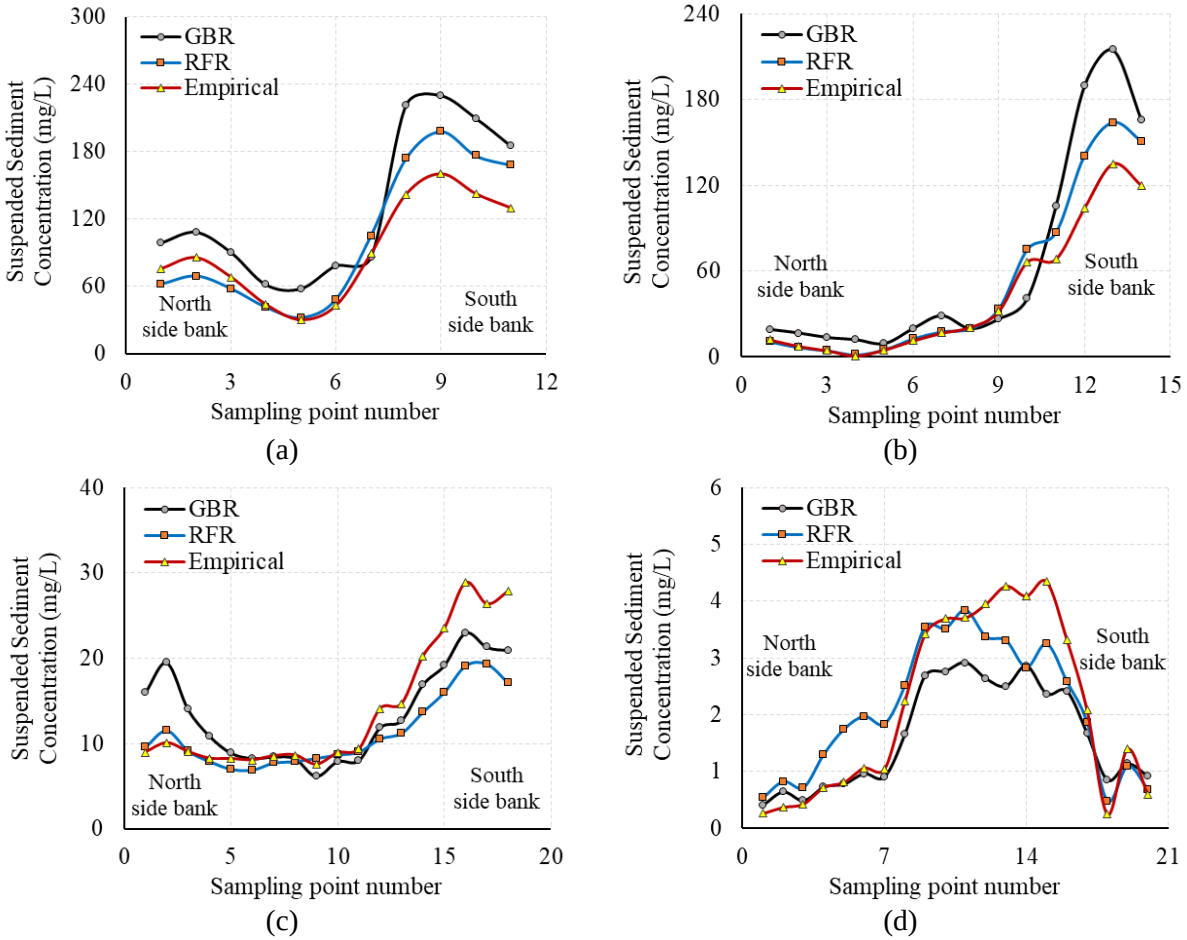


**Figure 4.15** Elevated suspended sediment concentration across Wilson Creek due to overland erosion corresponding to April 29, 2021 storm: a) Cross section CS-1, b) Cross section CS-2, c) Cross section CS-3, and d) Cross section CS-4. Cross sections are shown in Figure 4.14

Three longitudinal cross sections illustrate the variations of SSC estimated by different dispersion models along the creek . Figure 4.14a shows the longitudinal cross sections that were on the south side (L-1), center line (L-2), and north side (L-3) of the creek. The changes in elevated SSC along sections L-1 to L-3 are shown in Figure 4.16 for the PTM with the empirical equation, RFR, and GBR. According to Figure 4.16a, along the south longitudinal section (L-1), the maximum elevated SSC varied between 193 mg/L (PTM with empirical dispersion model) and 261 mg/L

(PTM with the GBR dispersion model). The high concentration values predicted for the area between 10 m and 30 m downstream of the bridge location were expected because of the proximity of this area to the sediment sources on both sides of the creek. Downstream of this high concentration area, the sediment concentration decreased gradually for all three dispersion models to approximately 47 mg/L 70 m downstream of the bridge on the south side. As shown in Figure 4.16a, the GBR estimated a higher concentration along L-1 up to 70 m downstream of the bridge than the PTM with the RFR and empirical dispersion model; from 70 m to the downstream sections, it estimated a lower sediment concentration than the other two PTM models. The PTM with the RFR and the empirical-based dispersion models showed similar SSC values in the downstream areas (100 m and further from the bridge), where the sediment plume became diluted with the creek flow.

The distribution of the suspended sediment concentration along the center line of the creek (line L-2) was estimated as 5 to 53 mg/L by three dispersion models in an area between 5 m to 51 m downstream of the bridge location (Figure 4.16b). The PTM with the GBR dispersion model resulted in higher concentration than the RFR and empirical dispersion models in an area from 5 m to almost 51 m downstream of the bridge location (Figure 4.16b). For areas beyond 50 m downstream of the bridge location along the center line, the PTM with the GBR estimated that the SSC was lower than the RFR prediction. The empirical model estimated a higher SSC 170 m downstream of the channel than the GBR model. Overall, the PTM with the empirical based dispersion model estimated the SSC in a range between the RFR and GBR estimates along the center line of creek for high flow conditions ($Q$ = 37.4 $m^3/s$ on April 29, 2021), except for a distance 37 m to 87 m downstream of the bridge, where the flow experiences the first meander of the channel.

Along the north side of the creek (line L-3), the PTM/ empirical dispersion model estimated that the sediment concentration was 40% higher than the PTM/ RFR dispersion model predicted and less than 6% than the PTM/GBR dispersion model for an area up to 16 m downstream of the bridge location (Figure 4.16c). More than 38 m downstream of the bridge location, the SSC from the PTM with the empirical dispersion model showed smaller values than those estimated by the PTM with the RFR and GBR dispersion models. The SSC from the PTM with the GBR was slightly higher than the result of the RFR dispersion models from 32 to 165 m downstream of the bridge. All three PTM models showed similar trends in the fully mixed area between 190 m to 350 m downstream of the bridge.

Figure 4.16 shows that the PTM with the GBR dispersion model predicted higher concentration values along the creek than the RFR and empirical model from the bridge location to approximately 50 m downstream, along the south, center, and north sides of the creek. In the downstream sections, the PTM with the empirical and RFR dispersion models showed similar concentration distributions. Unlike the south and center line of the channel, the PTM with the empirical dispersion model estimated higher sediment concentrations in areas near the bridge location, along the creek's north bank, than the RFR dispersion model. However, the PTM with the empirical dispersion model showed smaller concentrations than the RFR and GBR dispersion models in downstream sections on the north side of the creek.

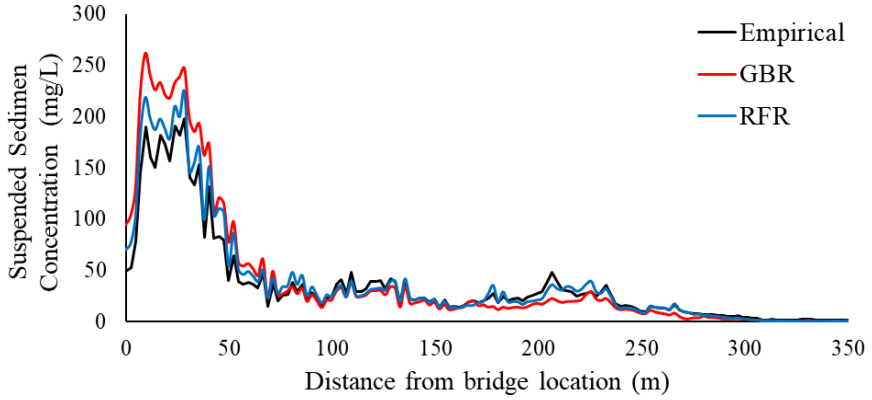


(a)

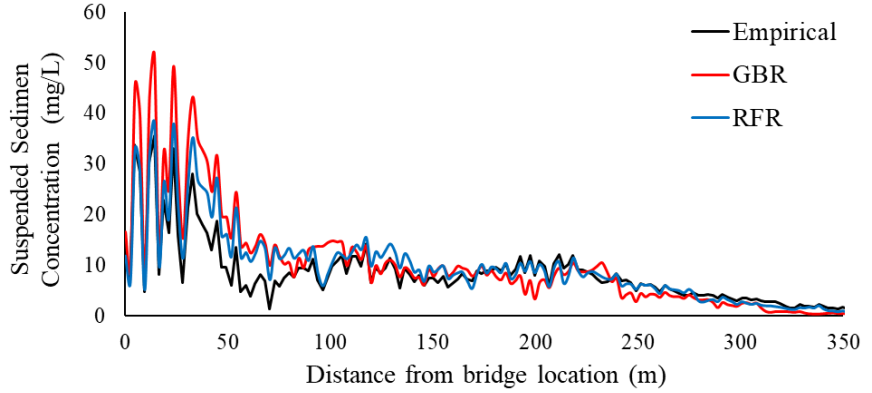


(b)

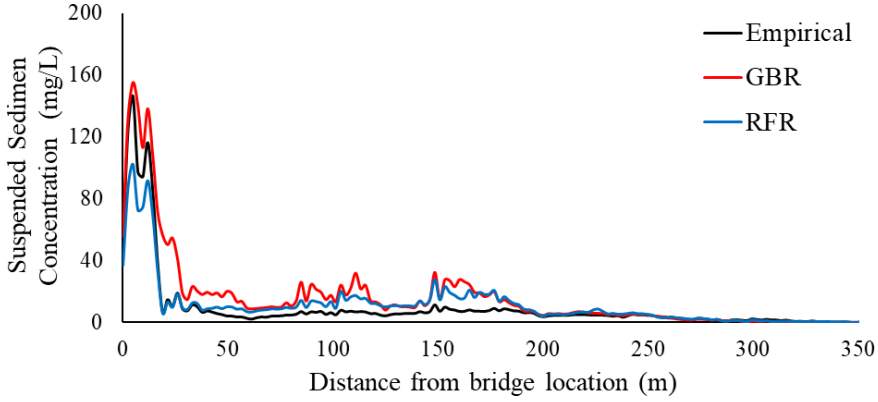


(c)

**Figure 4.16** Variation of suspended sediment concentration along a) south side (L-1), b) center line (L-2), and c) north side (L-3) of Wilson creek (April 29, 2021 storm)

***Suspended Sediment Concentration - November 3, 2021 Storm***

The increase in the suspended sediment concentration in Wilson creek was estimated using the PTM with different dispersion models for the low flow scenario (November 3, 2021). The results are presented in Figure 4.17.

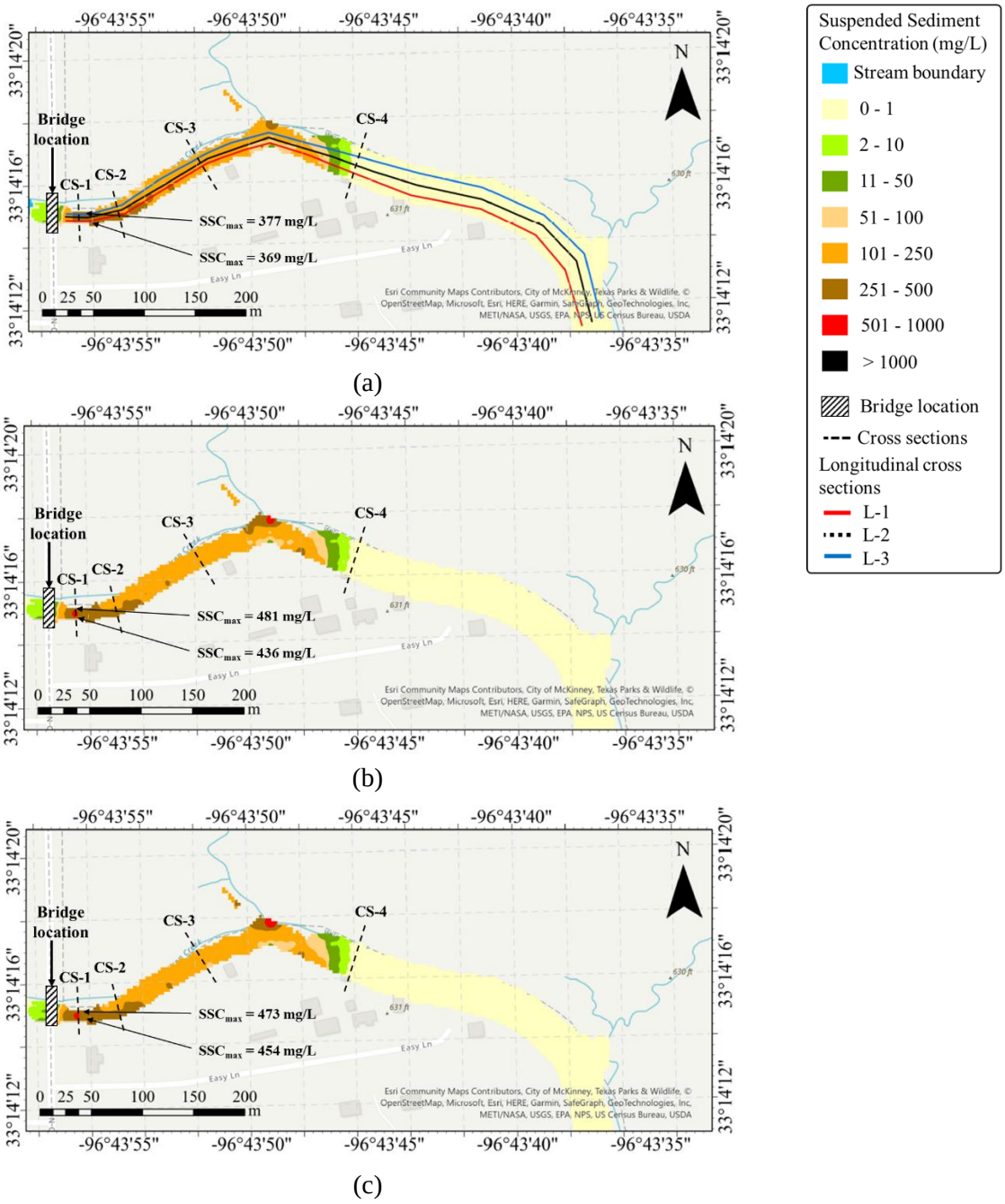


(a)

(b)

(c)

**Figure 4.17** Increase in suspended sediment concentration in Wilson Creek due to overland erosion corresponding to the November 3, 2021 storm estimated by the PTM using different dispersion coefficients: a) Empirical equation, b) RFR model, and c) GBR model

The increase in sediment concentration was due to the overland erosion in the north and south construction areas downstream of the bridge location. The same cross sections (CS-1 to CS-4) were used to compare the results of the PTM across the creek, using different dispersion models. The longitudinal profiles, L-1 to L-3 shown in Figure 4.17a, were used to investigate the

distribution of the sediment concentration along the creek. The elevated suspended sediment concentration across CS-1 to CS-4 on November 3, 2021 is depicted in Figure 4.18. The maximum elevated SSC across CS-1 was estimated as 421, 514, and 506 mg/L by the PTM with empirical equation, RFR, and GBR dispersion models, respectively (Figure 4.18a). The TSS was collected by the water sampler units on November 3, 2021 along the center line of the creek upstream of the bridge and at section CS-2 (Figure 4.5). The average TSS upstream of the bridge and at section CS-2 was measured as 35 mg/L and 174 mg/L, respectively. This means that the average TSS was elevated due to the local overland erosion by 139 mg/L along the center line of the creek from upstream to downstream of the bridge at CS-2 (Baharvand 2022b). The PTM estimated the elevated suspended sediment concentration at the creek's center line (sampling point 3 in Figure 4.18b) as 156, 146, and 143 mg/L, using the empirical equation, RFR, and GBR, respectively. Therefore, the PTM with the empirical equation, RFR, and GBR overestimated the elevated sediment concentration at the center line by 12, 5, and 2.8%.

According to Figure 4.18c, the PTM with the empirical equation, RFR, and GBR estimated the average elevated SSC in section CS-3 as 127, 113, and 114 mg/L, respectively. These values show that the PTM with the RFR and GBR models predicted similar sediment concentrations downstream of the creek, where the sediment was almost fully mixed across the channel. All three models predicted very small sediment concentration values at section CS-4 (< 0.1 mg/L). These values were negligible compared to the sediment concentrations estimated at sections CS-1 and CS-2 and their variations were less significant.

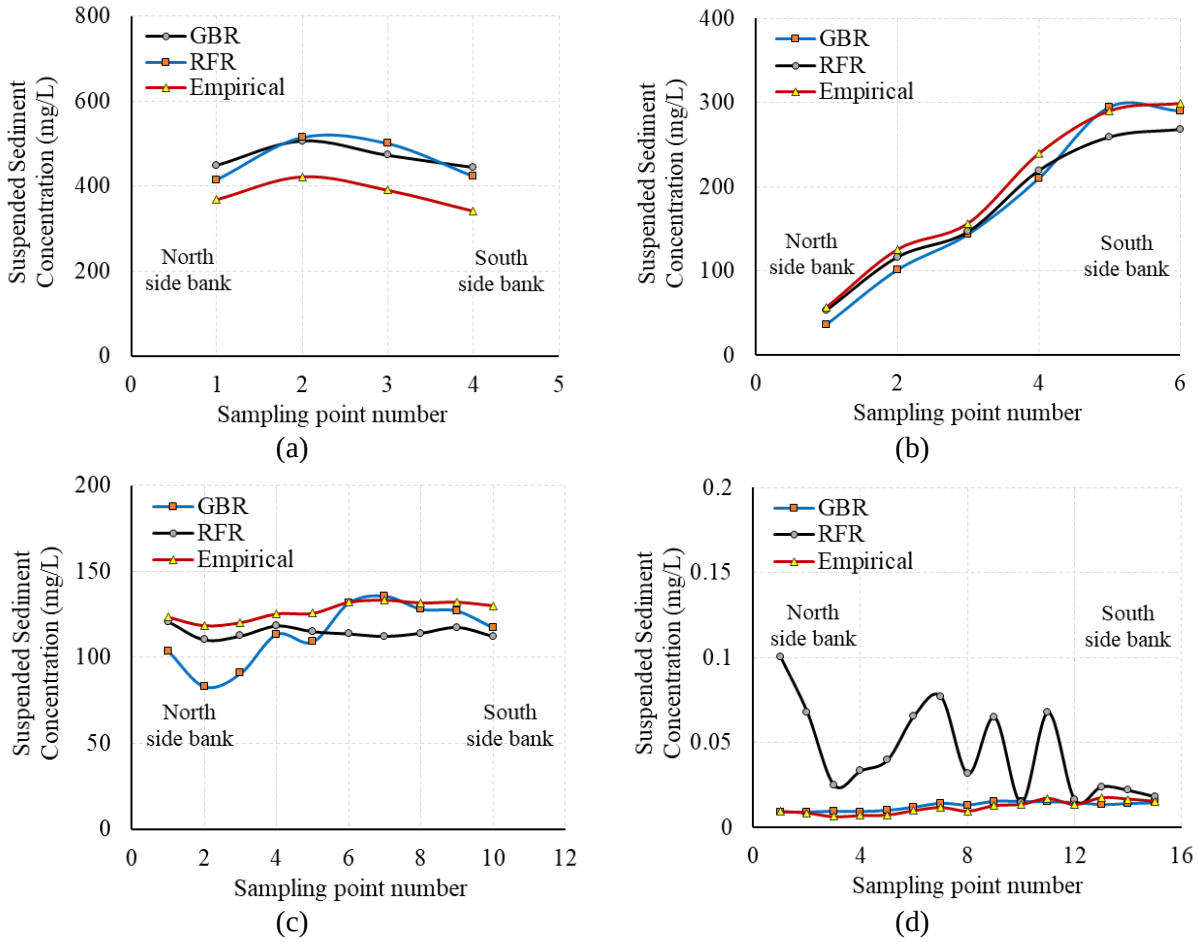


**Figure 4.18** Elevated suspended sediment concentration across Wilson Creek due to overland erosion corresponding to November 3, 2021 storm: a) Cross section CS-1, b) Cross section CS-2, c) Cross section CS-3, and d) Cross section CS-4. Cross sections are shown in Figure 4.17.

Three longitudinal profiles were used to extract the suspended sediment concentration distributions estimated by the PTM, using three dispersion models for the low flow scenario. The extent of each profile (L-1 to L-3) is depicted in Figure 4.17a. The increases in the SSC along L-1 to L-3 are shown in Figure 4.19 for different dispersion models.

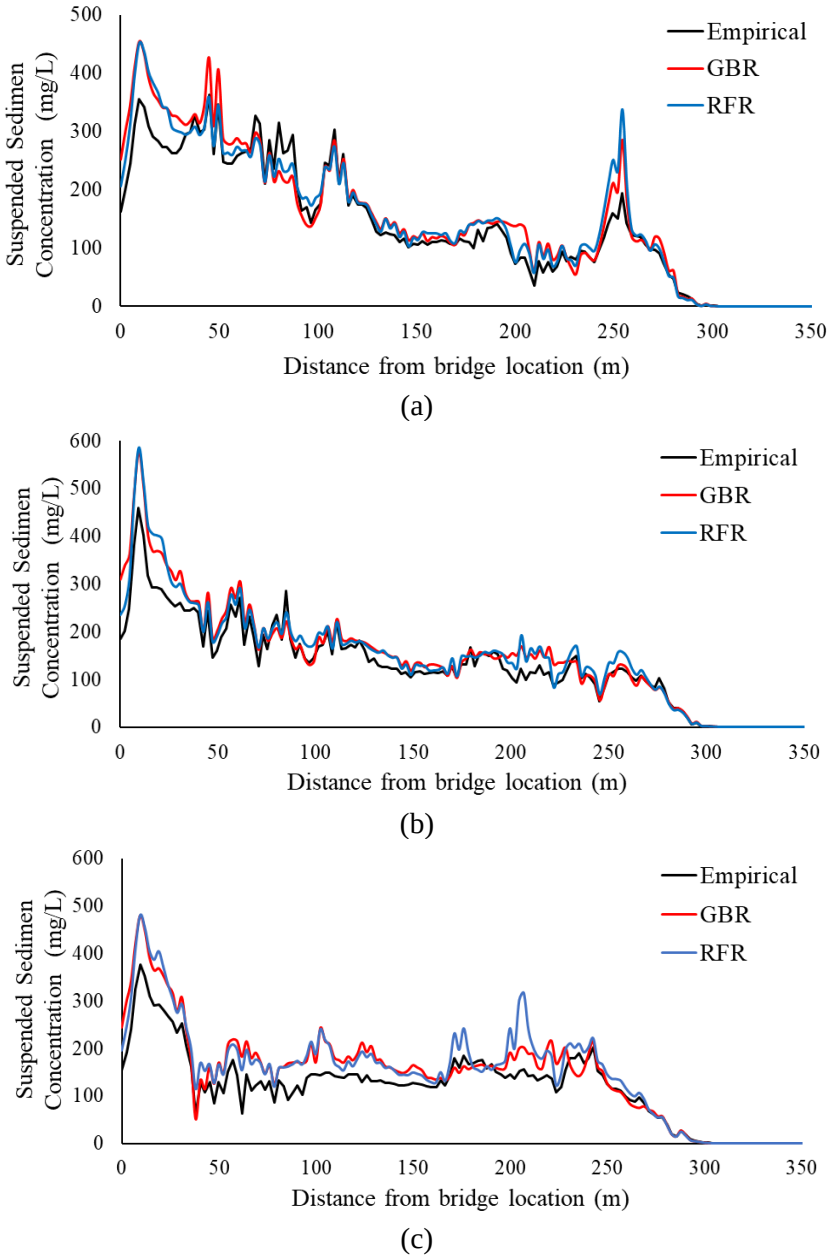


**Figure 4.19** Variation of suspended sediment concentration along a) south side (L-1), b) center line (L-2), and c) north side (L-3) of Wilson creek (November 3, 2021 storm)

Comparing Figure 4.19 with Figure 4.16 shows that the sediment concentration values of all the PTMs were significantly higher than those estimated for the high flow scenario. It could be argued that the smaller flow area and depth during the low flow resulted in locally higher SSC in the creek, even though the sediment load entering the creek during high flow (12.8 tonnes/day) was much higher than the sediment load entering the during the low flow condition (2.4 tonnes/day). The

average width of the creek 350 m downstream of the bridge was approximately 16 and 34 m during low and high flow scenarios, respectively. The average flow depth during the high flow scenario was approximately 2.5 times higher than during the low flow scenario. (The flow depth at the center line of CS-1 and CS-4 for the low scenario was 0.89 m and 2.3 m, respectively, while the flow depth at similar locations during the high flow scenario was 2.9 m and 5.5 m, respectively.) Most of the sediment particles entering the creek from the construction site were deposited before section CS-3 during the low flow scenario; fewer particles were transported to downstream sections during the high flow scenario (Baharvand et al., 2022b). Therefore, a higher concentration of suspended particles was expected between the bridge location and section CS-3 during the high flow scenario

The PTM with the empirical dispersion model predicted smaller values of sediment concentration along the north, south, and center line profiles in an area that extended between the bridge and 40 m downstream, as shown in Figure 4.19; the PTM with the RFR and GBR predicted similar sediment concentrations. On the south side of the creek (Figure 4.19a), 209 m downstream of the bridge, the suspended sediment concentration decreased from 452 mg/L to 63 mg/L for the PTM with RFR and GBR models. The maximum concentration estimated for the south side, using the PTM with the empirical dispersion model, was 341 mg/L 7 m downstream of the bridge and decreased to 36 mg/L 209 m. A sharp increase of more than 200 mg/L was detected in the area from 244 m to 254 m downstream of the bridge location on the south side, which is detectable in Figures 4.17b and c. The sharp increase in the SSC could be due to the shallower flow depth at this location (0.98 m) compared to adjacent areas. From here on, the creek bed elevation decreases, and the flow depth increases to 2.3 m in a distance of 18 m. The applied shear stress at this location was less than the particles' critical shear stress, and no deposition occurred at this point (Baharvand

et al., 2022b). Therefore, a large number of resuspended particles was expected at this location, which increases the sediment concentration significantly.

The maximum concentration estimated for the central part of the channel was 585 mg/L according to the PTM with RFR and GBR dispersion models; the PTM with an empirical dispersion model estimated a maximum concentration of 459 mg/L at this location (Figure 4.19b). On the north side of the creek (Figure 4.19c), the PTM with an empirical dispersion model predicted lower sediment concentration values in most areas along the longitudinal section than the PTM with the RFR and GBR dispersion models. The SSC was negligible along the north, south, and central profiles 285 m downstream of the bridge and, based on field observations and the results of numerical modeling of sediment deposition in Wilson Creek, was due to a high rate of sediment deposition after this segment of the creek (Baharvand et al., 2022b).

## CONCLUSION

Several empirical equations have been used by researchers in previous studies to estimate the longitudinal and transverse dispersion coefficients and model the evolution of pollution and sediment transport in natural streams. They evaluated the performance of some machine learning-based approaches in predicting dispersion coefficients in streams, but some approaches, such as bagging and boosting ensemble models, were not included in their studies. Although there are several studies on the application and sensitivity analysis of machine learning approaches to predict dispersion coefficients in natural streams, the methods they touted have not been used in Lagrangian-based sediment transport models.

The present study used data derived from previous studies to investigate the performance of two ensemble machine learning models, random forest regression and gradient boosting regression, in

predicting longitudinal and transverse dispersion coefficients in natural streams. The resulting data-driven dispersion models were integrated with a Lagrangian particle tracking model (PTM) to simulate suspended sediment concentration in natural streams.

Random forest regression (RFR) and gradient boosting regression (GBR) models were selected as two powerful ensemble learning-based approaches that can be used to accurately predict longitudinal and transverse dispersion coefficients, using the dataset from previous studies. The natural stream dispersion datasets were split into two stages, training (80%) and testing (20%), and the optimal principal parameters (hyperparameters) were identified for each ensemble model, using a grid-search cross-validation (GridsearchCV) technique. Various statistical measures were used to assess the performance of the RFR and GBR models in predicting the longitudinal and dispersion coefficients in streams. The results showed that the GBR model predicted the longitudinal dispersion coefficient more accurately, with a coefficient of determination of $R^2$ = 0.95 and total discrepancy ratio of $DR_s$ = -0.07 in the training stage and a coefficient of determination of $R^2$ = 0.9 and total discrepancy ratio of $DR_s$ = -0.1 in the testing stage. The GBR and RFR models predicted the transverse dispersion coefficient in the training stage as $R^2$ = 0.94 and 0.92, respectively. The RFR model was more accurate in predicting the transverse dispersion than the GBR in the testing stage, with $R^2$ = 0.94 and $DR_s$ = -0.118. According to these results, both the RFR and GBR models accurately predicted the longitudinal and transverse dispersion coefficients; however, the total discrepancy ratios showed that both models underestimated the dispersion coefficients for the hyperparameters of the study in longitudinal and transverse directions.

Since both ensemble models showed acceptable performance in predicting dispersion coefficients in natural streams, they were integrated with the Lagrangian particle tracking model developed by

Baharvand et al. (2022a) to simulate sediment transport in natural streams. The performance of the PTMs were evaluated using field data collected from a section of Wilson Creek near Highway FM 2478 in McKinney, Texas, where road and bridge expansion projects were expected to introduce additional sediment load to the creek during the construction period. The required hydrodynamic parameters were obtained from a HEC-RAS 2D model for two flow conditions with mean daily discharges of 37.4 $m^3/s$ and 7.4 $m^3/s$, corresponding to the April 29 and November 3, 2021 storm events.

The outputs of the PTMs showed that the increase in suspended sediment concentration in Wilson Creek was due to the excess sediment load caused by construction activities in the vicinity of the creek and were used to developed the suspended sediment concentration distributions across and along the channel. A comparison between the cross-sectional sediment concentrations and the field data showed acceptable accuracy of all three models in predicting suspended sediment concentration distributions in the creek. The average sediment concentrations from the PTM with the GBR model correlated better with the results of the field investigations for high and low flow scenarios, however, and the 2D sediment concentration maps showed that the mixing process of the GBR was faster than that of the PTM with RFR and empirical models.

The present model simulated suspended sediment load, using empirical and machine learning-based longitudinal and transverse dispersion models under a steady-state flow condition, and estimated the vertical dispersion coefficient using empirical relationships. In future research, the unsteady flow condition and bedload transport could be added to the PTM to enhance its capabilities, and the vertical dispersion coefficient could be modeled using the machine learning approaches. A limitation of this study is that the dataset that was used to predict the dispersion coefficient may not be applicable for different streams. Therefore, it is suggested that future

research enhance the model's reliability by increasing the number of dispersion coefficient datasets from different natural streams.

**Acknowledgment**

The present study was supported by Texas Department of Transportation (TxDOT) under project Number 0-7023.

**Conflict of Interest** The authors declare no conflict of interest.

## REFERENCES


Ahmad, Z. (2007). “Two-dimensional mixing of pollutants in open channels. ” A technical report submitted to DST, New Delhi, India.

Ahmari, H., Ahsan, M.R, Penner, L.A., and Gonzalez, N. (2013a). “Assessment of erosion and sedimentation for hydropower projects on the lower Nelson River, Manitoba.” Canadian Dam Safety 2013 Annual Conference, Oct. 5-10, Montreal, Quebec, Canada.

Ahmari, H. (2013b). “Shoreline erosion and sedimentation effects during construction. Keeyask Generation Project.” Technical Memorandum GN 9.2.10, Manitoba Hydro, Manitoba, Canada.

Ahmari, H., Baharvand, S., Pebworth, M. (2021). “Developing an ArcGIS Pro Toolkit for assessing bridge construction effects on sediment regime and aquatic habitat.” 20th *Iranian Hydraulic Conference*, Gorgan University of Agricultural Sciences and Natural Resources, Gorgan, Iran.

Ahmari, H., Randklev, C. R., Jaber, F., Yu, X., Baharvand, S., Pebworth, M., Kandel, S., and Goldsmith, A. M. (2022). “Determining downstream ecological impacts of sediment derived from bridge construction.” TxDOT Report No. 0-7023.

Alwated, B., and El-Amin, M. F. (2021). “Enhanced oil recovery by nanoparticles flooding: From numerical modeling improvement to machine learning prediction.” *Advances in Geo-Energy Research*, 5(3), 297–317.

Antonopoulos, V. Z., Georgiou, P. E., and Antonopoulos, Z. V. (2015). "Dispersion coefficient prediction using empirical models and ANNs." *Environmental Processes*, (2), 379–394.

Azamathulla, H. M., and Ahmad, Z. (2012). "Gene-expression programming for transverse mixing coefficient." *Journal of Hydrology*, 434-435, 142–148.

Azamathulla, H. M., and Ghani, A. A. (2011). "Genetic programming for predicting longitudinal dispersion coefficients in streams." *Water Resources Management*, 25(6), 1537–1544.

Azamathulla, H. M., and Wu, F.-C. (2011). “Support vector machine approach for longitudinal dispersion coefficients in natural streams.” *Applied Soft Computing*, 11(2), 2902–2905.

Baharvand, S., Jozaghi, A., Fatahi-Alkouhi, R., Karimzadeh, S., Nasiri, R., and Lashkar-Ara, B. (2021). “Comparative study on the machine learning and regression-based approaches to predict the hydraulic jump sequent depth ratio.” *Iranian Journal of Science and Technology, Transactions of Civil Engineering*, 45(4), 2719–2732.

Baharvand, S., Ahmari, H., Taghvaei, P. (2022a). “Developing A Lagrangian Sediment Transport Model For Open Channel Flows.” *International Journal of Sediment Research*, Elsevier, (*submitted*).

Baharvand, S., Ahmari, H., Kandel, S., Goldsmith, A., Jaber, F., and Yu, Z. (2022b). “Numerical assessment of sediment transport in natural streams using a Lagrangian particle tracking model - case study: Wilson Creek, McKinney, Texas, USA.” *Journal of Hydrology* (*will be submitted*)

Baharvand, S., Rezaei, R., Talebbeydokhti, N., Nasiri, R., and Amiri, S, M. (2022d). “Investigation of energy dissipation rate of stepped vertical overfall (SVO) spillway using physical modeling

and soft computing techniques." *KSCE Journal of Civil Engineering*, Springer, (*accepted*).

Baek, K. O. and Seo, I. W. (2008). "Prediction of transverse dispersion coefficient using vertical profile of secondary flow in meandering channels." *KSCE Journal of Civil Engineering*, 12 (6), 417–426.

Beltaos, S. (1979). "Transverse mixing in natural streams." *Canadian Journal of Civil Engineering*, 6 (4), 575–591.

Beschta, R. L. (1978). "Long-term patterns of sediment production following road construction and logging in the Oregon Coast Range." Water Resources Research, 14(6), 1011–1016.

Black, A. R. (1995). "Major flooding and increased flood frequency in Scotland since 1988." Physics and Chemistry of the Earth, 20(5–6), 463–468.

Breiman, L. (2001). "Random forests." *Machine Learning*.

De Baas, A. F., Van Dop, H., and Nieuwstadt, F. T. M. (1986). "An application of the Langevin equation for inhomogeneous conditions to dispersion in a convective boundary layer." *Quarterly Journal of the Royal Meteorological Society*, 112(471), 165–180.

Elder, J. W. (1959). "The dispersion of marked fluid in turbulent shear flow." *Journal of Fluid Mechanics*, 5(4), 544–560.

Fan, N., Singh, A., Guala, M., Foufoula-Georgiou, E., and Wu, B. (2016). "Exploring a semimechanistic episodic Langevin model for bed load transport: Emergence of normal and anomalous advection and diffusion regimes." *Water Resources Research*, 52(4), 2789–2801.

Fang, H.-W., and Rodi, W. (2003). "Three-dimensional calculations of flow and suspended sediment transport in the neighborhood of the dam for the Three Gorges Project (TGP) reservoir in the Yangtze River." *Journal of Hydraulic Research*, 41(4), 379–394.

Fischer, H. B., and Park, M. (1967). "Transverse mixing in a sand-bed channel." US Geological Survey Professional Paper, 267–272.

Fischer, H. B. (1965). "The mechanics of dispersion in natural streams." *Journal of the Hydraulics Division*, 93(6), 187–216.

Fischer, H. B. (1975) "Simple method for predicting dispersion in streams." Discussion by R.S. Mc Quivey and T.N. Keefer. J Environ Eng Div ASCE 101(3):453–455

Fuat Toprak, Z., and Savci, M. E. (2007). "Longitudinal dispersion coefficient modeling in natural channels using fuzzy logic." *Clean – Soil, Air, Water*, 35(6), 626–637.

Graf, B. (1995). "Observed and predicted velocity and longitudinal dispersion at steady and unsteady flow, Colorado River, Glen Canyon Dam to Lake Mead." *J. Am. Water Resour. Assoc.*, 31(2), 265–281.

Gualtieri, C., and Mucherino, C. (2008). "Comments on 'development of an empirical equation for the transverse dispersion coefficient in natural streams' by Tae Myoung Jeon, Kyong Oh Baek and Il Won Seo." *Environmental Fluid Mechanics*, 8(1), 97–100.

Guy, H.P., and Ferguson, G.E. (1963). "Sediment in small reservoirs due to urbanization." *Journal of Hydraulics Division*. 88(2): 22-37. Available from https://mountainscholar.org/bitstream/handle/10217/198027/CERF_64_06.pdf?sequence=1 [accessed 15 July 2020].

Hastie, L., Boon, P., Young, M., and Way, S. (2001). “The effects of a major flood on an endangered freshwater mussel population.” *Biological Conservation*, 98(1), 107–115.

Hastie, T., Tibshirani, R., and Friedman, J. (2009). "The elements of statistical learning." 2nd ed. New York: Springer.

Holley, E. R., and Abraham, G. (1973). "Laboratory studies on transverse mixing in rivers." *Journal of Hydraulic Research*, 11 (3), 219–253.

Jeon, T. M., Baek, K. O., Seo, I. W. (2007). "Development of an empirical equation for the transverse dispersion coefficient in natural streams." *Environmental Fluid Mechanics*, 7 (4), 317–329.

Kargar, K., Samadianfard, S., Parsa, J., Nabipour, N., Shamshirband, S., Mosavi, A., and Chau, K. (2020). “Estimating longitudinal dispersion coefficient in natural streams using empirical models and machine learning algorithms.” *Engineering Applications of Computational Fluid Mechanics*, 14(1), 311–322.

Kashefipour, S. M., and Falconer, R. A. (2002). "Longitudinal dispersion coefficients in natural channels." *Water Research*, 36(6), 1596–1608.

Krishnappan, B. G., and Lau, Y. L. (1977). "Transverse mixing in meandering channels with varying bottom topography." *Journal of Hydraulic Research*, 15 (4), 351–370.

Lane, A., and Prandle, D. (2006). “Random-walk particle modelling for estimating bathymetric evolution of an estuary.” *Estuarine, Coastal and Shelf Science*, 68(1–2), 175–187.

Lee, M. E., and Seo, I. W. (2013). "Spatially variable dispersion coefficients in meandering channels." *Journal of Hydraulic Engineering*, 139 (2), 141–153.

Ley, A. J., and Thomson, D. J. (1983). "A random walk model of dispersion in the diabatic surface layer." *Quarterly Journal of the Royal Meteorological Society*, 109(462), 867–880.

Lick, W. (2009). "Sediment and contaminant transport in surface waters." CRC Press, Taylor & Francis Group, Boca Raton, FL.

MacDonald, N. J., Davies, M. H., Zundel, A. K., Howlett, J. D., Demirbilek, Z., Gailani, J. Z., and Smith, J. (2006). "PTM: particle tracking model." Report 1: Model theory, implementation, and example applications. Engineering Research and development center Vicksburg MS Coastal and Hydraulic Lab.

Najafzadeh, M., Noori, R., Afroozi, D., Ghiasi, B., Hosseini-Moghari, S.-M., Mirchi, A., Torabi Haghighi, A., and Kløve, B. (2021). “A comprehensive uncertainty analysis of model-estimated longitudinal and lateral dispersion coefficients in open channels.” *Journal of Hydrology*, 603, 126850.

Nezaratian, H., Zahiri, J., Peykani, M. F., Haghiabi, A., and Parsaie, A. (2021). "A genetic algorithm-based support vector machine to estimate the transverse mixing coefficient in streams." *Water Quality Research Journal*, 56(3), 127–142.

Niño, Y., and García, M. (1998). "Using Lagrangian particle saltation observations for bedload sediment transport modelling." *Hydrological Processes*, 12(8), 1197–1218.

Nordin, C. F., and Sabol, G. V. (1974). "Empirical data on longitudinal dispersion in rivers." Water-Resources Investigations, 20-74, U.S. Geological Survey, Reston, VA.

Noori, R., Deng, Z., Kiaghadi, A., and Kachoosangi, F. T. (2016). “How reliable are ANN, ANFIS, and SVM techniques for predicting longitudinal dispersion coefficient in natural rivers?” *Journal of Hydraulic Engineering*, 142(1).

Oh, J. (2011). "Stochastic particle tracking modeling for sediment transport in open channel flows." *Ph.D. dissertation.* State University of New York at Buffalo.

Oh, J., and Tsai, C.W. (2018). "A stochastic multivariate framework for modeling movement of discrete sediment particles in open channel flows." *Stochastic Environmental Research and Risk Assessment*, 32(2).

Ouda, M., and Toorman, E. A. (2019). "Development of a new multiphase sediment transport model for free surface flows." *International Journal of Multiphase Flow*, 117, 81–102.

Park, I., and Seo, I. W. (2018). "Modeling non-Fickian pollutant mixing in open channel flows using two-dimensional particle dispersion model." *Advances in Water Resources*, Elsevier, 111(August 2016), 105–120.

Parsaie, A., and Haghiabi, A. H. (2015). "Computational modeling of pollution transmission in rivers." *Applied Water Science*, 7(3), 1213–1222.

Peacock, E., Haag, W. R., and Warren, M. L. (2005). “Prehistoric decline in freshwater mussels coincident with the advent of maize agriculture.” Conservation Biology, 19(2), 547–551.

Pedregosa, F., Varoquaux, G., Gramfort, A., Michel, V., Thirion, B., Grisel, O., Blondel, M., Prettenhofer, P., Weiss, R., Dubourg, V., Vanderplas, J., Passos, A., Cournapeau, D., Brucher, M., Perrot, M., and Duchesnay, É. (2011) “Scikit-learn: Machine learning in Python.” *Journal of Machine Learning Research* 12 (85): 2825−2830.

Piotrowski, A. P., Rowinski, P. M., and Napiorkowski, J. J. (2012). "Comparison of evolutionary computation techniques for noise injected neural network training to estimate longitudinal dispersion coefficients in rivers." *Expert Systems with Applications*, 39(1), 1354–1361.

Riahi-Madvar, H., Ayyoubzadeh, S. A., Khadangi, E., and Ebadzadeh, M. M. (2009). "An expert system for predicting longitudinal dispersion coefficient in natural streams by using ANFIS." Expert Systems with Applications, 36(4), 8589–8596.

Risken, H. (1989). “The Fokker-Planck Equation.” Methods of Solution and Applications. Springer Verlag.

Rossum, G. van., (1995). “Python tutorial.” Technical Report CS-R9526, Centrum voor Wiskunde en Informatica (CWI), Amsterdam.

Rutherford, J. C. (1994). "River mixing." Wiley, Chichester, UK.

Sahay, R. R., and Dutta, S. (2009). "Prediction of longitudinal dispersion coefficients in natural rivers using genetic algorithm." *Hydrology Research*, 40(6), 544–552.

Salazar, F., and Crookston, B. (2019). "A performance comparison of machine learning algorithms for arced labyrinth spillways." *Water*, 11(3), 544.

Seakem Group, ARA Consulting Group and Northwest Hydraulic Consultants Ltd., Yukon Placer Mining Implementation Review Committee, and North/South Consultants. (1992). “Yukon Placer Mining Study.” 1st ed. Yukon Placer Mining Implementation Review Committee, Sidney, British Columbia. p. 17.

Seo, I.W., Cheong, T.S., (1998). "Predicting longitudinal dispersion coefficient in natural streams." *J. Hydraul. Eng*. 124 (1), 25-32.

Shao, H., and X. Deng. (2018). "AdaBoosting neural network for short-term wind speed forecasting based on seasonal characteristics analysis and lag space estimation." *Comput. Modell. Eng. Sci*. 114 (3): 277–293.

Sulaiman, S. O., Al-Ansari, N., Shahadha, A., Ismaeel, R., and Mohammad, S. (2021). "Evaluation of sediment transport empirical equations: case study of the Euphrates River West Iraq." *Arabian Journal of Geosciences*, 14(10), 825.

Tayfur, G., and Singh, V. P. (2005). "Predicting longitudinal dispersion coefficient in natural streams by artificial neural network." *Journal of Hydraulic Engineering*, 131(11), 991–1000.

Tsai, C. W., Hung, S. Y., and Wu, T.-H. (2020). "Stochastic sediment transport: anomalous diffusions and random movement." *Stochastic Environmental Research and Risk Assessment*, 34(2), 397–413.

Tsai, C.W., Man, C., and Oh, J. (2014). "Stochastic particle-based models for suspended particle movement in surface flows." *International Journal of Sediment Research*, 29(2), 195–207.

Toprak, Z. F., Şen, Z., and Savci, M. E. (2004). "Comment on 'Longitudinal dispersion coefficients in natural channels.'" *Water Research*, 38(13), 3139–3143.

Toprak, Z. F., and Cigizoglu, H. K. (2008). "Predicting longitudinal dispersion coefficient in natural streams by artificial intelligence methods." *Hydrological Processes*, 22(20), 4106–4129.

Tu, L. X., Thanh, V. Q., Reyns, J., Van, S. P., Anh, D. T., Dang, T. D., and Roelvink, D. (2019). "Sediment transport and morphodynamical modeling on the estuaries and coastal zone of the Vietnamese Mekong Delta." *Continental Shelf Research*, 186, 64–76.

United States Environmental Protection Agency (2017). "EnviroAtlas. Total Suspended Solids (TSS)-EPA Method160.2." Retrieved: 01,19,2017, from: https://19january2017snapshot.epa.gov/sites/production/files/2015-06/documents/160_2.pdf.

Waskom, M. (2021). "Seaborn: statistical data visualization." *Journal of Open Source Software*, 6(60), 3021.

Wu, W. (2004). "Depth-averaged two-dimensional numerical modeling of unsteady flow and nonuniform sediment transport in open channels." *Journal of Hydraulic Engineering*, 130(10), 1013–1024.

Yotsukura, N., Fischer, H. B., and Sayre, W. W. (1970). "Measurement of mixing characteristics of the Missouri River between Sioux City, Iowa and Plattsmouth, Nebraska." U.S. Geological Survey Water-Supply Paper 1899-G, U.S. Government Printing Office, Washington, DC

Zahiri, J., and Nezaratian, H. (2020). "Estimation of transverse mixing coefficient in streams using M5, MARS, GA, and PSO approaches." *Environmental Science and Pollution Research*, 27(13), 14553–14566.

Zeng, Y., and Huai, W. (2014). "Estimation of longitudinal dispersion coefficient in rivers." *Journal of Hydro-environment Research*, 8(1), 2–8.

Zhu, M. (2007). “Kernels and ensembles: Perspectives on statistical learning.” *arXiv:0712.1027 [stat.ME]*

# CHAPTER 5

# GENERAL CONCLUSIONS AND FUTURE RESEARCH RECOMMENDATIONS

Sediment erosion and transport processes are critical processes that impact the health of the ecosystem and threaten aquatic species in natural streams; however, sediment transport models can help control and manage the nutrient and sediment loading. Lagrangian models were developed during the course of this research to effectively assess the advection and dispersion of sediment in open channels and evaluate the ability of various types of empirical relationships and machine learning-based approaches to predict the dispersion coefficient. The following section presents the findings and achievements of this research and offers suggestions and recommendations for future work.

## CONCLUSIONS

The following findings correspond to the objectives of this study:

- A Lagrangian stochastic particle tracking model was developed to simulate sediment transport in open channel flows. Two-dimensional discretized advection and three-dimensional dispersion terms were used to simulate sediment particles in an Eulerian flow domain. The model simulates the movement of sediment particles in suspension, and sediment deposition and resuspension were considered in the PTM, using a mobility factor based on the Shield criteria.
- The performances of three longitudinal dispersion equations (Elder 1959, Kashefipour and Falconer 2002, and Sahay and Dutta 2009) were examined to select the one best suited for

a PTM of a prismatic open channel, and it was determined that the longitudinal dispersion coefficient proposed by Elder (1959) was more accurate than the others for this purpose.

- The PTM's ability to generate vertical distribution of dimensionless sediment concentration ($C/C_{max}$) in prismatic open channels was assessed for a variety of sediment gradations, from very fine sand to medium sand, obtained from a laboratory study by Coleman (1986). The PTM that was developed using the longitudinal dispersion coefficient proposed by Elder (1959) more accurately predicted the sediment concentration for coarser material, with a correlation coefficient of 0.96 and standard deviation of 0.26; however, it was less accurate in estimating sediment concentrations in depths ($z/H$) ranging between 0.15 and 0.21 for all sediment gradations.
- The PTM results were compared to the analytical solution of the advection-dispersion model for a straight rectangular channel with an instantaneous sediment source. The longitudinal and transverse sediment concentrations from the analytical solution and the PTM showed an acceptable agreement, confirming the ability of the PTM to predict the SSC variation in a straight rectangular channel. However, the PTM model underestimated the maximum sediment concentration with 6.3% and 9.4% error from the analytical solution for time steps of t = 30 s and 50 seconds, respectively.
- The PTM was used to simulate sediment transport in a section of Wilson Creek in McKinney, Texas, during bridge and roadway construction activities to evaluate the model's ability to predict the suspended sediment concentration and depositional areas in a natural stream. The predicted increase in suspended sediment concentration was comparable to the expected values and the field data. The accuracy of the PTM in determining the potential depositional areas was acceptable and comparable to those

predicted by field measurements for different local sediment gradations that contributed to sediment loads from construction sites.

- Random forest regression (RFR) and gradient boosting regression (GBR) models were the two powerful ensemble learning-based approaches that were selected for predicting longitudinal and transverse dispersion coefficients, using the dataset from previous studies. A sensitivity analysis was conducted on the hyperparameters of each model, using a grid-search cross-validation (GridsearchCV) technique, and revealed the optimal principal parameters for modeling the longitudinal and transverse dispersion coefficients in streams. Both models showed an acceptable level of accuracy for predicting the dispersion coefficients in the training and testing stages, after splitting dataset with a fraction of 80% and 20%, respectively, and both underestimated the dispersion coefficients and had a coefficient of determination above 0.9 for the testing stage.
- The RFR and GBR models were integrated into the Lagrangian particle tracking model to investigate the performance of learning-based dispersion coefficients and empirical dispersion relationships, using the field data obtained downstream of a construction site at Wilson Creek for high ($Q = 37.4\ m^3/s$) and low flow ($Q = 7.4\ m^3/s$) scenarios. It was revealed that all three PTMs can accurately predict the sediment concentration distribution downstream of the bridge, but a comparison of the PTM with ensemble dispersion coefficients and empirical-based dispersion relationships revealed the superior performance of the GBR model. All of the models demonstrated an acceptable level of accuracy in predicting the suspended sediment concentration distribution in natural streams.

- The PTM with the GBR model showed a relatively higher maximum concentration in the upstream sections close to the construction site than the PTM with RFR and empirical-based dispersion models. It also showed lower cross-sectional concentration values in the downstream sections than the RFR model, which means that its mixing process could be faster.

The overall accuracy of the Lagrangian PTMs with different dispersion coefficient models was assessed using laboratory dataset, analytical solution, and field measurements, and it was concluded that the model has the ability to effectively simulate sediment transport in natural streams.

**RECOMMENDATION FOR FUTURE RESEARCH**

- The present study modelled sediment transport using the Lagrangian approach, considering longitudinal and transverse advection with three-dimensional dispersion coefficients. It is suggested that future studies consider the vertical velocity component in conjunction with the settling velocity of particles to better simulate the vertical motion of particles, using both advection and dispersion coefficients.
- The proposed model does not consider bedload transport or the geomorphologic evolution of channel beds. Therefore, it is suggested that a bedload transport model be coupled with the PTM developed in this study to provide a full range of sediment transport in open channels, including suspended and bedload transport.
- The PTM performance was evaluated for a range of particle gradations and may not be applicable for smaller or larger sediment particles. Therefore, it is recommended that future studies consider the applicability of PTMs for a wider range of sediment particle

sizes and modify the model based on the potential correction factors to address the motion of different particle sizes in natural streams.

- The present model simulates the suspended sediment load using empirical and machine learning-based longitudinal and transverse dispersion models under a steady state flow condition. Adding the unsteady flow condition and bedload transport to the PTM to enhance its capabilities could broaden the impact of this research.

The limited dataset used to predict the dispersion coefficient, using machine learning approaches, may not be applicable for natural streams with different ranges of hydrodynamic parameters that are not included in this study. Therefore, it is suggested that future researchers enhance the reliability of the model by increasing the number of dispersion coefficients by using other available datasets or conducting field measurements.

- In the present study, the vertical dispersion coefficient was estimated using empirical relationships. In future research, it could be modelled, using machine learning approaches.

## APPENDIX A

## DISPERSION COEFFICIENT DATASET FOR NATURAL STREAMS

This section discusses the correlation between feature and target data of the dataset for dispersion coefficients in natural streams. Figure A-1 shows the correlation of the feature dataset with the longitudinal dispersion coefficient, as well as the count of each feature parameter. The coefficient of determination ($R^2$) between longitudinal dispersion coefficient ($D_x$) with $H$, $u$, and $u^*$ is 0.33, 0.48, and 0.01, respectively.

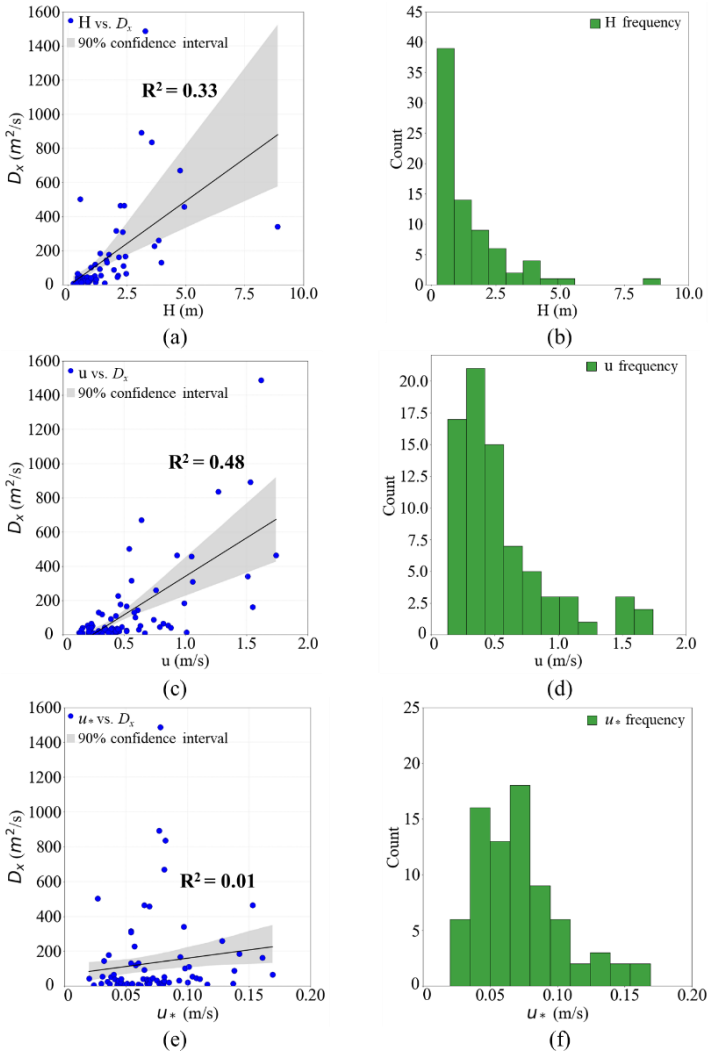


**Figure A. 1** Longitudinal dispersion coefficient against the feature datasets, and frequency of each feature dataset: (a) and (b) flow depth ($H$); (c), (d) flow velocity; (e), (f) shear velocity

Figure A.2 shows a similar plot for the transverse dispersion coefficient and shows that the transverse dispersion coefficient is more correlated with the flow depth, with a coefficient of determination of 0.81. The coefficient for flow velocity and shear velocity was estimated at 0.53 and 0.26, respectively.

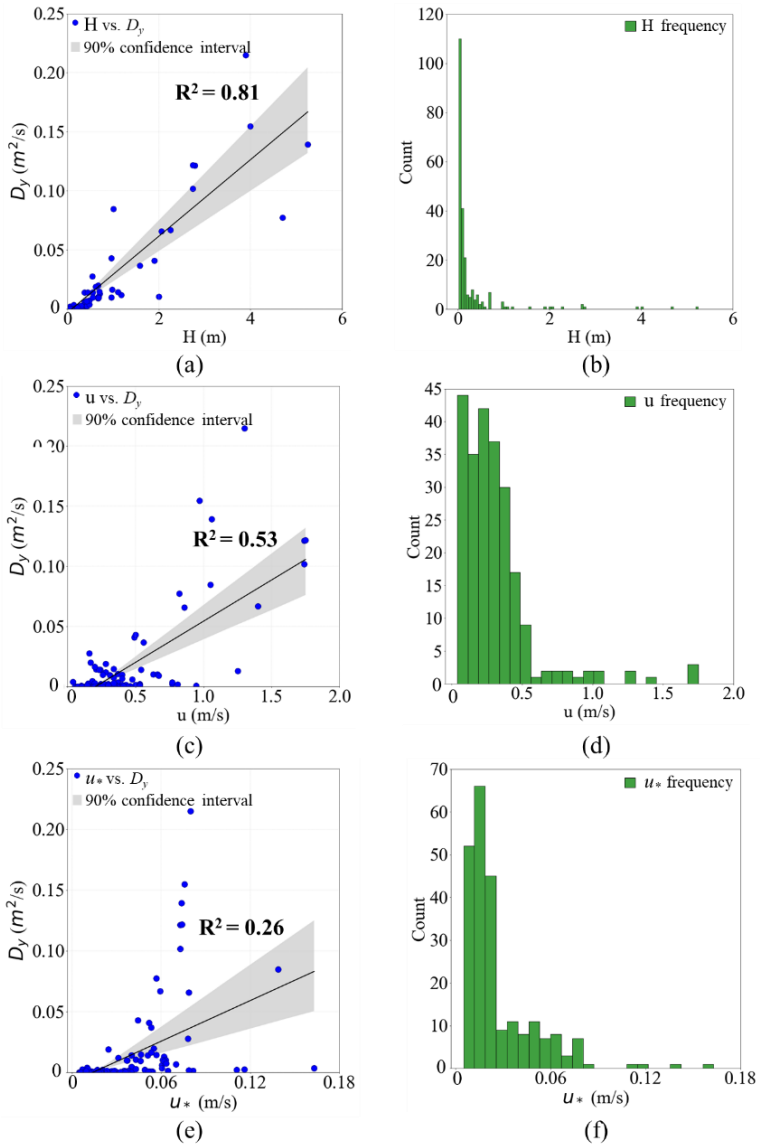


**Figure A. 2** Transverse dispersion coefficient against the feature datasets, and frequency of each feature dataset: (a) and (b) flow depth (*H*); (c), (d) flow velocity; (e), (f) shear velocity

The number of the longitudinal and transverse dispersion coefficients are shown as histograms in Figure A-3.

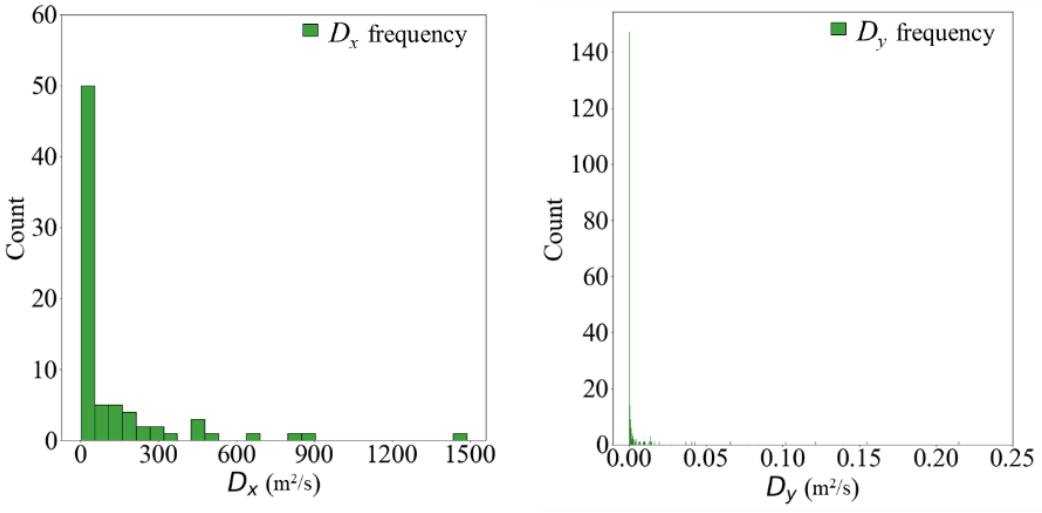


(a) (b)

**Figure A. 3** Frequency of target parameters: a) longitudinal dispersion coefficient ($D_x$), and b) transverse dispersion coefficient ($D_y$)

The datasets used in this study for longitudinal and transverse dispersion coefficients are shown in Tables A-1 and A-2, respectively. The longitudinal dispersion data was obtained from Fischer (1968), Yotsukura et al. (1970), McQuivey and Keffer (1974), Nordin and Sabol (1974), Rutherford (1994), Graf (1995), and Toprak and Cigizoglu (2008). The transvers dispersion data was from different sources collected by Nezaratian et al (2021).

**Table A. 1** Longitudinal Dispersion Datasets Used in this Study

| No. | $H$ | $u$ | $u_*$ | $D_x$ | No. | $H$ | $U$ | $u_*$ | $D_x$ |
|---|---|---|---|---|---|---|---|---|---|
| 1 | 0.49 | 0.21 | 0.079 | 19.52 | 40 | 0.55 | 0.35 | 0.044 | 30.19 |
| 2 | 0.84 | 0.52 | 0.1 | 21.4 | 41 | 1.13 | 0.39 | 0.075 | 32.52 |
| 3 | 0.49 | 0.25 | 0.079 | 9.5 | 42 | 1.35 | 0.39 | 0.065 | 92.9 |
| 4 | 0.86 | 0.28 | 0.067 | 13.93 | 43 | 0.98 | 0.59 | 0.098 | 101.5 |
| 5 | 2.13 | 0.86 | 0.104 | 53.88 | 44 | 0.66 | 0.43 | 0.085 | 20.9 |
| 6 | 2.09 | 0.79 | 0.107 | 46.45 | 45 | 0.71 | 0.16 | 0.046 | 41.4 |
| 7 | 0.39 | 0.14 | 0.116 | 9.85 | 46 | 0.65 | 0.62 | 0.044 | 29.6 |
| 8 | 0.85 | 0.16 | 0.055 | 9.5 | 47 | 1.15 | 0.32 | 0.058 | 119.8 |
| 9 | 0.58 | 0.3 | 0.049 | 8.08 | 48 | 0.41 | 0.23 | 0.04 | 66.5 |
| 10 | 1.56 | 0.67 | 0.043 | 9.57 | 49 | 0.69 | 0.23 | 0.064 | 40.8 |
| 11 | 0.94 | 0.34 | 0.067 | 32.52 | 50 | 0.41 | 0.15 | 0.081 | 29.3 |
| 12 | 0.91 | 0.4 | 0.067 | 39.48 | 51 | 1.13 | 0.63 | 0.081 | 53.3 |
| 13 | 0.41 | 0.29 | 0.044 | 13.94 | 52 | 1.95 | 0.74 | 0.138 | 88.9 |
| 14 | 0.39 | 0.32 | 0.06 | 9.29 | 53 | 2.44 | 0.52 | 0.094 | 166.9 |
| 15 | 0.52 | 0.43 | 0.069 | 16.26 | 54 | 0.5 | 0.24 | 0.038 | 52.2 |
| 16 | 0.71 | 0.52 | 0.081 | 25.55 | 55 | 0.31 | 0.25 | 0.062 | 1.9 |
| 17 | 0.32 | 0.21 | 0.043 | 4.65 | 56 | 0.22 | 0.39 | 0.053 | 7.1 |
| 18 | 0.45 | 0.32 | 0.051 | 13.94 | 57 | 0.45 | 0.32 | 0.024 | 5.8 |
| 19 | 0.87 | 0.44 | 0.07 | 37.16 | 58 | 1.4 | 0.2 | 0.031 | 54.7 |
| 20 | 2.23 | 0.93 | 0.065 | 464.52 | 59 | 0.52 | 0.54 | 0.027 | 501.4 |
| 21 | 3.56 | 1.27 | 0.082 | 836.13 | 60 | 0.59 | 0.27 | 0.08 | 10.3 |
| 22 | 3.11 | 1.53 | 0.077 | 891.87 | 61 | 0.81 | 0.48 | 0.072 | 45.1 |
| 23 | 0.98 | 0.88 | 0.11 | 41.81 | 62 | 0.4 | 0.34 | 0.02 | 44 |
| 24 | 2.16 | 1.55 | 0.161 | 162.58 | 63 | 1.62 | 0.61 | 0.032 | 143.8 |
| 25 | 0.3 | 0.43 | 0.046 | 9.29 | 64 | 3.96 | 0.29 | 0.06 | 130.5 |
| 26 | 0.42 | 0.46 | 0.046 | 20.9 | 65 | 3.66 | 0.45 | 0.057 | 227.6 |
| 27 | 0.56 | 1.01 | 0.137 | 13.94 | 66 | 1.74 | 0.47 | 0.036 | 177.7 |
| 28 | 2.46 | 0.82 | 0.169 | 65.03 | 67 | 1.65 | 0.58 | 0.054 | 131.3 |
| 29 | 0.26 | 0.31 | 0.043 | 6.97 | 68 | 2.32 | 1.06 | 0.054 | 308.9 |
| 30 | 0.41 | 0.37 | 0.055 | 13.94 | 69 | 0.5 | 0.13 | 0.037 | 12.8 |
| 31 | 0.81 | 0.29 | 0.068 | 23.23 | 70 | 0.51 | 0.23 | 0.03 | 14.7 |
| 32 | 0.8 | 0.42 | 0.068 | 30.19 | 71 | 0.93 | 0.36 | 0.035 | 24.2 |
| 33 | 2.04 | 0.56 | 0.054 | 315.87 | 72 | 4.94 | 1.05 | 0.069 | 457.7 |
| 34 | 4.75 | 0.64 | 0.081 | 668.9 | 73 | 8.9 | 1.51 | 0.097 | 341.1 |
| 35 | 2.35 | 0.43 | 0.101 | 111.48 | 74 | 1.37 | 0.99 | 0.142 | 184.6 |
| 36 | 3.84 | 0.76 | 0.128 | 260.13 | 75 | 2.38 | 1.74 | 0.153 | 464.6 |
| 37 | 0.81 | 0.37 | 0.077 | 13.94 | 76 | 1.16 | 0.21 | 0.069 | 14.76 |
| 38 | 1.2 | 0.45 | 0.093 | 32.52 | 77 | 3.28 | 1.62 | 0.078 | 1486.45 |
| 39 | 0.98 | 0.21 | 0.041 | 39.48 | | | | | |

**Table A. 2** Transverse Dispersion Datasets Used in this Study

| No. | $H$ | $u$ | $u_*$ | $D_y$ | No. | $H$ | $U$ | $u_*$ | $D_y$ |
|---|---|---|---|---|---|---|---|---|---|
| 1 | 1.9 | 0.49 | 0.052 | 0.041 | 40 | 0.0396 | 0.328 | 0.015084 | 0.0001 |
| 2 | 0.04 | 0.465 | 0.027 | 0.000189 | 41 | 0.04 | 0.243 | 0.013311 | 7.89E-05 |
| 3 | 0.33 | 0.247 | 0.0221 | 0.001065 | 42 | 0.174 | 0.5 | 0.0351 | 0.0015 |
| 4 | 0.36 | 0.2487 | 0.0215 | 0.001117 | 43 | 0.09 | 0.142 | 0.0151 | 0.000155 |
| 5 | 0.111 | 0.46 | 0.0199 | 0.000356 | 44 | 0.04 | 0.27 | 0.014377 | 0.000104 |
| 6 | 0.22 | 0.31 | 0.0141 | 0.000326 | 45 | 0.018 | 0.2 | 0.0239 | 0.000085 |
| 7 | 0.44 | 0.18 | 0.04 | 0.0047 | 46 | 0.06 | 0.126 | 0.0153 | 0.000122 |
| 8 | 0.4 | 0.18 | 0.0402 | 0.004663 | 47 | 0.171 | 0.35 | 0.0364 | 0.000674 |
| 9 | 0.027 | 0.5 | 0.0264 | 0.000119 | 48 | 0.06 | 0.1 | 0.0059 | 0.000063 |
| 10 | 0.015 | 0.31 | 0.0212 | 0.000064 | 49 | 0.148 | 0.235 | 0.0381 | 0.00133 |
| 11 | 0.04 | 0.056 | 0.0077 | 0.00004 | 50 | 0.09 | 0.129 | 0.0073 | 0.000116 |
| 12 | 2 | 0.37 | 0.043 | 0.0105 | 51 | 0.04 | 0.092 | 0.0125 | 0.000066 |
| 13 | 0.37 | 0.24 | 0.04 | 0.014 | 52 | 0.371 | 0.371 | 0.0604 | 0.00369 |
| 14 | 0.7 | 1.25 | 0.062 | 0.01302 | 53 | 0.06 | 0.1 | 0.0059 | 0.000063 |
| 15 | 0.158 | 0.945 | 0.0518 | 0.000665 | 54 | 0.028 | 0.3 | 0.0164 | 0.000079 |
| 16 | 0.28 | 0.24 | 0.0162 | 0.000249 | 55 | 0.09 | 0.1667 | 0.0115 | 0.000165 |
| 17 | 0.371 | 0.475 | 0.0604 | 0.00592 | 56 | 0.013 | 0.2 | 0.0269 | 0.000088 |
| 18 | 0.173 | 0.35 | 0.0166 | 0.000325 | 57 | 0.07 | 0.3913 | 0.019513 | 0.000153 |
| 19 | 0.04 | 0.081 | 0.0077 | 0.000044 | 58 | 0.025 | 0.2 | 0.0208 | 0.000092 |
| 20 | 0.09 | 0.167 | 0.0115 | 0.000165 | 59 | 0.09 | 0.171 | 0.0188 | 0.000225 |
| 21 | 0.09 | 0.129 | 0.0073 | 0.000116 | 60 | 0.064 | 0.299 | 0.0335 | 0.000418 |
| 22 | 0.041 | 0.35 | 0.019 | 0.000106 | 61 | 0.03 | 0.27 | 0.0157 | 0.000079 |
| 23 | 0.248 | 0.244 | 0.049 | 0.00234 | 62 | 0.04 | 0.27 | 0.014623 | 9.19E-05 |
| 24 | 0.016 | 0.2 | 0.0239 | 0.000074 | 63 | 0.09 | 0.129 | 0.0073 | 0.000116 |
| 25 | 0.04 | 0.072 | 0.0099 | 0.000052 | 64 | 0.05 | 0.23 | 0.014 | 0.000092 |
| 26 | 0.104 | 0.43 | 0.0506 | 0.000748 | 65 | 0.28 | 0.246 | 0.0274 | 0.000979 |
| 27 | 0.09 | 0.105 | 0.0115 | 0.000138 | 66 | 0.126 | 0.53 | 0.116 | 0.00238 |
| 28 | 0.053 | 0.43 | 0.0218 | 0.000143 | 67 | 0.034 | 0.2 | 0.0191 | 0.000088 |
| 29 | 0.066 | 0.45 | 0.0214 | 0.000204 | 68 | 0.032 | 0.2 | 0.0209 | 0.000116 |
| 30 | 0.053 | 0.43 | 0.0209 | 0.000133 | 69 | 0.06 | 0.108 | 0.0094 | 0.000082 |
| 31 | 0.125 | 0.31 | 0.0541 | 0.000938 | 70 | 0.67 | 0.66 | 0.061 | 0.010218 |
| 32 | 0.07 | 0.3387 | 0.017203 | 0.000123 | 71 | 0.04 | 0.056 | 0.0077 | 0.00004 |
| 33 | 0.028 | 0.2 | 0.0176 | 0.000067 | 72 | 0.017 | 0.33 | 0.0198 | 0.000079 |
| 34 | 0.033 | 0.19 | 0.0203 | 0.000088 | 73 | 0.065 | 0.33 | 0.016769 | 0.000113 |
| 35 | 0.06 | 0.126 | 0.0153 | 0.000122 | 74 | 0.06 | 0.1 | 0.0121 | 0.000096 |
| 36 | 0.079 | 0.312 | 0.016543 | 0.000129 | 75 | 0.053 | 0.43 | 0.0223 | 0.000133 |
| 37 | 0.04 | 0.081 | 0.0077 | 0.000044 | 76 | 0.073 | 0.23 | 0.012 | 0.000118 |
| 38 | 0.065 | 0.28 | 0.0155 | 0.000124 | 77 | 0.065 | 0.299 | 0.01563 | 0.000152 |
| 39 | 0.68 | 0.63 | 0.063 | 0.010282 | | | | | |

**Table A-2** (Continued)

| No. | $H$ | $u$ | $u_*$ | $D_y$ | No. | $H$ | $U$ | $u_*$ | $D_y$ |
|---|---|---|---|---|---|---|---|---|---|
| 78 | 0.04 | 0.075 | 0.0049 | 0.000034 | 117 | 0.06 | 0.128 | 0.0094 | 0.000087 |
| 79 | 0.04 | 0.098 | 0.0077 | 0.000047 | 118 | 0.039 | 0.2 | 0.0188 | 0.000111 |
| 80 | 0.09 | 0.14 | 0.0188 | 0.000222 | 119 | 0.05 | 0.31 | 0.016074 | 8.82E-05 |
| 81 | 0.06553 | 0.3764 | 0.018954 | 0.000146 | 120 | 0.064 | 0.46 | 0.0401 | 0.000352 |
| 82 | 0.04 | 0.098 | 0.0077 | 0.000047 | 121 | 0.07 | 0.359 | 0.017931 | 0.000218 |
| 83 | 0.06 | 0.108 | 0.0094 | 0.000082 | 122 | 0.07 | 0.311 | 0.015979 | 0.000133 |
| 84 | 0.132 | 0.77 | 0.111 | 0.00227 | 123 | 0.04 | 0.075 | 0.0049 | 0.000034 |
| 85 | 0.09 | 0.105 | 0.0115 | 0.000138 | 124 | 0.09 | 0.171 | 0.0188 | 0.000225 |
| 86 | 0.05 | 0.256 | 0.014377 | 0.000103 | 125 | 0.126 | 0.53 | 0.0814 | 0.00155 |
| 87 | 0.0519 | 0.3275 | 0.017075 | 0.000133 | 126 | 0.097 | 0.112 | 0.006 | 0.000092 |
| 88 | 0.06753 | 0.3831 | 0.019207 | 0.00024 | 127 | 0.053 | 0.42 | 0.0214 | 0.000121 |
| 89 | 0.09 | 0.19 | 0.0099 | 0.000097 | 128 | 0.065 | 0.345 | 0.017441 | 0.00015 |
| 90 | 0.127 | 0.3 | 0.0301 | 0.000372 | 129 | 0.04 | 0.092 | 0.0125 | 0.000066 |
| 91 | 0.023 | 0.2 | 0.0178 | 0.00005 | 130 | 0.06 | 0.1 | 0.0121 | 0.000096 |
| 92 | 0.04 | 0.098 | 0.0077 | 0.000047 | 131 | 0.04 | 0.082 | 0.0077 | 0.000044 |
| 93 | 0.04 | 0.2 | 0.0158 | 0.000088 | 132 | 0.04 | 0.069 | 0.0125 | 0.000065 |
| 94 | 0.09 | 0.171 | 0.0188 | 0.000225 | 133 | 0.055 | 0.3 | 0.036 | 0.0004 |
| 95 | 0.108 | 0.39 | 0.0186 | 0.000278 | 134 | 0.0665 | 0.306 | 0.0325 | 0.000346 |
| 96 | 0.173 | 0.31 | 0.016 | 0.00065 | 135 | 0.039 | 0.37 | 0.0373 | 0.000198 |
| 97 | 0.05 | 0.302 | 0.015749 | 0.000155 | 136 | 0.07903 | 0.4198 | 0.020571 | 0.000304 |
| 98 | 0.068 | 0.36 | 0.0501 | 0.000481 | 137 | 0.127 | 0.31 | 0.0646 | 0.00148 |
| 99 | 0.148 | 0.235 | 0.0381 | 0.000958 | 138 | 0.4 | 0.15 | 0.0105 | 0.002604 |
| 100 | 0.05 | 0.3 | 0.0172 | 0.000141 | 139 | 0.3 | 0.1 | 0.0068 | 0.000898 |
| 101 | 0.053 | 0.42 | 0.0212 | 0.000145 | 140 | 1.17 | 0.28 | 0.03108 | 0.012 |
| 102 | 0.09 | 0.167 | 0.0115 | 0.000165 | 141 | 0.96 | 0.4 | 0.037202 | 0.01 |
| 103 | 0.06 | 0.1 | 0.0153 | 0.000121 | 142 | 0.54 | 0.16 | 0.078 | 0.027799 |
| 104 | 0.017 | 0.2 | 0.0239 | 0.000059 | 143 | 0.67 | 0.17 | 0.055 | 0.019899 |
| 105 | 0.07 | 0.371 | 0.018415 | 0.000114 | 144 | 2.74 | 1.74 | 0.0729 | 0.10187 |
| 106 | 0.039 | 0.31 | 0.0182 | 0.000114 | 145 | 0.42 | 0.2 | 0.007 | 0.002499 |
| 107 | 0.031 | 0.2 | 0.0154 | 0.000062 | 146 | 0.48 | 0.04 | 0.01 | 0.003984 |
| 108 | 0.042 | 0.18 | 0.011 | 0.000074 | 147 | 0.3 | 0.1 | 0.0054 | 0.000275 |
| 109 | 0.05 | 0.2888 | 0.015249 | 0.0001 | 148 | 0.0372 | 0.268 | 0.0213 | 0.00103 |
| 110 | 0.04 | 0.075 | 0.0049 | 0.000034 | 149 | 0.0302 | 0.317 | 0.0266 | 0.001125 |
| 111 | 0.09 | 0.135 | 0.0149 | 0.000178 | 150 | 0.68 | 0.31 | 0.0462 | 0.009425 |
| 112 | 0.06 | 0.128 | 0.0094 | 0.000087 | 151 | 5.25 | 1.06 | 0.0738 | 0.139482 |
| 113 | 0.09 | 0.135 | 0.0149 | 0.000178 | 152 | 0.022 | 0.197 | 0.0168 | 0.000185 |
| 114 | 0.06 | 0.128 | 0.0094 | 0.000087 | 153 | 0.0203 | 0.19 | 0.0137 | 0.000195 |
| 115 | 0.67 | 0.67 | 0.062 | 0.009139 | 154 | 0.3 | 0.1 | 0.0054 | 0.000194 |
| 116 | 0.09 | 0.142 | 0.0151 | 0.000155 | 155 | 0.21 | 0.43 | 0.024 | 0.000857 |

**Table A-2** (Continued)

| No. | $H$ | $u$ | $u_*$ | $D_y$ | No. | $H$ | $U$ | $u_*$ | $D_y$ |
|---|---|---|---|---|---|---|---|---|---|
| 156 | 0.61 | 0.28 | 0.024526 | 0.019 | 195 | 0.173 | 0.37 | 0.0175 | 0.000286 |
| 157 | 0.0528 | 0.27 | 0.017 | 0.002154 | 196 | 0.245 | 0.344 | 0.049 | 0.00202 |
| 158 | 0.69 | 0.34 | 0.0465 | 0.014759 | 197 | 0.06 | 0.077 | 0.0094 | 0.000074 |
| 159 | 0.15 | 0.2 | 0.0117 | 0.000456 | 198 | 0.09 | 0.139 | 0.0188 | 0.000222 |
| 160 | 2.25 | 1.4 | 0.0594 | 0.066825 | 199 | 0.06 | 0.076 | 0.0094 | 0.000074 |
| 161 | 2.78 | 1.74 | 0.0729 | 0.121597 | 200 | 0.04 | 0.072 | 0.0099 | 0.000052 |
| 162 | 0.15 | 0.2 | 0.0133 | 0.000738 | 201 | 0.054 | 0.44 | 0.0218 | 0.000162 |
| 163 | 0.3 | 0.3 | 0.0204 | 0.002203 | 202 | 0.28 | 0.2448 | 0.02 | 0.000796 |
| 164 | 1.1 | 0.21 | 0.0569 | 0.014396 | 203 | 0.06 | 0.1 | 0.0121 | 0.000096 |
| 165 | 0.2 | 0.15 | 0.0084 | 0.000437 | 204 | 0.049 | 0.15 | 0.0093 | 0.000091 |
| 166 | 0.55 | 0.54 | 0.0402 | 0.01415 | 205 | 0.04 | 0.069 | 0.0125 | 0.000065 |
| 167 | 0.21 | 0.429 | 0.0286 | 0.001441 | 206 | 0.09 | 0.139 | 0.0188 | 0.000222 |
| 168 | 0.96 | 0.5 | 0.044348 | 0.043 | 207 | 0.042 | 0.34 | 0.0196 | 0.000134 |
| 169 | 0.48 | 0.34 | 0.0633 | 0.007292 | 208 | 0.131 | 0.77 | 0.163 | 0.00362 |
| 170 | 0.15 | 0.4 | 0.0233 | 0.001643 | 209 | 0.079 | 0.4 | 0.019294 | 0.000191 |
| 171 | 1.58 | 0.56 | 0.053222 | 0.037 | 210 | 0.06 | 0.1 | 0.0153 | 0.000121 |
| 172 | 0.3 | 0.2 | 0.0108 | 0.002851 | 211 | 0.173 | 0.306 | 0.016 | 0.00065 |
| 173 | 3.9 | 1.3 | 0.0799 | 0.215011 | 212 | 0.04 | 0.256 | 0.013994 | 7.13E-05 |
| 174 | 0.04 | 0.072 | 0.0099 | 0.000052 | 213 | 0.06 | 0.1 | 0.0059 | 0.000063 |
| 175 | 0.014 | 0.2 | 0.028 | 0.00006 | 214 | 0.087 | 0.41 | 0.0513 | 0.000603 |
| 176 | 0.079 | 0.382 | 0.018739 | 0.0002 | 215 | 0.06 | 0.077 | 0.0094 | 0.000074 |
| 177 | 0.107 | 0.42 | 0.0193 | 0.000209 | 216 | 0.06 | 0.108 | 0.0094 | 0.000082 |
| 178 | 0.018 | 0.2 | 0.0187 | 0.000036 | 217 | 0.079 | 0.342 | 0.017913 | 0.000137 |
| 179 | 0.055 | 0.42 | 0.022 | 0.000165 | 218 | 0.09 | 0.105 | 0.0115 | 0.000138 |
| 180 | 0.06 | 0.126 | 0.0153 | 0.000122 | 219 | 0.055 | 0.3 | 0.036 | 0.0004 |
| 181 | 0.04 | 0.056 | 0.0077 | 0.00004 | 220 | 4 | 0.97 | 0.0759 | 0.154836 |
| 182 | 0.065 | 0.356 | 0.017886 | 0.000181 | 221 | 0.21 | 0.14 | 0.0095 | 0.000379 |
| 183 | 0.102 | 0.15 | 0.0082 | 0.000091 | 222 | 2.05 | 0.86 | 0.078525 | 0.066 |
| 184 | 0.06 | 0.1 | 0.0153 | 0.000121 | 223 | 2.74 | 1.75 | 0.074 | 0.121656 |
| 185 | 0.127 | 0.53 | 0.053 | 0.000827 | 224 | 0.44 | 0.23 | 0.051 | 0.014137 |
| 186 | 0.035 | 0.32 | 0.0175 | 0.000087 | 225 | 0.97 | 0.2 | 0.0534 | 0.016575 |
| 187 | 0.04 | 0.092 | 0.0125 | 0.000066 | 226 | 0.41 | 0.4 | 0.07 | 0.006888 |
| 188 | 0.0485 | 0.363 | 0.02 | 0.00017 | 227 | 4.7 | 0.82 | 0.0568 | 0.077418 |
| 189 | 0.09 | 0.142 | 0.0151 | 0.000155 | 228 | 0.3 | 0.3 | 0.0161 | 0.001014 |
| 190 | 0.04 | 0.069 | 0.0125 | 0.000065 | 229 | 0.3 | 0.34 | 0.043 | 0.002967 |
| 191 | 0.038 | 0.19 | 0.0182 | 0.000093 | 230 | 0.55 | 0.26 | 0.037 | 0.009972 |
| 192 | 0.09 | 0.135 | 0.0149 | 0.000178 | 231 | 0.21 | 0.143 | 0.0095 | 0.000998 |
| 193 | 0.014 | 0.2 | 0.0209 | 0.000034 | 232 | 1 | 1.05 | 0.1389 | 0.084729 |
| 194 | 0.125 | 0.81 | 0.0786 | 0.00189 | - | - | - | - | - |